

**Development of Finger Clubbing Monitor  
And Serum Calcium Detector as an Early  
Indicator of Cardio-Pulmonary Diseases**

**Thesis submitted for the Degree of Doctor of  
Philosophy (Science)**

To

**Jadavpur University**

By

**Kaustav Sen**

Under the Joined Supervision of

**Prof. Jayoti Das**

**&**

**Dr. Syed Minhaz Hossain**



Department of Physics,  
Jadavpur University  
Kolkata 700032, India



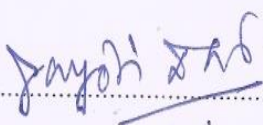
*Dedicated*

*To*

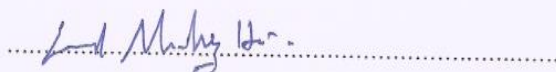
*My Parents*

### CERTIFICATE FROM THE SUPERVISOR(S)

This is to certify that the thesis entitled "**Development of Finger Clubbing Monitor and Serum Calcium Detector as an Early Indicator of Cardio-Pulmonary Diseases**" Submitted by **Sri Kaustav Sen** who got his name registered on **8<sup>th</sup> October, 2015** for the award of **Ph. D. (Science)** degree of Jadavpur University, is absolutely based upon his own work under the supervision of **Dr. Jayoti Das and Dr. Syed Minhaz Hossain** and that neither this thesis nor any part of it has been submitted for either any degree / diploma or any other academic award anywhere before.



**Dr. Jayoti Das**  
Professor  
Department of Physics  
Jadavpur University  
Kolkata - 700 032



(Signature of the Supervisor(s) date with official seal)



**Dr. S. M. Hossain**  
Associate Professor & Head  
Department Of Physics  
Indian Institute Of Engineering Science & Technology, Shibpur  
Howrah - 711103

# List of Publications

---

## Journal

1. **Kaustav Sen**, Tanusree Sarkar, Deeparati Basu, Syed Minhaz Hossain & Jayoti Das. “Calmodulin Functionalized Porous Silicon Based Electrical Calcium Detector and its Comparison with Optical Detector”. *Silicon*. (2022) (Accepted for Publication). DOI: 10.1007/s12633-022-02265-7 (Impact factor: 2.94)
2. **Kaustav Sen**, Deeparati Basu, Syed Minhaz Hossain & Jayoti Das. “Calcium selective optical sensor based on calmodulin functionalized porous silicon”. *Applied Physics: A* 127, no. 10 (2021): 1-8. DOI: <https://doi.org/10.1007/s00339-021-04869-z> (Impact factor: 2.98)
3. Deeparati Basu, **Kaustav Sen**, Syed Minhaz Hossain & Jayoti Das. “Influence of pore diameter on physical and sensing properties of free-standing Chitosan-Silica Nanocomposite membrane”. *Journal of Porous Materials* 28, no. 5 (2021): 1595-1607. DOI: <https://doi.org/10.1007/s10934-021-01079-z> (Impact factor: 2.52)
4. Deeparati Basu, Tanusree Sarkar, **Kaustav Sen**, Syed Minhaz Hossain & Jayoti Das. “Multi-Parametric optical glucose sensor based on surface functionalized nano-porous silicon”. *IEEE Sensors Journal* 18, no. 24 (2018): 9940-9947. DOI: 10.1109/JSEN.2018.2872846 (Impact factor: 4.32)
5. **Kaustav Sen**, Deeparati Basu, Syed Minhaz Hossain & Jayoti Das. “Effect of Etching time on Optical response of Calmodulin functionalized Porous silicon Calcium Detector”, *Journal of Nano-Particle Research* (2022) (In course of publication).
6. **Kaustav Sen**, Deeparati Basu, Syed Minhaz Hossain & Jayoti Das. “Etching time dependence of electrical response of calmodulin functionalized porous silicon based calcium detector”. (2022) (Communicated to *Material Research Express IOP*).

## Conference

1. **Kaustav Sen**, Arnesh Sen, Deeparati Basu, Syed Minhaz Hossain & Jayoti Das. “Automated technique based on image processing for accurate diagnosis of finger clubbing”. In 2018 IEEE SENSORS Conference, **2018**, pp. 1-4, DOI: 10.1109/ICSENS.2018.8589695.
2. **Kaustav Sen**, Arnesh Sen, Deeparati Basu, Syed Minhaz Hossain & Jayoti Das. “Automated detection of profile axis angle of human finger for quantitative digital clubbing diagnosis”. In 2019 10<sup>th</sup> International Conference on Computing, Communication and Networking Technologies (ICCCNT). pp. 1-4. IEEE, **2019**. DOI: 10.1109/ICCCNT45670.2019.8944519.
3. Arnesh Sen, **Kaustav Sen**, Jayoti Das “Ultrasonic blind stick for completely blind people to avoid any kind of obstacle”. In 2018 IEEE SENSORS Conference, **2018**, DOI: 10.1109/ICSENS.2018.8589680.
4. Arnesh Sen, **Kaustav Sen**, Jayoti Das, “In-house early detection of flat foot and high ankle foot using image processing”. In 2019 10<sup>th</sup> International Conference on Computing, Communication and Networking Technologies (ICCCNT). IEEE, **2019**. DOI: 10.1109/ICCCNT45670.2019.8944911.
5. Deeparati Basu, **Kaustav Sen**, Syed Minhaz Hossain & Jayoti Das.” Instrumentation and development of grating coupler sensor for cost-effective and precision measurement of biomolecule”. In 2019 10<sup>th</sup> International Conference on Computing, Communication and Networking Technologies (ICCCNT). IEEE, **2019**. DOI: 10.1109/ICCCNT45670.2019.8944788.



# Preface

---

Finger Clubbing is an important early clinical symptom indicating several severe health disorders, mostly related to cardio-pulmonary malfunctioning in human beings. Finger clubbing is identified as the deformation of the human finger into a bulbous tip appearance. This key clinical symptom is associated to several underlying health disorders including lung cancer. In this work the phalangeal depth ratio and the profile axis angle of the finger is monitored by the development of an automated instrument that undertakes and analyses the above mentioned parameters for quantitative and precise detection of finger clubbing by employing techniques of image processing and laser-photo-detector method. As the presence of finger clubbing in one is strongly associated with lung cancer, hence a more conclusive approach towards its diagnosis can be achieved by monitoring the serum calcium level. Since lung cancer is almost invariably associated with a drastic increase in serum calcium levels, a condition called “hyper-calcemia”, in this work a calmodulin surface-functionalized, porous silicon based calcium detecting biosensor has been developed.

Biosensors by definition is a device used to detect chemical compounds by using specific biochemical reactions mediated by isolated organelles, whole cells, tissues, enzymes or immune systems, usually by optical, electrical or thermal signals. In modern times a vast field of nanotechnology is ventured for fabrication of biosensing structures that includes nano-porous surfaces, porous membrane structures, composite and surface functionalized nanostructures that can act as high precision, accurate, sensitive and largely biocompatible biosensors.

Porous silicon, a nano-structured material is used in this work owing to its significantly high surface area for absorption, easily modulable porosity and high biocompatibility serves as perfect material for bio-sensing application. Calmodulin being a common protein in all eukaryotic cells acts as effective calcium binders due to its high affinity towards calcium ions. Porous silicon with its many-fold increase in surface area for absorption, surface-functionalized with calmodulin, acting as active calcium binder provides the perfect platform for calcium detector fabricated in this work.



Electrical response like the variation of current with varying voltage and variation of capacitance with varying frequency of input voltage, together with the optical parameter response like reflection peak intensity loss, scattering loss and absorption loss of the fabricated detector platform are analysed with calcium ion incubation at biologically relevant concentration, in order to establish the selectivity of the detector towards calcium ion. The detector displays high affinity towards calcium ion by exhibiting discriminative response for calcium in presence of other mono and bi-valent interfering ions at biologically relevant concentrations. Later, the optimization of the detector platform, to enhance its response as a calcium detector is performed by studying the change in the electrical and optical response of the detector by modulating the preparation etching parameter of the porous silicon substrate like etching time of preparation. The observations were conducted for both nano and macro porous silicon samples prepared under varying etching time. The optimized detecting platform provides a precise, sensitive, robust, cost-effective and level-free, multi-parametric approach towards calcium detection that may find use in scientific studies, food, drug and chemical industries and most importantly in medical and pharmaceutical industry as an effective clinical diagnosis tool. This study thus provides a two stage early diagnosis for any person with underlying cardio-pulmonary disorders like lung cancer, so that through this early screening process effective medical help can be sought at a very preliminary stage that can ensure better prognosis for such patients.

# Acknowledgements

---

I would like to take this opportunity to convey my sincere gratitude toward all who have physically, technically and morally supported me in this long endeavour of mine. It wouldn't have been possible without the help of these people to complete this work successfully.

I grab this opportunity to thank my first supervisor Prof. Jayoti Das (Department of Physics, Jadavpur University) for her sincere guidance throughout my research work. Her experience, knowledge and thoughtful advice has been immensely helpful in designing my research work. Her expert advice, as and when required has forged me ahead to overcome my problems and hurdles and conceive numerous exciting ideas as far as my research was concerned. Moreover, the healthy and open-minded environment maintained by her in the work-place has enabled free flow of ideas and discussions that has enriched me and my research work.

I would like to convey my gratitude towards my second supervisor Dr. Syed Minhaz Hossain (Department of Physics, IEST Shibpur) for his precious advices and guidance that has improved the scientific standard of this work immensely. The technical support provided by him in the designing of the optical analysing setup has been pivotal, without which this work wouldn't have been completed.

I would like to acknowledge Dr. Kaustuv Das (Department of Physics, Jadavpur University) for providing technical support and motivation throughout this journey. I convey my sincere gratitude towards Dr. Sanjay Kumar (Department of Physics, Jadavpur University) for his help and support in completing this work. I would like to thank Dr. Joydeep Chakraborty (Department of Physics, Jadavpur University) for the support and help provided by him in this work. I also thank Dr. Sanat Karmakar (Department of Physics, Jadavpur University), Dr. Nabin Baran Manikn (Department of Physics, Jadavpur University), Dr. Sukhen Das (Department of Physics, Jadavpur University), Dr. Kalyan Kumar Chattopadhyay (Department of Physics, Head, Jadavpur University) for their incite full words, motivations and ideas that has inspired me immensely during the course of my research. I take this opportunity to specially convey my gratitude towards Dr. Debiprasad Bhattacharya, former professor (Department of Physics, Jadavpur University) for being such an

inspiration to me. His insightful and motivational advices has immensely inspired me always and helped me throughout my research tenure.

I would like to thank RUSA, Government of India for providing me with fellowship through a long period of my research work.

I am pleased to have the opportunity to thank my fellow colleagues that includes everyone in the department of Physics in Jadavpur University, special mentions includes, Deeparati Basu, Tanusree Sarkar, Bittu Ray, Soumya Saha, Chandra Bhattacharaya, Mintu Mallick, Arnesh Sen, Shubhom Ray, Dheeraj Mondal, Moushumi, Bhaskar, Firoz. Without their support this work would have extremely difficult to complete. I would also extend my appreciation towards Sudipta, Shayari and Anupam, from department of physics, IEST Shibpur for their help when required. I would also like to thank Dr. Sayantan Chattopahayay for providing technical support and ideas that have immense influenced my research work.

I would take this rare opportunity to thank my family especially my Maa (Mrs. Kalpana Sen) and baba (Mr. Partha Sen) whose sincerity towards my wellbeing I have often taken for granted. Hence, now I grab the opportunity to acknowledge the immense love, care and support bestowed upon me by my parents that have often lifted my spirit and renewed by vigour to charge ahead in thick and thin.

Finally I would like to thank billions of my fellow citizens of India who have indirectly, supported my research work.

.....  
**KAUSTAV SEN**

**[Index No.: 163/15/Phys/24]**

Research Scholar, Department of Physics

Jadavpur University

**Date:**

Kolkata 700032, India.

**Place:**



**List of Publications (iii)**

**Preface (vi)**

**Acknowledgements (viii)**

## **1. Literature Review and Scope of Work (1)**

### **1.1 An understanding of Finger Clubbing (2)**

1.1.1 Finger Clubbing Causes (2)

1.1.2 Finger Clubbing Monitoring Techniques (3)

1.1.2.1 Qualitative Techniques (3)

1.1.2.2 Quantitative Techniques (3)

1.1.3 Benifits of Detection of Finger Clubbing (5)

### **1.2 Biosensors (5)**

1.2.1 Structure of Biosensor (6)

1.2.2 Classificatio of Biosensors (8)

1.2.3 Calssifiacion Based on Bio-Receptor (8)

1.2.3.1 Enzyme Based Biosensors (8)

1.2.3.2 Antibody Based Biosensors (10)

1.2.3.3 Aptamer Based Biosensors (10)

1.2.3.4 Whole Cell Based Biosensors (10)

1.2.3.5 Nanoparticle based Biosensors (11)

1.2.4 Attachment Techniques of Biosensors (11)

1.2.5 Classification Based on Transducer (13)

1.2.5.1 Electrochemical Biosensors (13)

1.2.5.2 Optical Biosensors (15)

1.2.5.3 Electronic Biosensors	(18)
1.2.5.4 Acoustic Biosensors	(19)
1.2.5.5 Thermal Biosensors	(19)
1.2.5.6 Gravimetric Biosensors	(20)
1.2.6 Development of Nanotechnology	(21)
1.2.7 Nano-Biosensors	(23)
1.2.8 Porous Silicon as Biosensor	(25)
1.2.9 Porous Silicon Properties	(27)
1.2.10 Optical Properties of Porous Silicon	(29)
1.2.11 Electrical Properties of Porous Silicon	(32)
<b>1.3 Calcium Detector</b>	<b>(32)</b>
<b>1.4 Scope of Work</b>	<b>(34)</b>
<b>1.5 Objective of Thesis</b>	<b>(35)</b>
<b>1.6 Thesis Outline</b>	<b>(36)</b>
<b>2. Design and Development of Multi-parametric Finger Clubbing Monitor</b>	<b>(49)</b>
2.1 Brief Introduction	(49)
2.2 Instrument Design	(50)
2.3 Mechanism of Detection	(52)
2.4 Real Time Application of the Instruments	(56)
2.5 Conclusion and Future Scope	(58)
<b>3. Porous Silicon: Synthesis &amp; Characterization</b>	<b>(62)</b>
3.1 Porous Silicon Fabrication Process	(62)
3.1.1 Electrochemical Etching Process of Fabrication of Porous Silicon	(63)
3.1.1.1 Cleaning of Silicon Wafers	(63)
3.1.1.2 Electro-Chemical Etching Method for PSi Fabrication	(64)
3.2 Mechanism of PSi Formation	(67)

3.3	Characterization	(68)
3.3.1	XRD	(69)
3.3.2	FESEM	(70)
3.4	Application of Porous Silicon	(72)
3.5	Conclusion	(73)
4.	Calmodulin Surface-Functionalized Porous Silicon Based Calcium Detector	(78)
4.1	Sample Preparation	(79)
4.1.1	Materials Used	(79)
4.1.2	Fabrication of Surface-Functionalized Detecting Platform	(80)
4.2	Structural Characterization	(81)
4.2.1	XRD	(81)
4.2.2	FESEM	(82)
4.2.3	FTIR Spectroscopy	(84)
4.3	Optical Data Acquisition Setup	(84)
4.4	Obtaining and Processing Optical Data	(85)
4.5	Optical Response	(87)
4.6	Discussion on Optical Response	(90)
4.7	Electrical Data Acquisition Setup and Processing	(92)
4.8	Electrical Characterization	(93)
4.9	Discussion on Electrical Response	(95)
4.10	Comparative Study of Optical and Electrical Response	(96)
4.11	Transient Response and Response Time of the Detector	(98)
4.12	Reproducibility of the Detector	(99)
4.13	Conclusion	(100)
5.	Effect of Etching Time on Detector Response	(107)
5.1	Fabrication of Nano and Macro Porous Silicon	(108)
5.1.1	Chemicals Required	(108)
5.1.2	Fabrication of CaM Surface-Functionalized Nano and Macro PSi with Varying Etching Time	(109)
5.2	Structural Characterization of Nano and Macro PSi with Changing Etching Time	(110)

5.2.1	XRD of Nano and Macro PSi with Varying Etching Time	(111)
5.2.2	FESEM	(112)
<b>5.3</b>	<b>Optical Characterization of Nano and Macro PSi With Changing Etching Time</b>	<b>(116)</b>
<b>5.4</b>	<b>Discussion of Optical Response</b>	<b>(119)</b>
<b>5.5</b>	<b>Electrical Characterization of Nano and Macro PSi With Varying Etching Time</b>	<b>(123)</b>
<b>5.6</b>	<b>Discussion of Electrical Response</b>	<b>(125)</b>
<b>5.7</b>	<b>Reproducibility of Nano and Macro-PSi With Changing Etching Time</b>	<b>(126)</b>
<b>5.8</b>	<b>Conclusion</b>	<b>(127)</b>
<b>6.</b>	<b>Conclusion &amp; Future Scope</b>	<b>(133)</b>
6.1	Conclusion	(133)
6.2	Future Scope	(135)
<b>7.</b>	<b>Annexure</b>	<b>(149)</b>





# Chapter-1



# Chapter 1: Literature Review and Scope of Work

---

Cardio-Pulmonary diseases have become one of the most common forms of medical conditions for humans all over the world. Owing to the fact of elevated carbon and toxic gas emissions in the environment, stressful life style, healthy air, food and water being increasingly scanty in supply, diseases such as ischaemic heart disease, bronchiectasis, cyanotic congenital heart disease, idiopathic pulmonary fibrosis, cirrhosis of liver, chronic obstructive lung disease and lung cancer are becoming increasingly common. In fact, several of these cardio-pulmonary conditions top the WHO ranking of the most common causes of deaths around the globe [1]. But, it has been proven that early detection of such diseases decreases its fatality rate significantly. As a matter of fact, early detection of these diseases plays a key role in their treatment and facilitates better prognosis.

The investigation undertaken here is to device a detector for quantitative detection of such cardio-pulmonary health conditions, most importantly lung cancer, at a rudimentary stage hence to expedite treatment and significantly decrease the mortality rate of such disease. Finger clubbing is a common clinical symptom for early manifestation of many cardio-pulmonary conditions including lung cancer [1-7]. Presence of finger clubbing provides a substantial early precursor of the presence of many underlying health disorder, most commonly in the case of lung cancer [7], though not confirmatory. Thus to confirm, serum calcium level in blood is another parameter undertaken in the investigation. Lung cancer is almost inevitably associated with an elevated level of serum calcium, a condition called “hypercalcemia” [8]. Association of hypercalcemia with lung cancer is most common; in fact it is the most prevalent metabolic anomaly accompanying malignancies [8-12]. Thus in reference to the study a finger clubbing detector is devised for quantitative detection of finger clubbing and a serum calcium detector is fabricated using Calmodulin functionalized porous silicon.

## **1.1 AN UNDERSTANDING OF FINGER CLUBBING**

Finger clubbing is a clinical condition characterized by the drumstick or bulbous appearance of fingers [13]. It is actually a distortion of the general shape of the finger that now takes a bulging appearance, resembling a drumstick or a bird's beak. It causes the structural change in the appearance of the finger which results in the increase in antero-posterior and lateral diameter of the nails [1]. Finger clubbing was first diagnosed, in the 5<sup>th</sup> century B.C by Hippocrates as a sign of underlying disorder [1-2,13-15]. Since then finger clubbing has been associated with a numerous diseases.

### **1.1.1 FINGER CLUBBING CAUSES**

Finger clubbing is caused due to unfragmented platelets precursor in the pulmonary circulation which accumulates in peripheral vasculature, releasing platelet derived growth factor resulting in digital clubbing [3]. This condition generally stems from the lack of oxygen carrying capacity of the blood [3]. Thus finger clubbing is a common symptom associated with numerous cardio-pulmonary diseases namely lung cancer, bronchiectasis, cyanotic congenital heart disease, idiopathic pulmonary fibrosis, cirrhosis of liver, cystic fibrosis, mesothelioma, inflammatory bowel disease and hepatic cirrhosis [1-7]. Moreover the association of finger clubbing has also been confirmed with intrathoracic tumours and Crohn's disease [14].

Finger clubbing generally occurs in steps [1,16].

- ❖ Initially the nail bed softens, giving it a spongy appearance.
- ❖ Second step results in the loss of lovi-bond angle that is the angle between the nail plate and the proximal nail fold. The lovi-bond angle increases from its normal measure of nearly 170° to greater values [2, 3, 5-7, 14, 17-18].
- ❖ Eventually, the depth of distal phalanx increases, thus disruption of distal and inter phalangeal depth ratio occurs [1]
- ❖ Finally the nail appears shinny [1].

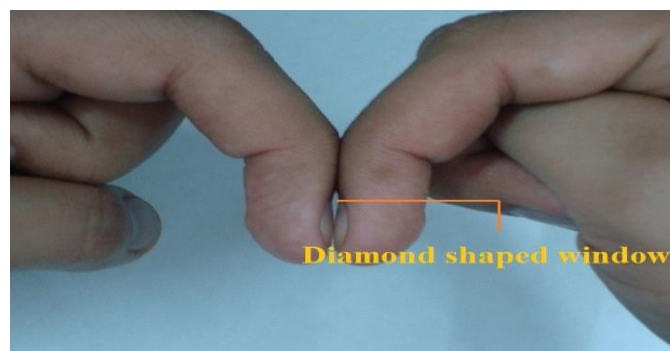
### 1.1.2 FINGER CLUBBING MONITORING TECHNIQUES

Numerous techniques both qualitative and the more accurate, quantitative are known for monitoring finger clubbing. Here we discuss the universally accepted standard techniques, both qualitative and quantitative.

#### 1.1.2.1 QUALITATIVE TECHNIQUES

This technique of monitoring of finger clubbing in patients includes visual techniques that helps to detect only the presence of the disease or symptom but provides little or no information about the degree or measure of the symptom. This technique though effective in monitoring the advance stage of the symptom, often fails when the symptom is its initial stage.

- ❖ **Schamroth's Window Test:** Named after Dr.Schamroth of South Africa this test provides a qualitative detection of finger clubbing. Carried out by placing the dorsal surface of the terminal ends of the phalanges together of left and right hand correspondingly [1]. For a normal finger a diamond shaped window is created when dorsal surfaces of the terminal end of the phalanges of similar fingers are touched as shown in figure 1.1. Any obliteration of this diamond shaped window indicates the presence of finger clubbing in an individual.



**Fig 1.1 Schamroth's window test [1]**

**Visual method:** This method does not involve any technique but is totally dependent of visual interpretation of a human finger. If by observing the terminal end of the phalange appears bulging, or a resemblance is observed to a drumstick or a bird's beak, the finger is stated to be clubbed [1].

#### 1.1.2.2 QUANTITATIVE TECHNIQUES

This technique undertakes different parameters of the phalange to measure quantitatively the degree of finger clubbing for a particular patient. Distal phalangeal

depth (DPD) and inter phalangeal depth (IPD) ratio together with the lovi-bond angle measure provides important parameters for quantitative diagnosis of finger clubbing [2, 5, 7, 13, 19-26].

- ❖ **Shadow Diagram Technique:** In this method the shadow of the human finger is projected upon a screen to obtain the outline of the finger from where the lovi-bond angle of the finger is calculated as the degree of finger clubbing [26]. This process is an effective way to quantify finger clubbing by considering lovi-bong angle, which is an important parameter for finger clubbing determination. This technique is manual and may be subjected to error. Repetitive measurement is required in this method to obtain accuracy.
- ❖ **Vernier-Calliper Method:** This method includes measurement of Distal phalangeal depth and inter phalangeal depth ratio using a vernier calliper and computation of their ratio to provide a quantitative manifestation of finger clubbing in an individual [16, 22]. This technique is an effective way of determination of advance stage of finger clubbing. This technique though useful, requires human intervention and not automated.
- ❖ **Digital photographic method:** In this method the digital image of the finger is manually analysed using computer software for the determination of lovi-bond angle of a finger in order to determine the presence of finger clubbing [13]. This method undertakes a single parameter for determination of finger clubbing and involves manual intervention hence is not automated.
- ❖ **Ultrasound imaging technique:** This method involves the analysis of ultrasound image of a finger and the measurement of soft tissue depth under nail with naked eye [21]. This method also undertakes the DPD-IPD ratio parameter for determination of finger clubbing [21]. This method introduces a new parameter for finger clubbing analysis, which is the soft tissue depth measurement. Though effective in early diagnosis in finger clubbing, this method involves heavy machinery and is expensive relative to the other above mentioned methods. Moreover, the image analysis is manual and may be subjected to errors. Repetitive measurement is required to obtain an errorfree diagnosis.

### **1.1.3 BENIFITS OF DETECTION OF FINGER CLUBBING**

Finger clubbing is an early precursor to numerous underlying disorders, mostly cardio-pulmonary [1-7]. Association of finger clubbing in case of lung cancer is most common [7]. As such finger clubbing provides a vital, early symptom of such underlying diseases, thus enabling early diagnosis and better prognosis for such patients. Though the presence of finger clubbing in a patient is not a confirmatory symptom but since its presence is almost inevitable for any cardio-pulmonary malfunctions, diagnosis of finger clubbing provides a key role in investigation of such serious health conditions thus triggering further and more confirmatory tests for diagnosis of cardio-pulmonary diseases and most importantly lung cancer so that early management can be enabled and the disease can be dealt with at a rudimentary stage and better prognosis can be warranted.

Since our key focus is on early detection of cardio-pulmonary health conditions mainly lung cancer, in this work we further ventured into the topic for a more confirmatory parameter for the detection of lung cancer. As discussed earlier, serum calcium level in humans acts as an excellent confirmatory detecting parameter for lung cancer [8-12]. In-fact “hypercalcemia”, a state of elevated serum calcium level is considered as the most common symptom of lung cancer [8-12]. Hence in this work a calmodulin (CaM) surface-functionalized, porous silicon (PSi) based biosensor is designed for serum calcium detection. This detector can act as an excellent marker for the elevated calcium level in human serum and hence facilitate early confirmatory detection of lung cancer.

## **1.2 BIOSENSORS**

Biosensors by definition are devices used to detect chemical compounds by using specific biochemical reactions mediated by isolated organelles, whole cells, tissues, enzymes or immune-systems, usually by optical, electrical or thermal signals [27]. In plain words, a sensor capable of qualitative or quantitative detection of biological analytes or contains any biological element can be termed as a biosensor. In-fact human beings themselves are full with biosensors. Eyes as optical sensors, skin as temperature and pressure sensor, tongue and nose as chemical sensors and ears as acoustic sensors [27]. In fact tropic movements in plants are excellent examples of bio sensing capability of living beings [27].

The human race was introduced to the world of biosensor by Lenad C. Clark, who first invented glucose sensor in 1962 by detecting glucose with amperometric enzyme electrode [28]. Since then biosensors has been the field of interest for many scientific studies. Development of calcium biosensor by the use of calcium sensor dyes was first introduced in 1987 by W. Melzer and M F Schneider [29, 30]. Later Calmodulin (CaM) based indicator method for calcium sensing was introduced in 1997 by A. Miyawaki [31]. Since then several methods of calcium detection has been introduced, be it chromatography technique [32], electrochemical technique [33,34], potentiometric technique [35-37] and spectroscopic techniques [38-41]. In-fact different new approaches have been introduced in bio-sensing methods and materials in order to increase the accuracy and sensitivity of biosensors appreciably. In modern times a vast field of nanotechnology is ventured for fabrication of biosensing structures that includes nano-porous surfaces, porous membrane structures, composite and surface functionalized nanostructures that can act as high precision, accurate, sensitive and largely biocompatible biosensors [42]. Thus now a days, biosensor includes a huge interdisciplinary field of research that merges different branches of science including physics, chemistry, biology, electronics, nanotechnology and pharmaceutical providing a huge horizon of scientific studies.

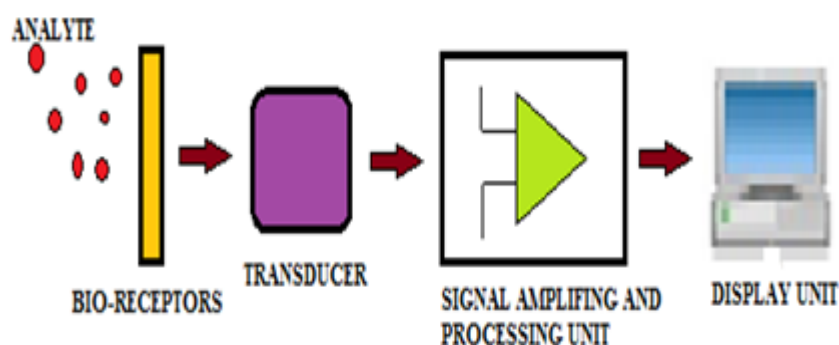
### **1.2.1 STRUCTURE OF BIOSENSOR**

Since a biosensor is programmed to detect qualitatively as well as quantitatively a biological analyte, we firstly need to state what these analytes could possibly be. Any biological or bio-chemical substance can act as an analyte for a biosensor. These substances can include simple elements to complex bio-chemical compounds. Since one of the major applications of biosensors is in the field of human health diagnostics, simple elements and compounds like calcium, sodium, potassium, glucose, uric-acid, etc which requires constant monitoring can act as analytes for biosensors. Again complex compounds like an entire cell of a living microorganism like bacteria, virus, other pathogens, DNA, RNA, antigens can act as analytes for biosensors.

Thus to design a biosensor for health monitoring, a biomarker or a marker analyte that is a parameter for specific ailment is selected and their biological relevant range is studied. For the interaction of these specific analyte with the biosensor,



specific chemical compound that have affinity towards the marker analyte termed as bio-receptor is selected and implanted upon the surface of the biosensor using different techniques, the most easy and popular among them being the surface-functionalization technique [43]. These implanted compounds acts as specific attachment sites for the biomarker intended to be analysed by the biosensor. As in the case for antigen-antibody interaction, the antibody is capable to get selectively attach to the antigen in a complex bio-chemical compound by means of weak forces like hydrogen-bond, Vander Waal force or by means of hydrophobic and electrostatic interaction [43]. Similarly the targeted biomarkers are able to get attached to the biosensor surface by the help of biomarker-bioreceptor interaction, in spite of the presence of other interfering molecules. The sensing technique of the biosensor is then carried out by the help of transducers. Transducer helps in converting energy from one form to the other. The material of the biosensor that ranges from thin films, to composite structures to membranes to porous structures to almost anything is selected according to the requirement of the biomarker that need to be sensed by the biosensor. These problem specific materials chosen as the base of the biosensor act as transducers since all the properties of the biosensor, be it optical, electrical or mechanical are controlled by this material. Any change in these properties of the biosensor after the introduction, implantation and immobilization of the analyte molecule indicates the change in transducer signal that may be further processed for better accuracy of the biosensor. A block structure of a typical biosensor in its sequence is represented in fig 1.2.



**Fig 1.2 Schematic Block Structure of Biosensor.**

## **1.2.2 CALSSIFICATION OF BIOSENSORS**

It is possible to classify biosensors in various different ways depending upon parameters like bio-receptors, transducers, biosensor material and technology and based upon detection system, as shown in the classification scheme depicted in fig 1.3.

### **1.2.3 Classification Based on Bio-receptor**

As we know bio-receptors plays a vital role in biosensor designing, thus biosensors are mainly classified on basis of bio-receptors which includes catalytic and non-catalytic biosensors [43]. In a catalytic biosensor, the analyte interacts with the bio-receptor to produce biochemical reaction products [44]. Examples of catalytic biosensors include enzyme, whole cell, microorganisms and tissue. In case of non-catalytic biosensor the analyte gets irreversibly attached to the receptor, without formation of any interaction product. This type of biosensor includes antibodies, nucleic acids and cell receptors [44].

#### ***1.2.3.1 Enzyme Based Biosensor***

Enzyme based biosensors are one of the most common category of biosensors. Being common biocatalysts, enzymes are known to increase biological reaction rate under specific ambient conditions. Enzyme based biosensors work under the principle of catalytic reaction and binding of target analyte to the sensor surface for detection [45]. Enzyme based biosensors employs various mechanisms for detection of target analyte, like metabolises of the analyte by the enzyme, thus estimation of the enzyme concentration to give a direct measurement of the catalytic transformation caused by the enzyme upon the targeted analyte. Analyte based activation or inhibition of the enzyme, to measure the analyte concentration, which is directly related to the decrease in product formation of the enzymatic reaction serves as another mechanism for enzyme based biosensors [45]. Lastly, measurement of enzyme characteristics due to a specific analyte is yet another mechanism employed for enzyme based biosensing action [46-49]. Glucose and urea biosensors are the most common form of enzyme-biosensors known till date. In recent times, C.A Cordeiro developed enzyme base glucose biosensor for real time glucose monitoring of the brain [50]. D.A Uygun developed nanoparticle based potentiometric urea biosensors that acts upon

analyte-enzyme interaction for the sensing of urea [51]. Lately, with the emergence of

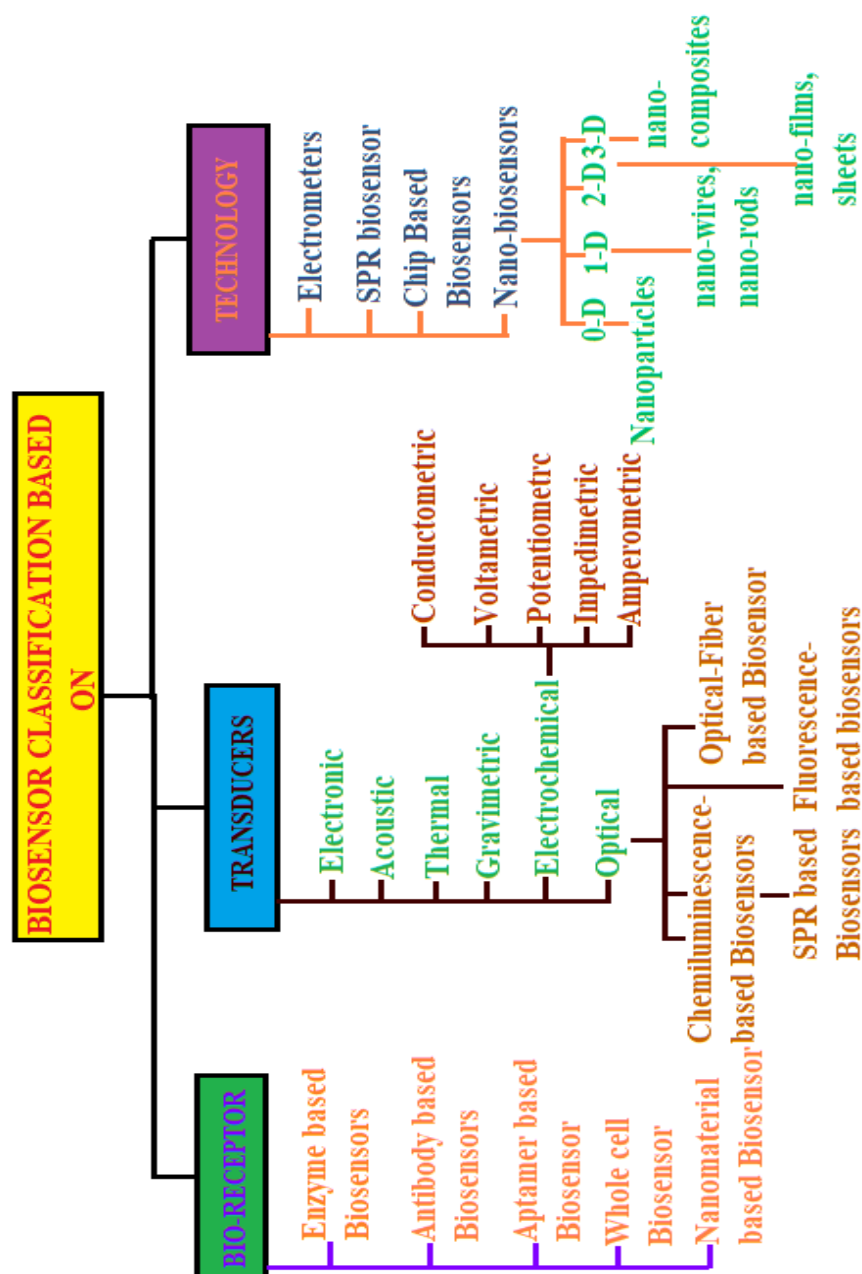


Fig 1.3 Biosensor classification

nanotechnology, nanoparticle integrated with enzymes has become a hugely popular in the field of biosensors, where recently enzyme used as receptor material has become hugely popular [52].

### ***1.2.3.2 Antibody Based Biosensor***

Antibody based biosensors work on the principle of antigen-antibody reaction for detection of target analyte [52]. The antibody embedded in biosensor contains signature 'Y' shaped immunoglobulins that acts as receptor molecule for antigen-antibody reaction. These types of antibody-based biosensors are called immuno-sensors [52]. Immuno-sensors are further divided in labeled and label-free category. In case of labeled immunosensors an antigen-antibody specific label is introduced and the antigen-antibody complex is sensitively calibrated through measurement of the label [53]. In case of label-free immunosensors the physical changes brought about by the development of the antigen-antibody complex is directly measured for biosensing purpose [54].

### ***1.2.3.3 Aptamer Based Biosensor***

Aptamer based biosensors consists of single stranded molecules of RNA and DNA as receptor molecule which are highly flexible and can get folded into 2-D and 3-D structures and get selectively binded to target molecules. Aptamer based biosensors exhibit excellent binding capabilities due to its reduced steric blocking and larger surface density [55-57]. A great advantage of aptamer based biosensors is that unlike enzymes or antibodies they can be synthesized chemically and modified according to target analytes and detection conditions [58].

### ***1.2.3.4 Whole Cell Based Biosensor***

Whole cell biosensors include microbes like bacteria, viruses, fungi, protozoas and algae as the receptor element in their construction. These single whole cell organisms contains potential bio-recognition element like antibodies and are self-replicating hence whole cell based biosensors do not require any extraction and purification of the detection element [59, 60]. The whole cell that act as recognition elements in whole cell based biosensors reacts with wide range of target analytes and produces significant electrochemical response for the transducers to process [61]. Whole cell based biosensors exhibits extremely high sensitivity and selectivity hence finds

immense use in the fields of pharmacology, drug analysis and screening, organic contaminants monitoring, food industry, pesticides, etc [62].

#### ***1.2.3.5 Nanoparticle Based Biosensor***

- With the advancement of nanotechnology in recent years, nano-membranes and nano-particles have gained a lot of importance in the field of biosensors. Presently a wide variety of nano-membranes are employed as bioreceptors in biosensors [63]. Since nano-membranes in many applications act both as bioreceptor and transducer like in the case of cerium oxide base nano-membranes that shows biomimetic catalytic activity for bioreception [64]. Due to presence of immensely interesting properties in many nano-structured materials like graphene, carbon nano tubes and noble metal nano-particles, they can be and are effectively employed as transducers in biosensing.

#### **1.2.4 Attachment techniques of Bio-Receptors on biosensors**

Appropriate attachment or immobilization technique plays an important role in the designing of the biosensor. As there are chances of the bio-receptor element to get deteriorated and become inactive, appropriate choice of the immobilization technique helps immensely in proper working of the biosensor. One must be careful that the bio-molecule to be recognized should retain its biological activity, function and structure during the working of the biosensor. Two most popular immobilization techniques involved in case of enzyme biosensors are physical or reversible and chemical or irreversible techniques. Suitable attachment technique is mainly dependent on the bio-analyte characteristics, bio-receptor chosen, the transducer employed and the physical-chemical environment of working [65, 66].

In physical or reversible technique the enzymes are attached to sensor surface by weak interacting forces and does not includes formation of chemical bonds. Physical attachment techniques includes physical absorption method, where the bio-receptor molecule is immobilized on the free surface of the biosensor by weak interactive forces like hydrogen bonding, electrostatic bond, van der waals forces or ionic bonding. Besides being an economic process, physical absorption method is the most simple and easy way of attachment and does not includes generation of matrix or modification of the biological element. In spite of the stated advantages, the

drawbacks of this method includes susceptibility of the method to varying physical and chemical conditions like temperature, pH and due to the presence of weaker forces of attachment this method do not exhibits good storage or operational stability [65-69]. Another physical or reversible technique includes physical entrapment process. In this process 3D matrix is used for the physical entrapment of the recognition element by covalent or non-covalent bonds. The receptor gets attached in the 3D network of inorganic and organic molecules. Porous ceramic materials and activated carbon are generally used as inorganic materials in the matrix where as photopolymer, polydimethylsiloxane, acetate phthalate, modified polypropylene, gelatin, cellulose, acetate phthalate etc are used as organic molecules. Popularly used techniques in physical entrapment process includes electro-polymerization, sol-gel technique and microencapsulation [65-69].

Chemical or irreversible attachment technique involves strong attachment of the recognition element to the transducer surface of the biosensor by covalent bond formation. Based on the type of covalent bond produced, chemical or irreversible attachment techniques are of two types: direct covalent binding and cross-linked covalent binding [65-69]. Direct covalent binding the most employed method of binding of the recognition element to the inner transducer matrix or the surface of the transducer. Here the functional polymer is synthesized and attached strongly to the transducer by covalent bonds. The advantage of this method lies in the fact that environmental changes has little to no effect on the attached molecule, there is little to no chance of the biorecognition element to get leached as the method involves strong bond formation. The disadvantage of the method is due to stable formation of the recognition element-transducer matrix, it becomes non-reusable [65-69]. In cross-linkage covalent bond method the bioreceptor element is attached to the analyte by the help of cross-linked covalent bonds which is brought about by multi-functional reagents that helps to link the 3D cross linked enzyme molecules to the transducer surface. The advantage of the process is it increase the catalytic activity of the enzymes, provides stronger attachment and shorter response time of the biosensor. Disadvantage of the process is, due to the formation of cross-linked covalent bonds between protein molecules there is a partial denaturation of the protein molecules limits the application of the process [65-69].The different binding techniques are illustrated in fig 1.4.

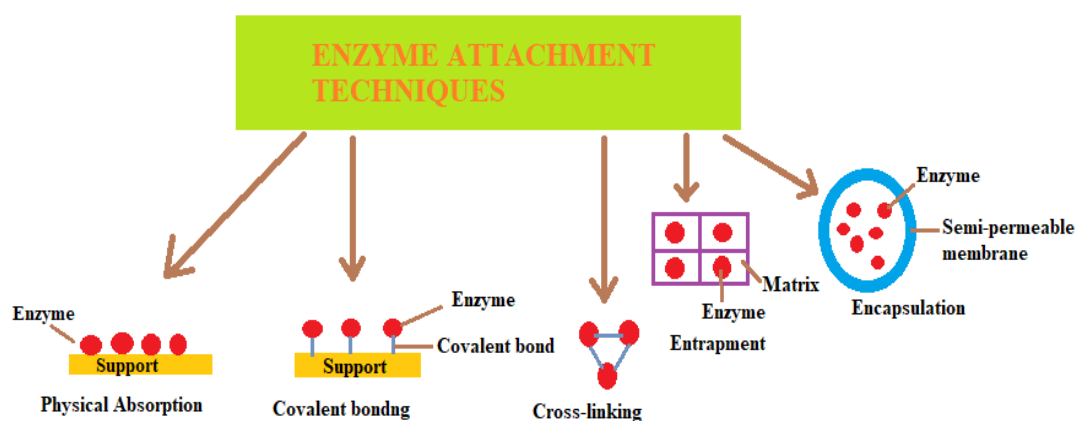


Fig 1.4 Different attachment techniques of enzyme to receptors

## 1.2.5 Classification Based on Transducer

Biosensors are broadly classified in terms of the transducers used for bio-sensing, namely they are electrochemical, optical, thermal, gravimetric and electronic, as shown in fig 1. 3.

### 1.2.5.1 *Electrochemical Biosensors*

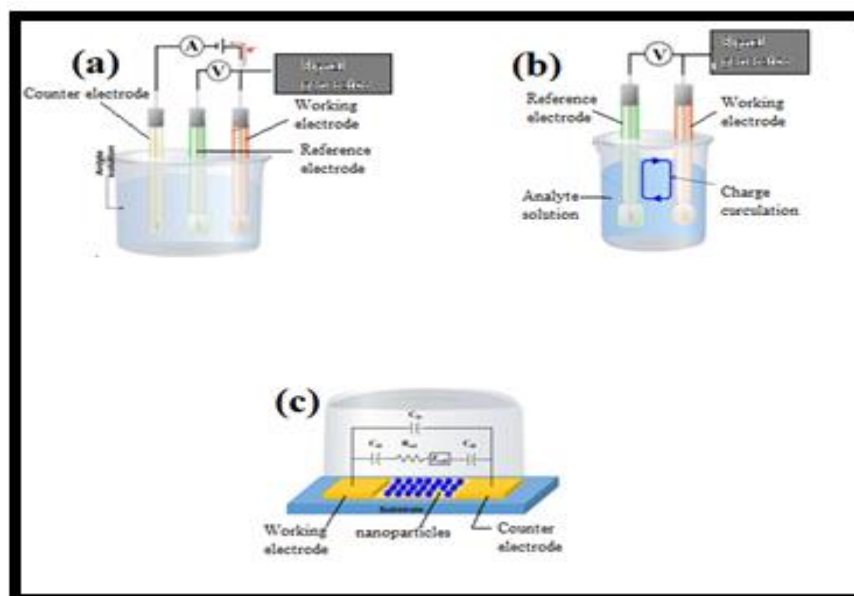
Electrochemical based biosensors are one of the most popular and widely used biosensors that work on the principle of electrochemical properties of the transducer and analyte. In electrochemical based biosensors, the electrochemical reaction that occurs between the analyte and bio-receptor on the transducer surface produces detectable electrochemical signals in form of current, voltage, impedance or capacitance are analysed for detectable biosensing activity[70-72]. Electrochemical based biosensors are largely preferred owing to its high selectivity and sensitivity. Based on the electrochemical signal produced the electrochemical biosensors are further classified as Conductometric, voltametric, Potentiometric, impedimetric and amperometric biosensors. The different class of electrochemical based biosensors is illustrated in fig 1.5. [70].

- ❖ **Conductometric Biosensors:** Conductometric biosensors are largely used in detection of changes produced due to metabolic processes in biological systems. Conductometric sensors are sensitive to the change in conductance produced between two electrodes, brought

about by the electrochemical reaction between the analyte and the bio-receptor molecule [70, 73, 74].

- ❖ ***Voltametric Biosensors:*** Voltametric biosensors are highly sensitive biosensors and are capable of simultaneous, multiple analyte detection. These biosensors work on the principle of analyte detection by detecting the change in current with controlled alteration of the potential difference applied [70, 73].
- ❖ ***Potentiometric Biosensors:*** Potentiometric biosensors employ ion-selective electrodes or ion selective field effect transistors for the biosensing activity. In these biosensors the change accumulated due to the analyte-bioreceptor electrochemical reaction in the working or active electrode is compared to that of the control or reference electrode and the biochemical reaction is then transformed into potential signals for sensing [70-73, 75, 76].
- ❖ ***Impedimetric Biosensors:*** Impedimetric biosensors make use of a small alternative excitation signal at the electrolyte-electrode interface to measure electrical impedance produced. AC voltage of minimal amplitude is applied at the sensor electrode to measure the in or out of phase current response with variation of frequency by the use of an impedance analyser [70, 73, 77].
- ❖ ***Amperometric Biosensors:*** Amperometric biosensors take quantitative measurement of the current produced at the working of active electrode in comparison to the reference or control electrode, due to electrochemical reduction or oxidation of the active species present in the working electrode when a constant potential is applied across it. Generally amperometric biosensors employ two or three electrode arrangement [70-73, 75]. Amperometric biosensors are advantageous to potentiometric biosensors as they provide linear, sensitive and fast response, at the same time substantial interference from other active substance resulting in reduced selectivity is a common disadvantage of the process [70, 78, 79].





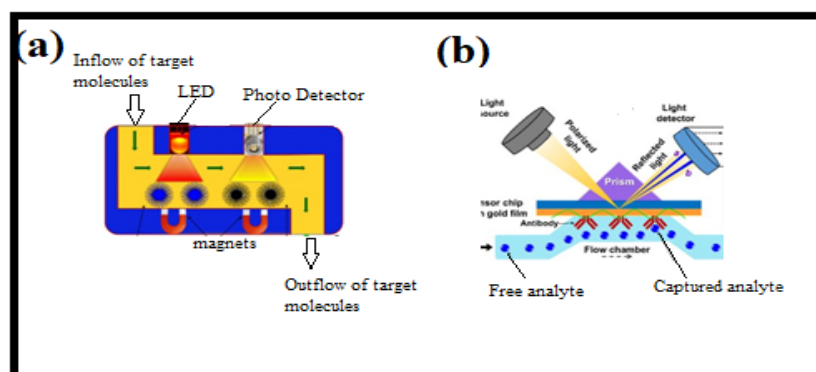
**Fig.1.5. Schematic diagram of (a) Voltammetric (b) Potentiometric and (c) impedimetric biosensors. [70]**

#### **1.2.5.2. Optical Biosensors**

Optical based biosensors work under the principle of generation of optical signals, proportional to the analyte concentration by the use of optical transducer system. Optical biosensors are further subdivided as label-free and label-based systems. In a label-free optical biosensor the analyte-transducer interaction produces the required optical signal which is sensed by the biosensor, whereas label-based methods use luminescence, fluorescence or calorimetric methods for the generation of the optical signal. Optical based biosensors use enzymes, whole cells, tissues, aptamers and antibodies as bio-recognition or bio-receiving elements. In an optical biosensor the bio-receptor produces changes in reflection, refraction, absorption, transmission, frequency, phase and/or polarization of light in order to produce detectable sensing signals. Different optical principles, based on the optical properties of the transducing element, are employed for the designing of an optical biosensor; they include chemiluminescence, refractive index, fluorescence, evanescent wave (EW) fluorescence, surface-enhanced Raman scattering, optical waveguide interferometry and surface plasmon resonance (SPR) [66, 70, 80-82]. Schematic depictions of different optical biosensors are shown in fig 1.6 [70].

- ❖ ***Chemiluminescence-based Biosensors:*** Chemiluminescence based optical biosensors works on the principle of generation of light waves due to chemical reaction. Due to the mere simplicity of the detection method chemiluminescence biosensors have gained relevance in recent years. Again, this method provides economic instrumentation, provides wide range of calibration, have low detection limit which makes this method a popular choice as far as optical based biosensors are concerned. Moreover, introduction of this method in nonomaterials has provided substantial betterment to its sensitivity and has opened various new application fields [83]. Z. He developed grapheme oxide based chemiluminescence optical sensor, capable of precise DNA sensing [84].
- ❖ ***SPR based Biosensors:*** SPR is a phenomenon that is caused when polarized light waves, incident at a certain angle (called resonance angle) fall on the metal surface, at the interface of two media having different refractive indices. This incident radiation produces plasmons, which are electron charge density waves. This phenomena causes the decrease in intensity of reflected light from the metal surface in comparison to the incident radiation, the decrease being proportional to the mass of substance on the metal surface [85, 86]. SPR based biosensors works on the principle of detection of changed refractive index caused by surface plasmon resonance due to interaction of molecule to the metal surface. In fact SPR sensors detection technique depends on the variation of refractive index caused due to the analyte-bioreceptor interaction on the transducer surface. Instead of metal surface metal based nano-particle (NP) such as gold or silver NPs can also be employed for development of SPR based biosensors. The only difference is that a new phenomenon called local surface plasmon resonance (LSPR) is observed in case of NPs, the difference being that in case of LSPRs is the plasma oscillation is governed by total internal reflection principle at the NP surface instead of metal surface as observed in SPRs [82, 85, 86]. This method is a label freer method of optical sensing. SPR based biosensors find immense use in disease diagnosis, food monitoring and environmental monitoring. S.N Hosseini developed silver nano-columns based biosensor for endotoxin detection that uses LSPR technique for detection [87].

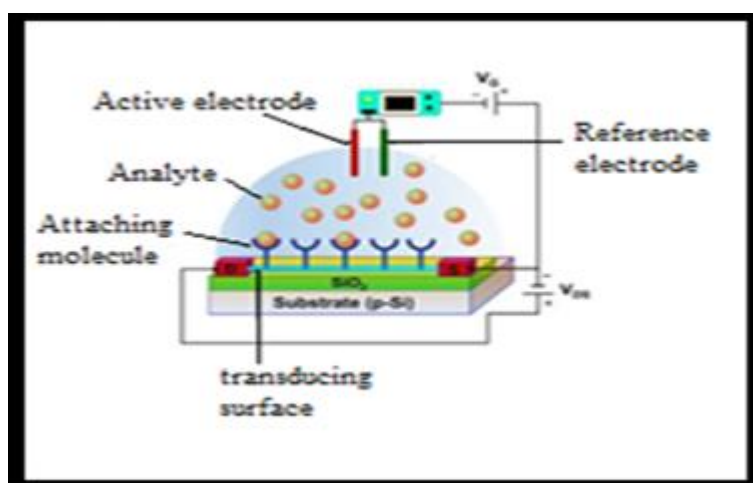
- ❖ **Fluorescence-based biosensors:** This is labeled method of optical biosensing and requires labeled agents for the detection of the analyte. Different fluorescent dyes like fluorescent proteins are used in the process. Three approaches of fluorescence base biosensors are utilized; they are Fluorescent quenching, fluorescent enhancement and fluorescence resonance energy transfer(FRET). Out of the above mentioned process, FRET as prevailed as the most widely used due to its higher sensitivity in compared to the other processes. FRET based biosensors includes non-radiative transfer of energy from donor to acceptor molecule, both being in ground state, through multipole long range interaction. FRET based sensors are capable of detecting changes in angstroms to nanometer range. Due to this high sensing quality, FRET biosensors finds use in clinical diagnosis such as aptamer analysis and cancer therapy [71, 88].
- ❖ **Optical-Fibre based Biosensor:** Optical biosensors based biosensors is an emerging alternative to traditional optical biosensing methods. Optical fibre base biosensors works on the principle of evanescent field sensing technique. Tapered optical fibres are used for the process. When light is passed through an optical fibre, evanescent waves are produced at the fibre-sample interface due to the phenomena of total internal reflection. With distance from the interface; the evanescent wave shows an exponential decay. This wave is used to produce fluorescence near the sensing surface [89]. Transducing process employed by these tapered optical fibre involves analysis of the variation in SPRs, refractive index, fluorescence and absorption [90, 91].



**Fig.1.6. Schematic diagrams of (a)chemiluminescence (b)surface Plasmon resonance biosensor. [70]**

### 1.2.5.3 Electronic Biosensors

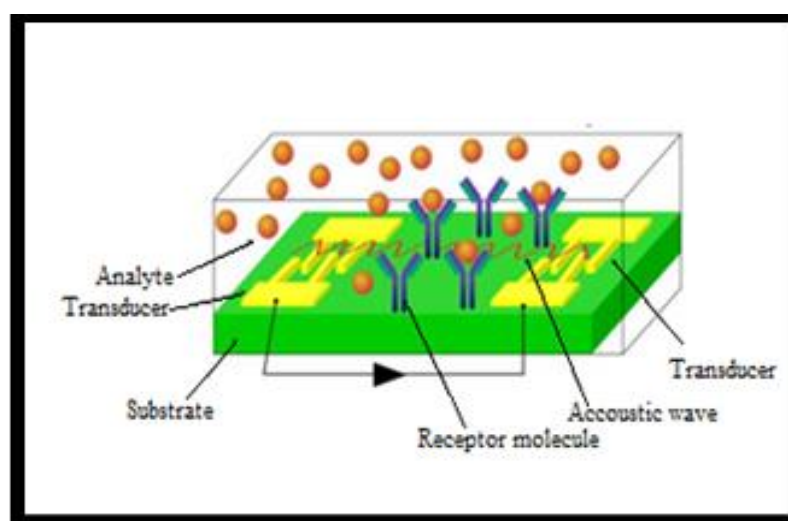
Electronic based biosensors uses silicon nano wires based field-effect-transistors (FET) biosensors or porous silicon surface based biosensors for analyte sensing. Porous silicon surface based electronic biosensors uses the alteration of electrical or optical signals caused due to analyte-bioreceptor reaction on the porous surface for transducer action [92, 93]. FET based electronic biosensors works under the principle of FET conductivity action. FETs are three terminal devices, consisting of drain, source and gate terminals, where the current flowing through source and drain terminal can be manipulated by the potential at the gate terminal or in other words by the electric field produced between the gate and the channel [94-96]. FETs based biosensors are capable of direct translation of the analyte-FET surface interaction that is the attachment of the analyte to the bio-receptor changes the channel width of FET which in turn alters the drain current [96]. Ion-based FETs and Metal-oxide FETs are most commonly used FET based electronic biosensors. The chemical changes due to analyte-bioreceptor interaction is analyzed by FET based sensors by the use of their high input impedance. High sensitivity and high spatial resolution are some advantages of this method of biosensing, however limitation of this method lies in in-vitro applications [97, 98]. Pictorial description of an electronic based sensor is shown in fig 1.7.



**Fig.1.7. Schematic diagram of electronic biosensor, nano-wire based FET biosensor [70].**

#### 1.2.5.4 Acoustic Biosensors

Acoustic biosensors measure the change in the acoustic wave's physical properties that is highly dependent on the amount of analyte absorbed by the acoustic transducer [99]. Acoustic biosensors use piezoelectric materials as transducers due to their ability of producing and transmitting frequency dependent acoustic waves. Since the optimum resonance frequency, for wave propagation is highly dependent on the physical properties of the piezoelectric transducer crystal, like its dimension, any variation in its mass due to surface absorption of analyte leads to measurable changes in the resonance frequency of the crystal [100, 101]. Acoustic wave biosensors are broadly divided into surface acoustic wave (SAW) transducer and bulk acoustic wave (BAW) transducer. In a SAW transducer acoustic waves are transmitted on a single surface of the crystal, from one location to another, whereas in BAW devices acoustic waves are transmitted from on surface to another crystal surface [102, 103]. The SAW device mechanism is depicted in fig 1.8.



**Fig.1.8. Surface acoustic wave based biosensors [70].**

#### 1.2.5.5. Thermal Biosensors

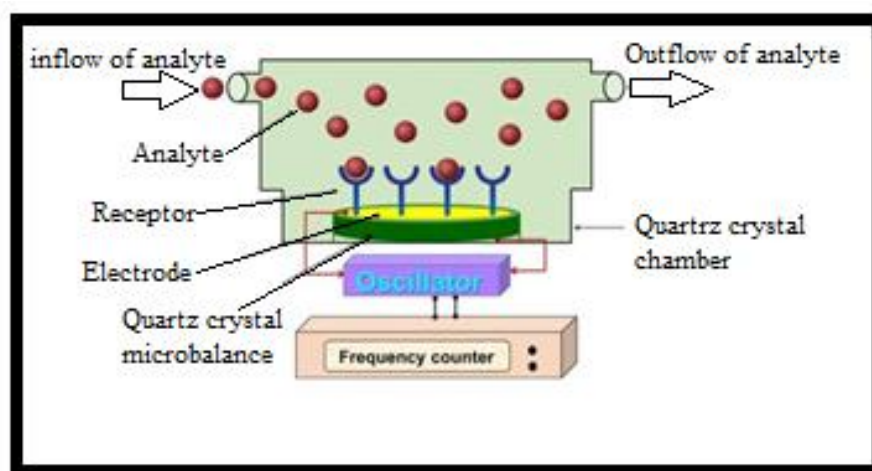
Thermal based biosensors works on the principle of measurement of heat energy absorbed (endothermic) or released (exothermic) during biological reactions. due to the biochemical reaction, the change in temperature ( $\Delta T$ ) calibrated by the thermal biosensor is proportional to the change in enthalpy ( $\Delta H$ ), the total number of molecules produced ( $\eta_p$ ) and inversely proportional to the specific heat capacity ( $C_p$ ).

Thus the temperature change can be calculated according to the equation  $\Delta T = -(\eta_p \Delta H) / C_p$  [104-108]. As the heat released or absorbed is proportional to the extent of biochemical reaction or the dynamics of structure of biomolecules in dissolved state, calorimetric based biosensors works on this principle [107, 109]. The drawbacks of calorimetric based biosensors like lack of specific temperature measurement and long experimental procedures are overcome in enzyme-thermistor based biosensors [106]. A thermal biosensor is configured such that a thermistor or thermopile that acts as a thermal transducer to be attached across an immobilized enzyme column. The catalytic reaction of the analyte-bioreceptor within the enzyme column generates measurable thermal signals, sensed by the thermal transducer. This thermal signal is processed for sensing and gives a direct measurement of the substrate concentration. Generally enzymatic catalysis shows an energy change of the range of 10-200 kJ/mol, which is sufficient for substrate concentration analysis at biological relevant levels for many metabolites [70, 105-109]. Thermistors and thermopiles are the most common thermal transducers used in thermal biosensors. Thermistor use the principle of variation in electrical resistance with temperature for temperature sensing, whereas thermopile consist of series of thermocouple junctions of metal semiconductor and substrate semiconductor components, where the temperature difference of two junctions are measured for temperature sensing [107, 108].

#### ***1.2.5.6. Gravimetric Biosensors***

Gravimetric biosensors make use of the piezoelectric properties of quartz crystals for measurement of signals generated due to small alteration in mass caused by binding of the analyte to the receptor molecule on the sensor surface. The piezoelectric quartz crystal vibrates at certain resonance frequency dependent on its mass and the applied current [110, 111]. Most commonly found gravimetric biosensors are piezoelectric biosensors, Quartz Crystal Microbalance (QCM) and Magnetoelastic based Biosensors (MES). Piezoelectric based gravimetric biosensors works under the principle of wave production at specific frequency of alternating current applied on the crystal. The change in this frequency due to absorption of the analyte or desorption of the analyte to the bioreceptor on the transducer surface causes change of this frequency that acts as the necessary signal for biosensing [112]. In QCM

based biosensor the change in resonance frequency due to attachment of analyte to the biorecognition element on the quartz crystal surface, that is sandwiched between electrodes gives the necessary signal for biosensing [113]. MES based biosensors consist of film like ferromagnetic amorphous ribbons that possess high tensile strength. MES based biosensors work under the principle of magnetostriction, where applied magnetic field causes mechanical deformation. On application of time varying magnetic field magnetoelastic vibrations are produced that in turn produces longitudinal vibrations. Thus the longitudinal vibrations produce magnetic flux within the magneto-elastic element that provides detectable signals for the biosensor functioning. Use of MES has become frequent in recent years due to certain advantages it provides like being wireless and passive and is useful in determination of force, pressure, strain and stress. Moreover MES is an ideal choice for biomedical applications owing to the stated advantages and due to its long lifetime, cost effectiveness and wireless fabrication [114]. The pictorial depiction of common gravimetric biosensors is shown in fig 1.9.



**Fig.1.9. Schematic diagram of quartz crystal based biosensor working under gravimetric sensing technique [70].**

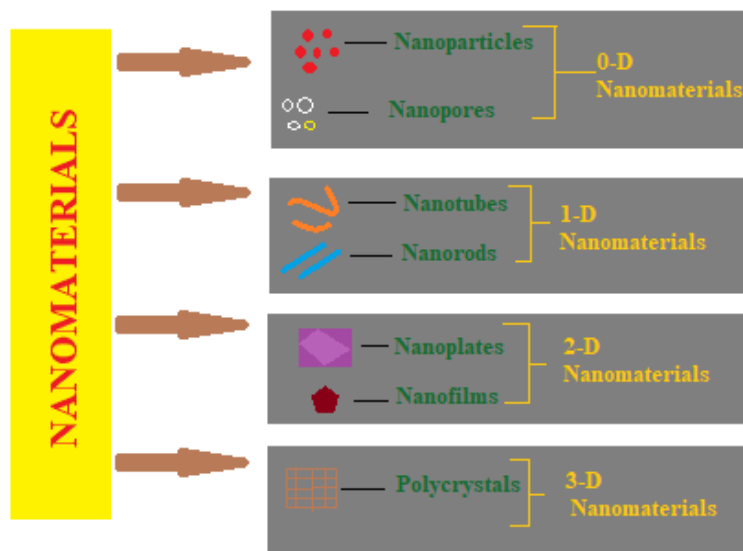
Since Biosensors classification based on technology has already been included and discussed in biosensors classification based on transducers, no separate portion of the chapter is devoted to it.

### **1.2.6. Development of Nanotechnology**

Due to the increase in demand of improved sensitivity, noise reduction and overall development in sensor technology, new approaches are ventured that lead to

altogether a new way of development of sensors with application of various new technologies like the development of nanotechnology. With the development of nanotechnology, its applications has been found in almost all field of basic and applied science like physics, chemistry, bioscience, bioinformatics, biotechnology, electronics, aerospace, healthcare, medical science, food processing and engineering and in environmental studies. The application of nanotechnology in biosensing application has been impactful. It leads to new avenues and approaches in the development of biosensors with improved sensitivity and increased bandwidth of its application. As nanotechnology includes manipulation of materials at its molecular or atomic level that largely affects various characteristics of the nanomaterial has lead to new approaches in nanomaterial based biosensor development. As the physical, chemical, optical, electrical and biological characteristics of a nanomaterial is largely dependent on its dimensionality, nanomaterials are classified based upon their nano-range dimensions. This classification includes 0D materials where the measureable dimensions of the material arenano-sized, such as nano-particles or quantum dots. For 1D materials one dimention is nano-sized while the other being larger, examples are nano-rods, nano-wires, nano-tubes excreta. For 2D nano-materials, two dimensions are or nano order while the the other dimension is of larger size like nano-sheets, nano-films, nano-walls, nano-prisms. 3D nanomaterials are those that are bulk nanomaterials like nano-balls, nano-cones, nano-pillars, multilayered nano-structures [115, 116]. Various techniques are employed for nanomaterial fabrications which are grossly categorized into top-down approach and bottom-up approach. In top-down includes restructuring of bulk materials into nano scale structures, while in bottom up approach molecular or atomic assembling is done to obtain nano sized materials. Famous top-down approaches includes chemical etching, ion milling, lithography and laser ablation, while most employed bottom-up technique includes chemical and physical vapor deposition, molecular beam epitaxy and several other bio-chemical processes like protein-polymer nanocomposites, supra-molecular complexes [115, 116]. Schematic descriptions of different nonomaterial are shown in fig1.10.





**Fig 1.10 Nanomaterial Classification according to Dimension.**

### 1.2.7. Nano-biosensors

Nanomaterial based biosensors are broadly categorized as nanobiosensors. Over the years research on nanomaterials lead to the development of nano-particles, nano-wires, nano-rods, nano-tubes and nano-composites. Owing to the different advantages presented by these nano-structures and easily modulable size and structure, use of nanomaterials have drastically improved the sensitivity and performance of biosensors. The basic advantages of nanobiosensors over other conventional biosensors includes the ability to reach and monitor different physical and chemical processes at areas difficult to reach, ability to detect and traces biochemicals liberated in minute amounts by cellular organelles that provides them an edge in medical and clinical diagnosis, Ability to interact and detect traces of ultra-low dimension harmful substances and dimensional analysis of microscopic particle in industrial and environmental studies [117].

Nanoparticle based biosensors are one of the most widely used nanomaterials in biosensing applications. Due to their nano shape and size their physical and chemical properties are hugely affected by their binding to target analytes, owing to which they find immense biomedical applications like clinical diagnosis, clinical imaging and drug delivery [118]. Nanoparticle base biosensors includes various transitional metal-oxides, metas and noble metals such as ZnO, SnO, TiO<sub>2</sub>, MnO, Palladium (Pd), Iron (Fe), Copper (Cu), Cobalt (Co), Gold (Au), Platinum (Pt) and Silver (Ag).

Nanoparticle based biosensors shows tremendous advantage due to their easy fabrication procedures, biocompatibility, chemical stability and excellent optical, electrical, electronic, chemical, mechanical and magnetic properties [70, 119-121].

Quantum dots based biosensors falls under the category of 0-D nanobiosensors. They are mainly inorganic nano-crystals that exhibit excellent optical properties like broad excitation, size-modulable spectra for emission, and appreciably high photochemical stability [122]. Quantum dots based biosensors has find immense use in the development of optical based biosensors as they are capable of precise detection of organic compounds, biomolecules like amino acids, carbohydrates, enzymes and neurotransmitters that find application in pharmaceutical analysis [123]. The most effective application of quantum dots based biosensors lies in the field of multiplexed optical analysis, as quantum dots based biosensors shows excellent sensitivity, high selectivity, quick detection time, miniaturized dimension and wavelength emission that is largely size-dependent [124].

Nano-wire or nano-tunnels based biosensors works under the principle of ion selective FET operation that includes influence of external charge on the carriers of the semiconductor that results in the sensitivity of the transducer [125]. Nano wire and tunnel based biosensors are employed for the fabrication of electrical and optical based biosensors that exhibits high reproducibility. In fact nano wire based biosensors provides the fabrication of biosensors with high sensitivity, selectivity and robust structure, capable of monitoring bioanalytes. Since the flow of current in such 1-D structure is through paths extremely close to the surface, nano-wire based biosensors are extremely sensitive to analyte attachment to the surface [126]. As the diameter of the nano-wires are comparable to the bio-analytes the combined effect of molecular attachment to the wire surface and the adjustable conductivity of the sensor provides generation of label-free detectable electrical signals for sensing [127].

Nano-rod based biosensors are mainly made of graphene, zinc, iron oxide, gold, manganese or from combination of the mentioned materials [128, 129]. Simple application of nano-rod based biosensors uses the principle of simple electrochemical modifiers to provide for a specific process. The most common applications for nano-rod based biosensors include detection and sensing of bio-molecules like glucose, nucleic acids and hydrogen peroxide [130].

Carbon-nano-tube (CNT) base biosensors are one of the most widely used sensors for biosensing applications. It consists of one, two or multi concentric layered hollow tube composed of graphite layers with fullerenes hemispheres as caps. CNTs exhibits excellent characteristics that serves as reason for its wide application in the field of biosensing, they are high electrical and thermal conductivity, great mechanical properties, huge chemical stability, huge surface to volume ratio and exhibits unique structural properties [131-133]. Together with biosensing applications CNTs also find use in tissue engineering, diagnosis, cell tracking and drug delivery [70]. Since CNTs possess large surface area any molecular attachment to its surface hugely affects its noble electron transport property, thus influencing its electronic conductance, this plays the key principle for CNT based biosensing. CNT based biosensors find immense use in glucose sensing, together with it they are employed also in sensing of neurotransmitters, amino acids, albumin, immunoglobulin, C-reactive protein, cancer biomarkers, DNA, microorganisms and other biomolecules [134-138]. Thus CNT based biosensors find immense application in the field of healthcare monitoring, food monitoring industry, chemical industries and in environmental studies [70].

Dendrimer based biosensors consist of 3-D macromolecules that have its dimension in nano range. They may be star-shaped, hyper-branched and mono-dispersed. Since the dendrimers have high density of functional groups at its surface, this structure provides large surface area that facilitates analyte attachment. A typical structure of a dendrimer consists of the external surface with functional group, the Dendron in the interior and the core [139, 140]. Dendrimer based biosensors exhibit high selectivity, sensitivity and reproducibility hence find application in biosensing, drug delivery and medical diagnosis [141-143].

### **1.2.8 Porous-Silicon as Biosensor**

Discovery of Porous Silicon (PSi) dates back to 1956 [144], where PSi was accidentally discovered during electrochemical polishing of Silicon in Bell's laboratories in USA. Vastly neglected over the years, PSi gained a significant amount of interest on the discovery of photoluminescence exhibited by it in visible light range upon excitation by UV spectrum, in the year 1990 [145]. This discovery gained a lot of scientific interest as silicon materials did not exhibit this property due to its indirect band gap. Since then Porous silicon (PSi) has emerged with manifold

application in microelectronics [146]. Unlike crystalline silicon, the direct and wider band-gap of PSi due to its quantum-confinement effect have rendered PSi as an ideal candidate for sensing application [146]. The phenomena of photoluminescence exhibited by PSi have found wide range use in optical sensor applications [147-149]. The exceptionally high surface area of PSi makes it a perfect material for absorption and interaction of bio-molecules [150-152]. Its easily adjustable surface morphology and porosity makes PSi a popular choice for bio-sensors [151, 153-157]. With the help of its high loading capacity, PSi finds wide-spread use in arena of chemical sensors, bio-sensors, ionic-sensors, to name a few [158-160]. Due to its biocompatibility and high absorption capacity, PSi finds use as bio-vehicles for highly targeted drug delivery [161,162].

PSi has been broadly categorized into three categories, namely microporous of pore size  $\leq 2\text{nm}$ , mesoporous of pore size ranging from 2-50nm and macroporous of pore size  $> 50\text{nm}$  [163]. Since any structure with size  $< 100\text{nm}$  is termed nanostructured, PSi with pore size ranging from 1-100nm is termed as nanoporousPSi. Moreover, the porosity, pore size, structure and morphology of PSi are dependent on the factors like anodization condition, electrolytic composition, wafer resistivity and dopant type, and can be easily modulated by changing any one or more of these mentioned factors [164,165]. Due to these mentioned properties of PSi it finds tremendous application as a transducing material in the field of gas, vapour and humidity sensing [166-170], chemical sensing [171] and biosensing [172, 173]. In this work the electro-chemical etching method of preparation of PSi on bulk silicon substrate is discussed together with different physical, chemical, electrical, optical and structural properties of the prepared macro and nanoPSi is presented. Later the chapter various application of PSi has been discussed in different fields of science.

Porous silicon (PSi) has lately emerged with manifold application in microelectronics [174]. Unlike crystalline silicon, the direct and wider band-gap of PSi due to its quantum-confinement effect have rendered PSi as an ideal candidate for sensing application [174]. The phenomena of photoluminescence exhibited by PSi have found wide range use in optical sensor applications [175-177]. The exceptionally high surface area of PSi makes it a perfect material for absorption and interaction of bio-molecules [178-180]. Its easily adjustable surface morphology and

porosity makes PSi a popular choice for bio- sensors [179, 181-185]. With the help of its high loading capacity, PSi finds wide-spread use in arena of chemical sensors, bio-sensors, ionic-sensors, to name a few [186-188]. Due to its biocompatibility and high absorption capacity, PSi finds use as bio-vehicles for highly targeted drug delivery [189, 190]. In recent years, PSi based ionic sensors have gained importance with wide applications in clinical diagnosis, food industry and in scientific laboratories.

Since the surface morphology of porous silicon can easily be altered by altering the etching conditions during its preparation, The electrical and optical properties of PSi, that are largely dependent on its surface morphology can also be altered, which renders PSi as an ideal electronic, electrical and optical transducer for sensing application. H. A. Hadi showed that the electrical properties of PSi can be substantially altered by altering the etching time and current density during formation of PSi, which showed decrease in build in voltage with increasing in etching time and current density [174]. S. J. Kim showed the tremendous absorption capability of PSi by using it as an alcohol gas sensor, capable of sensing alcohol at extremely low concentration of 0-0.5% at room temperature [178]. PSi finds application in organic analyte sensitivity as shown by F. A. Harraz, who established organic analyte sensor based on PSi and studied the capacitive property of the same with front and back Ag contacts [186]. E. A. Kabba established extended gate field effect transistors (EGFET) based on PSi that is capable of sensing sodium, potassium, calcium and manganese ions at room temperature within concentration range of  $10^{-4}$  to 1M by the use of altered current-voltage sensitivity of PSi based EGFET that works as a transducer for the process [188]. G. N. Tovar established meso-porous based PSi particles for effective antigen delivery to targeted molecule where the PSi particles are used as carriers [189].

### **1.2.9 Porous-Silicon properties**

Porous silicon (PSi), a product of electrochemical etching of bulk silicon exhibits a lot of exciting properties, due to its natural nano-structure, unlike its bulk counterpart. Domination of quantum effects in nano-structured materials with reduction in size of bulk materials to nano-range brings about numerous new properties in materials which are otherwise not exhibited in their bulk state. In case of PSi, it was reported in 1970 that the silicon in PSi can be thermally oxidized to

silicon dioxide and be used as a dielectric [191-195]. Similarly on the report of luminescence property of PSi in visible range, in the year 1990 [196], made the scientific world indulge in exploring various structural properties of PSi [197, 198], studying the mechanism of light emission and optical properties [199, 200], together with the study of other properties for possible optoelectronic and various more applications [201, 202]. It is due to these favourable properties of PSi, it finds tremendous application as multilayer structure in photonic crystals [203], light emitting structures [202], bio and chemical sensors [204-209], targeted systems for drug delivery [210], micro-engineering [211], signal processing [212] and many more. The Structural morphology of PSi can be easily modulated by bringing small changes in anodization conditions [164, 165], this adds widely to the acceptability of PSi as a sensing and transducing material. In this work the structural, electrical and optical properties of PSi have been emphasized upon. Table 1.1 gives a comparative study of certain properties of bulk and porous silicon.

**Table 1.1: Comparative study of Bulk Silicon and PSi. [213]**

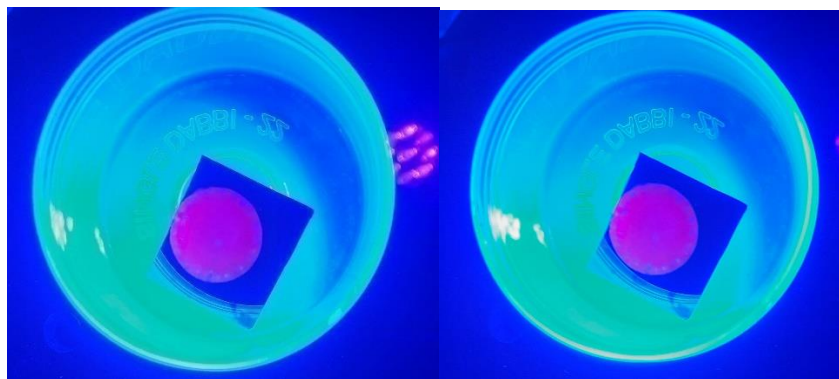
	<b>PROPERTIES</b>	<b>BULK SILICON</b>	<b>POROUS SILICON</b>
<b>STRUCTURAL</b>	Density	2.33g/cm <sup>3</sup>	0.12-1.9 g/cm <sup>3</sup>
	Porosity	-	20-95%
	Surface to Volume Ratio	1m <sup>2</sup> /cm <sup>3</sup>	500m <sup>2</sup> /cm <sup>3</sup>
	Lattice Structure	Diamond	Diamond
<b>MECHANICAL</b>	Young's Modulus	160 GPa	1-100 GPa
	Hardness	11.5 GPa	0.2-10 GPa/0.05-1 GPa
	Yield strength	7 GPa	-
<b>EMISSIVE</b>	PL Wavelength	1000-2000nm	400-1300nm
	PL Efficiency	10 <sup>-6</sup>	0.01-0.23-Films
			0.01-0.6-Suspensions
	EL Efficiency	10 <sup>-8</sup>	0.01-0.1
<b>ELECTRICAL</b>	Resistivity	10 <sup>-2</sup> - 10 <sup>3</sup> Ωm	10 <sup>3</sup> -10 <sup>12</sup> Ωm
	Electron Mobility	1305 cm <sup>2</sup> /Vs	0.1-30 cm <sup>2</sup> /Vs
	Hole Mobility	480 cm <sup>2</sup> /Vs	2-6 cm <sup>2</sup> /Vs
	Dielectric Constant	11.5	2-8

<b>OPTICAL</b>	Band-gap	1.1eV	1.1-3.2eV
	Infrared Refractive Index	3.5	1.1-3.0
	Reflectivity (500-1000nm)	10-35%	0.1-10%
<b>BIOCHEMICAL</b>	Biodegradability	-	Hours (Nanoparticles)
			Days (Microparticles)
			Months (Implants)

### 1.2.10 Optical Properties of porous Silicon

PSi predominantly exhibits two optical properties, photoluminescence on external excitation and optical reflectivity [191]. Photoluminescence (PL) is one of the widely used optical characterization methods use for optical property investigation of PSi. Photo creation of electron and hole pair is manifested upon incident light excitation on a material surface. The excess carriers created, recombines, often radiatively and this emitted light is termed as PL. Many important properties like electronic band structure, nature of defects and impurity enters and electron-photon coupling can be derived from the study of PL [214].

Unlike crystalline Silicon (Si) that emits extremely weak PL in infrared region due to its small and indirect bang gap, electrochemically etched PSi exhibits very efficient PL emission in the visible region, as shown in fig 1.11.



**Fig 1.11. PL emitted by PSi of different porosity upon ultra-violet excitation.**

As stated earlier that with approach towards nano scale dimension of particle size, new properties are manifested in materials that are otherwise not present in their bulk state. Quantum confinement (QC) effect is one such effect exhibited by PSi samples [215]. EL emission of PSi can be explained by this QC effect observed in PSi. The EL emitted can be explained by the recombination of quantum confined carriers in the crystalline Si structure present in PSi [214] that rendered PSi to have direct band-gap, unlike its bulk counterpart. But later, studies conducted on hydrogenated silicon compounds like silicon hydride complexes and siloxene derivatives found in oxidized PSi structures gives further incites in explanation of PL and its peak shifts [216, 217]. Moreover other optical properties like Cathodoluminescence and electroluminescence is explained thoroughly by the above mentioned models.

PSi And other Si based nanostructures has reported efficient exhibition of PL from infra-red to visible light region and into near ultra-violet region. This broad spectrum is attributed to distinct luminescence of different origin [214]. The most attention received by far is that of the ‘S-Band’ luminescence, that has been tuned effectively over the entire visible range starting from deep red to blue. This band has gained a lot of significance due to its technological applications and as it can be easily electrically excited [214]. The ‘F-Band’ luminescence has been the subject of recent study due to its blue-green PL emission. This PL emission is generally observed in oxidized structures and arises due to contamination of defects in Silicon oxides [214]. Infra-red emission of PL is observed for materials annealed under high vacuum conditions and can be attributed to dangling bonds seen in PSi [214]. Ultraviolet PL emission is also observed upon soft X-ray excitation. It is present with the blue-green ‘F-Band’ emission and observed in oxidised samples due to the presence of defective oxide states [214]. Different origin of PL bands together with their peak wavelength is shown in table 1.2.



**Table 1.2: Luminescence bands for PSi.**

<b>SPECTRAL RANGE</b>	<b>PEAK WAVELENGTH (nm)</b>	<b>LUMINESCENCE BAND</b>	<b>PL</b>	<b>CL</b>	<b>EL</b>
Near IR	1100-1500	IR band	Present	Nil	Nil
Blur-Red	400-800	S-Band	Present	Present	Present
Blue-Green	~470	F-Band	Present	Present	Nil
UV	~350	UV-Band	Present	Present	Nil

One of the most attractive property of PSi is that it can emit as well as reflect light in visible range. In-fact refractive is an important property of PSi that controls the transmission and reflection of waves incident upon the PSi-air interface. Bruggeman's approach is the most accepted approximation for the calculation of refractive index of PSi which is given by the use of the following formula [191].

$$(1 - P) \frac{(E_{Si} + EPSi)}{(E_{Si} + 2EPSi)} + (P) \frac{(E_{air} + EPSi)}{(E_{air} + 2EPSi)} = 0$$

Where, P= Porosity of PSi

$E_{Si}$ = Dilelectric constant Of Si

$EPSi$ = Dilectric constant Of PSi and

$E_{air}$ = Dilecetric constant of air.

In-fact Optical reflective spectrum of PSi shows Febry-Perot fringe pattern [191], where the interference fringe pattern is highly dependent upon the nnodization current density of PSi fabrication [191]. 9-12 fringe of wavelengths ranging from 500-1000nm are obtained for PSi samples of Thickness of approximate 3000nm [191]. A patter of decreasing fringe numbers is also reported with increasing annodization current density, with almost no fringe visible above current density of 600mA/cm<sup>2</sup> [191].

### 1.2.11 Electrical Properties of Porous Silicon

PSi being an inherently disordered solids, consists of several defective states. Its disorders are not only limited to compositional or structural impurities and defects but is predominated by numerous defective states and surface dangling bonds, created during its fabrication [218]. These dangling bond full surface of PSi plays a major role in charge transport mechanism in PSi.

The charge transport mechanism of inherently defective solids like PSi is dominated by several mechanisms, like hopping, Poole- Frenkel (P-F) and Trap-Assisted-Tunnelling (TAT) [218]. For dielectric materials like PSi, different mechanism for conduction can dominate at different applied electric field range and at different temperatures. In-fact, all the mechanisms for conduction can occur simultaneously. At lower voltage range (up-to 1.5V), the  $I$  Vs  $V$  characteristic of PSi is observed to be linear, which can be attributed to the process of hopping of carriers, thermally excited between discrete isolated defect states, giving an ohmic conduction region at low field range [218]. Observations on electrical property of PSi suggests that the conductance of PSi is proportional to exponent of  $V^{0.5}$ , which is suggestive of P-F conduction that basically is the electric field induced, thermal excitation of carriers from traps, which is played by numerous defective states present in PSi [218]. In higher electric field region, TAT mechanism predominates the conduction of PSi, which involves two-step trap assisted tunnelling mechanism for conduction of carriers [218]. So the high density of defect states, numerous dangling bonds on PSi surfaces provides hopping sites for charge carriers and thus controls the conduction mechanism of PSi [218].

## 1.3 CALCIUM SENSOR

Mineral ions in suitable concentration is essential for proper maintenance of life functioning. Calcium ion among them plays a very vital role. Calcium ion is the second most abundant ion and plays an essential role in cellular signalling process [211-222]. Moreover calcium regulates numerous cellular processes like skeletal and cardiac muscle excitation, blood coagulation and neurotransmission [223-224]. As stated previously, utility of calcium in the human body and abnormal calcium ion concentration in serum is a clear

indicator of numerous diseases. Increase in serum calcium level or hypercalcemia, primarily indicates hyperthyroidism, hyperparathyroidism but mostly is found in case of malignancies [8]. Association of hypercalcemia with lung cancer is quite common; in fact it is the most prevalent metabolic anomaly accompanying malignancies [8-12]. As stated earlier, the history of calcium sensor dates back to 1987, when W. Melzer and M F Schneider detected by the use of calcium sensor dyes [29, 30]. Later calcium sensor was developed by A. Miyawaki by the use of calmodulin (CaM), a calcium binding enzyme [31]. Since then various calcium detecting techniques were developed like the chromatography technique [32], electrochemical technique [33,34], potentiometric technique [35-37] and spectroscopic techniques [38-41] to name a few. Chromatographic technique includes high performance liquid chromatography for detection of mineral ion in water [31]. A. H. Ismail developed a calcium sensor that works on the principle of altered electrical impedance in supersaturated serum due to aggregation of mineral ions [34]. Rafiq Ahmad developed a highly conducting solution-gated FET sensor that employs CaM for effective calcium sensing [35]. The conductivity of the FET sensor shows remarkable change in conductivity on introduction of calcium ions of different concentration. This solution-gated FET calcium sensor shows an excellent example of potentiometric calcium sensor. Y. C Torres developed a lipophilic photoacid polymer that is capable of active proton exchange with calcium ion when illuminated with photons of wavelength 470nm [41].

Ionic calcium sensing using any transducer naturally requires a calcium receptor as required in case of any analyte for the analyte to be immobilized on the transducer surface. Calsequestrin [219], oligosaccharides [220], Ethylenediamine-tetra-acetic acid (EDTA) [164], cholesteric liquid crystalline polymer with benzoic acid metal binding site and calmodulin (CaM) [35,222, 226, 228] are calcium receiving materials, commonly used for calcium binding to transducers. Out of them CaM is often preferred due to some evident advantages of CaM protein that makes it a popular choice as calcium binder in case of fabrication of calcium biosensors. CaM is prototypical calcium sensing protein [225-228]. Present in all eukaryotic cells, CaM regulates essential cellular processes [225, 226]. Having the capability of calcium detection in

biologically relevant concentration range, CaM also shows additional discrimination towards calcium ions [225-227]. Thus CaM surface functionalized porous silicon structure is effective in calcium binding.

#### **1.4 SCOPE OF WORK**

Finger clubbing being an early symptom for numerous cardio-pulmonary disorders most importantly in case of lung cancer, it requires precise monitoring. The techniques for detection of finger clubbing as discussed in section 1.1.2, are mostly qualitative and some quantitative. As we know, qualitative analysis of phenomena is liable to be erroneous and may be largely prejudiced. Moreover the quantitative techniques discussed for the diagnosis of finger clubbing employs a single parameter for its analysis and in many cases expensive. Single parameter analysis of a phenomenon consists of drawbacks like incapability for detection of minor changes, compromised sensitivity and lack of precision. Inclusion of multiple parameters for diagnosis of finger clubbing enhances considerably the performance, sensitivity and the overall reliability of the technique.

Finger clubbing is not a confirmatory diagnosis parameter for cardio-pulmonary disease hence to build a more confirmatory approach in diagnosis, serum calcium detection is required, and as it is a confirmative indication of several cardio-pulmonary disorders including small cell lung carcinoma, as discussed earlier. Calcium detector techniques discussed in section 1.3 employs complex and expensive instrumentation, requires complex and time consuming fabrication procedures and also most of them depend on single parametric response. As discussed previously single parametric response for a sensor holds certain disadvantages as far as its precision, sensitivity and linearity is concerned. These drawbacks can be done away with when multi-parametric approach is undertaken, hence a considerable reliability and efficient performance can be achieved with multi-parametric detection technique.

Electrical and optical based detection system together is quiet an unprecedented approach towards the development of detection systems. Simple electrical parameters like current versus voltage and capacitance versus

frequency together with optical parameters like reflectance, absorption and scattering loss are simple, cost effective and multi-parametric approach towards the development of detectors. Together with this, Image processing based optical detection system is another field in detection system that is not quiet ventured before. The image of the reflected spot form the incubated sensor surface posses several spectral information that can be easily deciphered by the use of simple software and such information can be utilised for effective detection of optical parameters essential in the sensing process. Thus software based image processing optical sensors together with the analysis of electrical parameters is capable of contributing hugely towards the development and designing of reliable, efficient, simple and cost-effective biosensors.

Section 1.2.2 discussed the classification and types of biosensors used, among them nano-structured and nanopores based biosensors possess certain advantaged that makes them a great choice in the fabrication of biosensors. Their absorption capability owing to their tremendously large surface-area to volume ratio provides enough surfaces for biomolecule absorption and interaction. Certain nano-structured material like carbon and silicon exhibits great biocompatibility. Moreover their quick response time together with other interesting physical, chemical, electrical and optical properties makes them a natural choice for their use in biosensing filed in comparison to other biosensing materials.

## **1.5 OBJECTIVE OF THESIS**

As per the discussion in section 1.4 the objective of the thesis is listed as follows:

- ❖ Designing and development of quantitative and automated finger clubbing monitor capable of precise detection of finger clubbing, that utilizes image processing technique and laser-motor technique, developed in this pretext using MATLAB GUI environment.
- ❖ Fabrication and characterization of sensing platform for calcium detection, capable of detecting calcium in biologically relevant concentration.

- ❖ Verification of the selectivity of the fabricated detector platform towards calcium in presence of other commonly interfering ions by the use of optical and electrical parameters.
- ❖ Optimization of the calcium detecting platform by modulation of fabrication parameters.

## 1.6 THESIS OUTLINE

This work involves a gradual progression towards the development of finger clubbing monitor and the calcium detector that helps in early, precise and conclusive detection of cardio-pulmonary disease, mainly lung cancer. To start with, a substantial review of the existing finger clubbing monitor and a quiet a detailed discussion on biosensors and biosensing materials is provided in **chapter 1**, with emphasis on calcium sensor. In the following chapters the objectives discussed in section 1.5 is gradually and systematically developed.

**Chapter 2** contains the designing and development of automated and quantitative finger clubbing monitor. The monitor uses finger clubbing technique and laser-motor technique for quantitative measurement of profile axis angle and DPD-IPD ratio for accurate detection of finger clubbing.

**Chapter 3** consist of the development and fabrication of porous-silicon (PSi) based calmodulin (CaM) surface functionalized calcium detecting platform and their extensive physical characterization.

**Chapter 4** is used to discuss the sensing parameters of the developed calcium detector and extensively examine its selectivity towards calcium in presence of other interfering monovalent and divalent ions. Alteration of optical and electrical parameters is studied to determine the selectivity of the detector surface.

**Chapter 5** deals with the optimization of the prepared detector surface for better response. The fabrication condition of the PSi based calcium detector, namely the etching time of preparation of PSi is altered to study the change in characteristic electrical and optical response of the detector surface.

**Chapter 6** finally concludes the study and presents any further future scope of work on this topic.

# Reference

- [1] B Malay Sarkar, D. M. Mahesh, and Irappa Madabhavi, "Digital clubbing", *Lung India*, 29(4), pp. 354-362, (2012).
- [2] Kerith E. Spicknall, BA, Matthew J. Zirwas, MD, and Joseph C. English III, MD, "Clubbing: An update on diagnosis, differential diagnosis, pathophysiology, and clinical relevance", *Journal of the American Academy of Dermatology*, 52(6), pp. 1020-1028, (2005).
- [3] Motswaledi MH, Mayayise MC, "Nail changes in systemic diseases", *South African Family Practice*, 52( 5), pp.409-413, (2010).
- [4] X. Vandemergel, B. Rennboog, "Prevalence, aetiologies and significance of clubbing in a department of general internal medicine", *European Journal of Internal Medicine*, 19(5), pp. 325-329, (2008).
- [5] Chun Wai Chan, "Evaluation of digital clubbing", *Australian Family Physician*, 44(3), pp.113-116, (2015).
- [6] Archana Singal, Rahul Arora, "Nail as a window of systemic diseases", *Indian Dermatology online journal*, 6(2), pp. 67-74, (2015).
- [7] Gurcharan Singh, Nayeem Sadath Haneef, Uday A, "Nail changes and disorders among the elderly", *Indian Journal Of Dermatology, Venereology and Leprology*, 71(6 ), pp.386-392, (2005).
- [8] J. Matsumoto, T. Kojima, T. Shimizu, S. Kitashiro, K. Konishi, Y. Matsumura, Y. Kawarada, H. Ikeda, T. Yoshiki, "A Case of Lung Cancer with Hypercalcemia which was Incidentally Complicated with Primary Hyperparathyroidism due to Parathyroid Adenoma," *Ann Thorac Cardiovasc Surg*, vol. 8, no. 3, pp. 151-153, 2002.
- [9] D. Seccareccia, "Cancer-related hypercalcemia," *Can Fam Physician*, vol. 56, no. 3, pp. 244-246, 2010.
- [10] W. Goldner, "Cancer-Related Hypercalcemia," *Journal of Oncology Practice*, vol. 12, no. 5, pp. 426-432, 2016.
- [11] S. Nemr, S. Alluri, D. Sundaramurthy, D. Landry, G. Braden, "Hypercalcemia in Lung Cancer due to Simultaneously Elevated PTHrP and Ectopic Calcitriol Production: First Case Report," *Case Reports in Oncological Medicine*, vol. 2017, pp. 1-3, 2017.
- [12] J. Zagzag, M. I. Hu, S. B. Fisher, N. D. Perrier, "Hypercalcemia and Cancer: Differential Diagnosis and Treatment," *CA: A Cancer Journal for Clinicians*, vol. 68, pp. 377-386, 2018.
- [13] Daniela Husarik, Stephan R. Vavricka, Michael Mark, Andreas Schaffner, Roland B. Walter, "Assessment of digital clubbing in medical inpatients by digital photography and computerised analysis", *Swiss Medical Weekly*, 132, pp.132-138 (2002).
- [14] G. Kitis, H. Thompson, R. H. Allan, "Finger clubbing in inflammatory bowel disease: its prevalence and pathogenesis." *British Medical Journal*, 2(6194), pp. 825-828, (October 1979).
- [15] Dickinson CJ, "Lung disease associated with digital clubbing", *Clin Exp Rheumatol*, 10(7), pp.23-25, (1992).
- [16] R D Djojodibroto, MD, P T Thomas, MD, Kamarudin T Kana, MD, Hla Myint, MBBS, "Finger Clubbing: Do We Require Digital Index Quantitator?", *Med J Malaysia*, 69(2), pp.60-63, (April 2014).
- [17] Kathryn A Mayers, Donald R.E. Farquhar, "Does this patient have clubbing?", *The rational clinical examination*, 286(3), pp. 341-347, (July 18 2001).
- [18] T J Pitts-Tucker, M G Miller, and J M Littlewood, "Finger clubbing in cystic fibrosis", *Archives of Disease in Childhood*, 61, pp. 576-579, (1986).
- [19] R D Djojodibroto, MD, P T Thomas, MD, Kamarudin T Kana, MD, Hla Myint, MBBS, "Finger Clubbing: Do We Require Digital Index Quantitator?", *Med J Malaysia*, 69(2), pp.60-63, (April 2014).
- [20] Bernard Kernath, "Digital clubbing: A sign of underlying disease", *Hospital Physician*, 39(9), pp.25-27, (2003).
- [21] Homagni Sikha Roy, Zhigang Wang, Haitao Ran et.al., "Diagnosis of digital clubbing high-frequency ultrasound imaging". *International Journal of Dermatology*, 52(1), pp. 1-5, (2012).

- [22] James Y. Paton, Daisy B. Bautista, Michael W. Stabile et.al., "Digital clubbing and pulmonary function abnormalities in children with lung disease", *Pediatric pulmonology*, 10(1), pp. 25-29, (1991).
- [23] José da Silva Moreira, Marlene Hass, Ana Luiza Schneider Moreira, James de Freitas Fleck, José de Jesus Peixoto Camargo," Reversal of digital clubbing in surgically treated lung cancer patients", *Jornal Brasileiro de pneumologia*, 34(7), pp. 481-489 (2008).
- [24] S. M. W. Masra1, K. L. Goh, J. S. Henry, M. S. Muhammad, R. D. Djojodibroto and R. Sapawi,"Development of Finger Clubbing Meter", Conference: UNIMAS STEM Engineering Conference 2015, At Kuching, Sarawak, 833, Masra, Masniah. (2015). Development of Finger Clubbing Meter. . 10.4028/www.scientific.net/AMM.833.190.
- [25] Lindsey A. Torre, Freddie Bray, Rebecca L. Siegel et.al., "Global Cancer Statistics ,2012", *A Cancer Journal for Clinicians*, 65(2), pp. 87-108, (2015).
- [26] Donald Bentley, Angela Moore, Harry Shwachman, "Finger clubbing: a quantitative survey by analysis of the shadowgraph ". *The Lancet*, 2(7978), pp. 164-167, (1976).
- [27] IUPAC. Compendium of Chemical Terminology, 2nd ed. (The "Gold Book"). Compiled by A. D. McNaught and A. Wilkinson. Blackwell Scientific Publications, Oxford (1997). Online Version (2019) Created by S. J. Chalk. ISBN 0-9678550-9-8. <http://doi.org/10.1351/goldbook>.
- [28] L. C. Clark, C. Lyons, " Biosensors-A Practical Approach", *Jnr. Ann. NY Acade. Sci* 102 (1962): 29-45.
- [29] W. Melzer, E. Rios, and M. F. Schneider, "a general procedure for determining the rate of calcium release from the sarcoplasmic reticulum in skeletal muscle fibers". *elsevier*, 51 (6), pp. 849-863, (1987).
- [30] M F Schneider, B J Simon, G Szucs, "Depletion of calcium from the sarcoplasmic reticulum during calcium release in frog skeletal muscle". *The journal of physiology*, 392 (1), pp. 167-192, (1987)
- [31] Atsushi Miyawaki, Juan Llopis, Roger Heim, J. Michael McCaffery, Joseph A. Adams, Mitsuhiro Ikura , Roger Y. Tsien, "Fluorescent indicators for  $Ca^{2+}$  based on green fluorescent proteins and calmodulin". *Nature*, 388, pp. 882-887, (1997).
- [32] G. P. Cartoni, F. Coccioli, "Characterization of Mineral Waters by High-performance Liquid Chromatography," *J. Chromatogr. A*, vol. 360, pp. 225-230, 1986.
- [33] M. J. A. Shiddiky, A. A. J. Torriero, "Application of ionic liquids in electrochemical sensing systems," *Biosens. Bioelectron.*, vol. 26, pp. 1775-1787, 2011.
- [34] A. H. Ismail, C. Schafer, A. Heiss, M. Walter, W. Jahnen-Dechent, S. Leonhardt, "An Electrochemical Impedance Spectroscopy (EIS) Assay Measuring the Calcification Inhibition Capacity in Biological Fluids," *Biosens. Bioelectron.*, vol. 26, pp. 4702-4707, 2011.
- [35] R. Ahmad, N. Tripathy, M.S. Ahn, J.Y. Yoo, Y. B. Hahn, "Preparation of a Highly Conductive Seed Layer for Calcium Sensor Fabrication with Enhanced Sensing Performance," *Acs Sensors*, vol. 3, pp. 772-778, 2018.
- [36] S. Y. Lin, S. W. Liu, C. M. Lin, C. H. Chen, "Recognition of Potassium Ion in Water by 15-crown-5 Functionalized Gold Nanoparticles," *Anal. Chem.*, vol. 74, pp. 330-335, 2002.
- [37] P. J. Greenawalt, S. Amemiya, "Voltammetric Mechanism of Multiion Detection with Thin Ionophore-Based Polymeric Membrane," *Anal. Chem.*, vol. 88, pp. 5827-5834, 2016.
- [38] M. Moirangthem, R. Arts, M. Merkx, A. P. H. J. Schenning, "An Optical Sensor Based on a Photonic Polymer Film to Detect Calcium in Serum," *Advanced Functional Materials*, vol. 26, pp. 1154-1160, 2016.
- [39] X. Hun, Z. Zhang, "Preparation of a novel fluorescence nanosensor based on calcein-doped silica nanoparticles, and its application to the determination of calcium in blood serum," *Microchim Acta*, vol. 159, pp. 255-261, 2007.
- [40] H. Buening-Pfaue, "Analysis of Water in Food by Near Infrared Spectroscopy," *Food Chem.*, vol. 82, pp. 107-115, 2003.
- [41] V. K. Johns, P. K. Patel, S. Hassett, P. Calvo-Marzal, Y. Qin, K. Y. Chumbimuni-Torres, "Visible Light Activated Ion Sensing Using a Photoacid Polymer for Calcium Detection," *Anal. Chem.*, vol. 86, pp. 6184-6187, 2014.
- [42] C. Jianrong, M. Yuqing, H. Nongyue, W. Xiaohua, L. Sijiao, " nanotechnology and Biosensors", *Biotechnology advances* 22, no. 7 (2004): 505-518.



- [43] C. J. V. Oss, R. J. Good, M. K. Chaudhury, "Nature of the antigen-antibody interaction: Primary and secondary bonds: optimal conditions for association and dissociation", *Journal of Chromatography B: Biomedical Science and Applications* 376 (1986): 111-119. [https://doi.org/10.1016/S0378-4347\(00\)80828-2](https://doi.org/10.1016/S0378-4347(00)80828-2).
- [44] Nguyen, H.H.; Lee, S.H.; Lee, U.J.; Fermin, C.D.; Kim, M. Immobilized enzymes in biosensors or applications. *Materials* 2019, 12, 121. [CrossRef]
- [45] Shukla, S.K.; Govender, P.P.; Tiwari, A. Polymeric micellar structures for biosensor technology. In *Advances in Biomembranes and Lipid Self Assembly*, 1st ed.; Iglic, A., Kulkarni, C.V., Rappolt, M., Eds.; Academic Press: Cambridge, MA, USA, 2016; pp. 143–161.
- [46] Morrison, D.W.; Dokmeci, M.R.; Demirci, U.; Khademhosseini, A. *Clinical Applications of Micro- and Nanoscale Biosensors*; John Wiley & Sons, Inc.: Hoboken, NJ, USA, 2007.
- [47] Justino, C.I.L.; Freitas, A.C.; Pereira, R.; Duarte, A.C.; Santos, T.A.P.R. Recent developments in recognition elements for chemical sensors and biosensors. *Trends Anal. Chem.* 2015, 68, 2. [CrossRef]
- [48] Lim, S.A.; Ahmed, M.U. Introduction to food biosensors. In *Food Chemistry, Function and Analysis*, 1st ed.; Ahmed, M.U., Zourob, M., Tamiya, E., Eds.; Royal Society of Chemistry: Cambridge, UK, 2016; pp. 1–21.
- [49] Perumal, V.; Hasim, U. *Advances in biosensors: Principle, architecture and applications*. *J. Appl. Biomed.* 2014, 12, 1–15. [CrossRef]
- [50] Liu, H.; Ge, J.; Ma, E.; Yang, L. Advanced biomaterials for biosensor and the nanostics. In *Biomaterials in Translational Medicine*, 1st ed.; Yang, L., Bhaduri, S., Webster, T., Eds.; Academic Press: Cambridge, MA, USA, 2019; pp. 213–255.
- [51] Cordeiro, C.A.; Sias, A.; Koster, T.; Weterink, B.H.C.; Cremers, T.I.F.H. In vivo "real-time" monitoring of glucose in the brain with an amperometric enzyme-based biosensor based on gold coated tungsten (W-Au) microelectrodes. *Sens. Actuators B Chem.* 2018, 263, 605–613. [CrossRef]
- [52] Ondes, B.; Akpinar, F.; Uygur, M.; Muti, M.; Uygur, D.A. High stability potentiometric urea biosensor based on enzyme attached nanoparticles. *Microchem. J.* 2021, 160, 105667. [CrossRef]
- [53] Schroeder, W.H.; Cavacini, L. Structure and function of immunoglobulins. *J. Allergy Clin. Immunol.* 2010, 125, S41–S52. [CrossRef]
- [54] Lim, S.A.; Ahmed, M.U. Electrochemical immuno sensors and their recent nanomaterial-based signal amplification strategies: A review. *RSC Adv.* 2016, 6, 24995–25014. [CrossRef]
- [55] Lim, S.A.; Ahmed, M.U. Introduction to immunosensors. In *Detection Science*; Ahmed, M.U., Zourob, M., Tamiya, E., Eds.; Royal Society of Chemistry: Cambridge, UK, 2019; pp. 1–20.
- [56] Tombelli, S.; Minunni, M.; Mascini, M. Analytical applications of aptamers. *Biosens. Bioelectron.* 2005, 20, 2424–2434. [CrossRef]
- [57] Dhiman, A.; Kalra, P.; Bansal, V.; Bruno, J.G.; Sharma, T.K. Aptamer-based point-of-care diagnostic platforms. *Sens. Actuators B Chem.* 2017, 246, 535–553. [CrossRef]
- [58] Hong, P.; Li, W.; Li, J. Applications of aptasensors in clinical diagnostics. *Sensors* 2012, 12, 1181–1193. [CrossRef]
- [59] Kumar, A.; Malinee, M.; Dhiman, A.; Kumar, A.; Sharma, T.K. Aptamer technology for the detection of food born pathogens and toxins. In *Advanced Biosensors for Health Care Applications*, 1st ed.; Inamuddin, R.K., Mohammad, A., Asiri, A., Eds.; Elsevier: Cambridge, MA, USA, 2019; pp. 45–69.
- [60] Gui, Q.; Lawson, T.; Shan, S.; Yan, L.; Liu, Y. The application of whole-cell-based biosensors for use in environmental analysis and in medical diagnostics. *Sensors* 2017, 17, 1623. [CrossRef]
- [61] Kyllis, N.; Riangrunroj, P.; Lai, H.-E.; Salema, V.; Fernández, L.F.; Stan, G.-B.V.; Freemont, P.S.; Polizzi, K.M. Whole-cell biosensor with tunable limit of detection enables low-cost agglutination assays for medical diagnostic applications. *ACS Sensors* 2019, 4, 370–378. [CrossRef] [PubMed]
- [62] Ron, E.Z.; Rishpon, J. Electrochemical cell based sensors. *Adv. Biochem. Eng. Biotechnol.* 2010, 117, 77–84.

- [63] Berepiki, A.; Kent, R.; Machado, L.F.M.; Dixon, N. Development of high-performance whole-cell biosensors aided by statistical modeling. *ACS Synth. Biol.* 2020, 9, 576–589. [CrossRef]
- [64] Galvez, A.Z.; Narvaez, E.M.; Martinez, C.C.M.; Merkoci, A. Nanomaterials connected to antibodies and molecularly imprinted polymers as bio/receptors for bio/sensor applications. *Appl. Mater. Today* 2017, 9, 387–401. [CrossRef]
- [65] Singh, K.R.B.; Nayak, V.; Sarkar, T.; Singh, R.P. Cerium oxide nano particles: Properties, biosynthesis and biomedical application. *RSC Adv.* 2020, 10, 27194–27214. [CrossRef]
- [66] Arya, A.; Gangwar, A.; Kumar, A. Biosensors in animal biotechnology. In *Nanotechnology in Modern Animal Biotechnology: Concepts and Applications*, 1st ed.; Maurya, P.K., Singh, S., Eds.; Elsevier: Cambridge, MA, USA, 2019; pp. 75–95.
- [67] Martinkova, P.; Kostelnik, A.; Valek, T.; Pohanka, M. Main trends in the construction of biosensors and their applications. *Int. J. Electrochem. Sci.* 2017, 12, 7386–7403. [CrossRef]
- [68] Nguyen, H.H.; Kim, M. An Overview of techniques in enzyme immobilization. *Appl. Sci. Conver. Technol.* 2017, 26, 157–163. [CrossRef]
- [69] Sassolas, A.; Blum, L.J.; Leca Bouvier, B.D. Immobilization strategies to develop enzymatic biosensors. *Biotechnol. Adv.* 2012, 30, 489–511. [CrossRef] [PubMed]
- [70] Sneha, H.P.; Beulah, K.C.; Murthy, P.S. Enzyme immobilization methods and applications in the food industry. In *Enzymes in Food Biotechnology*, 1st ed.; Kuddus, M., Ed.; Academic Press: London, UK, 2019; pp. 645–658.
- [71] V. Naresh, N. Lee, “A Review on Biosensors and recent Development of Nanostructured Materials-Enabled Biosensors”. *Sensors*, vol. 21, no. 1109, 2021. <https://doi.org/10.3390/s21041109>.
- [72] Malhotra, B.D.; Ali, M.A. Nano materials in biosensors: Fundamentals and applications. In *Nanomaterials for Biosensors*, 1st ed.; Malhotra, B.D., Ali, M.A., Eds.; Elsevier: Cambridge, MA, USA, 2017; pp. 1–73.
- [73] Shanker, A.; Lee, K.; Kim, J. Synthetic hybrid biosensors. In *Encyclopedia of Molecular Cell Biology and Molecular Medicine*, 2nd ed.; Meyers, R.A., Ed.; Wiley-VCH Verlag GmbH & Co. KGaA: Weinheim, Germany, 2014; pp. 1–36.
- [74] Grieshaber, D.; MacKenzie, R.; Janos Vörös, J.; Reimhult, E. Electrochemical biosensors—Sensor principles and architectures. *Sensors* 2008, 8, 1400–1458. [CrossRef]
- [75] Dzyadevych, S.; Renault, N.J. Conductometric biosensors. In *Biological Identification*, 1st ed.; Schaudies, R.P., Ed. Elsevier: Cambridge, MA, USA, 2014; pp. 153–193.
- [76] Chaubey, A.; Malhotra, B.D. Mediated biosensors. *Biosens. Bioelectron.* 2002, 17, 441–456. [CrossRef]
- [77] Pisoschi, A.M. Potentiometric biosensors: Concept and analytical applications—An editorial. *Biochem. Anal. Biochem.* 2016, 5, 19–20. [CrossRef]
- [78] Radhakrishnan, R.; Suni, I.I.; Bever, C.S.; Hammock, B.D. Impedance biosensors: Applications to sustainability and remaining technical challenges. *ACS Sustain. Chem. Eng.* 2014, 2, 1649–1655.
- [79] Borgmann, S.; Schulte, A.; Neugebauer, S.; Schuhmann, W. Amperometric biosensors. In *Advances in Electrochemical Science and Engineering*, 1st ed.; Alkire, R.C., Kolb, D.M., Jacek Lipkowski, J., Eds.; Wiley-VCH Verlag GmbH & Co. KGaA: Weinheim, Germany, 2011; pp. 1–84.
- [80] Alaejos, M.S.; Montelongo, F.J.G. Application of amperometric biosensors to the determination of vitamins and  $\alpha$ -amino acids. *Chem. Rev.* 2004, 104, 3239–3266.
- [81] Touhami, A. Biosensors and nanobiosensors: Design and applications. In *Nanomedicine*, 1st ed.; Seifalian, A., De Mel, A., Kalaskar, D.M., Eds.; One Central Press: Cheshire, UK, 2014; pp. 374–403.
- [82] Lazcka, O.; Campo, F.J.D.; Munoz, F.X. Pathogen detection: A perspective of traditional methods and biosensors. *Biosens. Bioelectron.* 2007, 22, 1205–1217. [CrossRef] [PubMed]
- [83] Chen, C.; Wang, J. Optical biosensors: An exhaustive and comprehensive review. *Analyst* 2020, 145, 1605–1628.

- [84] Dippel, A.B.; Anderson, W.A.; Evans, R.S.; Deutsch, S.; Hammond, M.C. Chemiluminescent biosensors for detection of second messenger cyclic di-GMP. *ACS Chem. Biol.* 2018, 13, 1872–1879.
- [85] Luo, M.; Chen, X.; Zhou, G.; Xiang, X.; Chen, L.; Jia, X.; He, Z. Chemiluminescence biosensors for DNA detection using graphene oxide and a horse radish peroxidase-mimicking DNAzyme. *Chem. Commun.* 2012, 48, 1126–1128. [CrossRef]
- [86] Solaimuthu, A.; Vijayan, A.N.; Murali, P.; Korrapati, P.S. Nano-biosensors and their relevance in tissue engineering. *Curr. Opin. Biomed. Eng.* 2020, 13, 84–93. [CrossRef]
- [87] Damborsky, P.; Svitel, J.; Katrlík, J. Optical biosensors. *Essays Biochem.* 2016, 60, 91–100.
- [88] Zandieh, M.; Hosseini, S.N.; Vossoughi, M.; Khatami, M.; Abbasian, S.; Moshaii, A. Label-free and simple detection of endotoxins using a sensitive LSPR biosensor based on silver nano columns. *Anal. Biochem.* 2018, 548, 96–101.
- [89] Demchenko, A.P. Fluorescence detection techniques. In *Introduction to Fluorescence Sensing*, 1st ed.; Springer: Dordrecht, Netherlands, 2009; pp. 65–118.
- [90] Srivastava, K.R.; Awasthi, S.; Mishra, P.K.; Srivastava, P.K. Biosensors/molecular tools for detection of waterborne pathogens. In *Waterborne Pathogens: Detection and Treatment*, 1st ed.; Prasad, M.N.V., Grobelak, A., Eds.; Butterworth-Heinemann: Cambridge, MA, USA, 2020; pp. 237–277.
- [91] Leung, A.; Shankar, P.M.; Mutharasan, R. A review of fiber-optic biosensors. *Sens. Actuators B Chem.* 2007, 125, 688–703. [CrossRef]
- [92] Monk, D.J.; Walt, D.R. Optical fiber-based biosensors. *Anal. Bioanal. Chem.* 2004, 379, 931–945.
- [93] D. Basu, T. Sarkar, K. Sen, S. M. Hossain, J. Das, “Multi-parametric Optical Glucose Sensor based on Surface Functionalized nano-Porous Silicon,” *IEEE Sensors Journal*, vol. 18, no. 24, 2018.
- [94] T. Sarkar, D. Basu, N. Mukherjee, J. Das, “Comparison of Glucose Sensitivity of Nano and Macro Porous Silicon,” *Materials today proceedings*, vol. 5, no. 3, pp. 9798–9803, 2018.
- [95] Presnova, G.; Presnov, D.; Krupenin, V.; Grigorenko, V.; Trifonov, A.; Andreeva, I.; Ignatenko, O.; Egorov, A.; Rubtsova, M. Biosensor based on a silicon nano wire field-effect transistor functionalized by gold nanoparticles for the highly sensitive determination of prostate specific antigen. *Biosens. Bioelectron.* 2017, 88, 283–289. [CrossRef] [PubMed]
- [96] Zhang, G.J.; Zhang, L.; Huang, M.J.; Luo, Z.H.H.; Tay, G.K.I.; Lim, E.J.A.; Kang, T.G.; Chen, Y. Silicon nanowire biosensor for highly sensitive and rapid detection of dengue virus. *Sens. Actuators B Chem.* 2010, 146, 138–144. [CrossRef]
- [97] Makowski, M.S.; Ivanisevic, A. Molecular analysis of blood with micro-/nanoscale field-effect transistor biosensors. *Small* 2011, 7, 1863–1875. [CrossRef] [PubMed]
- [98] Chalklen, T.; Jing, Q.; Kar Narayan, S. Biosensors Based on Mechanical and electrical detection techniques. *Sensors* 2020, 20, 5605. [CrossRef]
- [99] Estrela, P.; Stewart, A.G.; Yan, F.; Migliorato, P. Field effect detection of biomolecular interactions. *Electrochim. Acta* 2005, 50, 4995–5000.
- [100] Fogel, R.; Limson, J.; Seshis, A.A. Acoustic biosensors. *Essays Biochem.* 2016, 60, 101–110.
- [101] Skladal, P. Piezo electric biosensors. *TrAC Trends Anal. Chem.* 2016, 79, 127–133. [CrossRef]
- [102] Su, L.; Zou, L.; Fong, C.C.; Wong, W.L.; Wei, F.; Wong, K.Y.; Wu, R.S.S.; Yang, M. Detection of cancer biomarkers by piezoelectric biosensor using PZT ceramic resonator as the transducer. *Biosens. Bioelectron.* 2013, 46, 155–161.
- [103] Griffiths, D.; Hall, G. Biosensors What real progress is being made? *Trends Biotechnol.* 1993, 11, 122–130.
- [104] Länge, K.; Bastian, E.; Rapp, B.E.; Rapp, M. Surface acoustic wave biosensors: A review. *Anal. Bioanal. Chem.* 2008, 391, 1509–1519.
- [105] Gopinath, S.C.B.; Lakshmipriya, T. An introduction to biosensors and biomolecules. In *Nanobiosensors for Biomolecular Targeting*, 1st ed.; Gopinath, S.C.B., Lakshmipriya, T., Eds.; Elsevier: Cambridge, MA, USA, 2019; pp. 1–17.
- [106] Yakovleva, M.; Bhand, S.; Danielsson, B. The enzyme thermistor A realistic biosensor concept. A critical review. *Anal. Chim. Acta* 2013, 766, 1–12. [CrossRef]
- [107] Ramanathan, K.; Danielsson, B. Principles and applications of thermal biosensors. *Biosens. Bioelectron.* 2001, 16, 417–423. [CrossRef]

- [108] Xie,B.;Danielsson,B.Thermal biosensors and microbiosensor techniques. In Handbook of Biosensors and Biochips, 1sted.;Marks,R.S., Cullen,D.C. ,Karube,I., Lowe,C.R.,Weetall,H.H.,Eds.;JohnWiley&Sons:NewJersey,NJ,USA,2007;Volume2,pp .1–19.
- [109] Vasuki,S.;Varsha,V.;Mithra,R.;Dharshni,R.A.;Abinaya,S.;Dharshini,R.D.;Sivar ajasekar,N.Thermal biosensors and their applications .Am.Int. J.Res. Sci.Tech.Eng.Math.2019,262–264.
- [110] Danielsson,B.Calorimetric biosensors.Biochem.Soc.Trans.1991,19,26–28.
- [111] Cali,K.;Tuccori,E.;Persaud,K.C.Gravimetric biosensors. Methods Enzymol. 2020, 642, 435–468.[PubMed]
- [112] Walton,P.W.;O’Flaherty,M.R.;Butler,M.E.;Compton,P.Gravimetric biosensors based on acoustic waves in thin polymer films. Biosens.Bioelectron.1993, 8,401–407.
- [113] Lim, J.Y.; Lee, S.S. Sensitive detection of microRNA using QCM biosensors: Sandwich hybridization and signal amplification byTiO<sub>2</sub>nanoparticles.Anal.Methods2020,12,5103–5109.[CrossRef]
- [114] Grimes,C.A.;Roy,S.C.;Rani,S.;Cai,Q.Theory,instrumentation and applications of magnetoelastic resonance sensors: A review. Sensors2011,11,2809–2844.
- [115] Dolez,P.Nanomaterials definitions, classifications, and applications. In Nano engineering,1sted.;Dolez,P.,Ed.;Elsevier:Cambridge,MA,USA,2015;pp.3–40.
- [116] Khan,F.A.Nanomaterials:Types,classifications,andsources.In Applications of Nanomaterials in Human Health,1sted.;Khan,F.,Ed.;Springer:Singapore,2020;pp.1–13.
- [117] Karim,R.A.;Reda,Y.;Fattah,A.A.Review—Nanostructured materials-based nanosensors. J.Electrochem. Soc.2020,167,037554.
- [118] Vanden Berg,B.; Wain,R. ;Dobson,C.M.; Ellis,R.J. Macro molecular crowding perturbs protein refolding kinetics: Implications for protein folding inside the cell.EMBOJ.2000, 19, 3870–3875.[CrossRef] [PubMed]
- [119] Maduraiveeran,G.;Sasidharan,M.;Ganesan,V.Electrochemical sensor and biosensor platforms based on advanced nanomaterials for biological and biomedical applications. Biosens.Bioelectron.2018,103,113–129.
- [120] Li,Y.;Schluesener,H.J.;Xu,S.Goldnanoparticle-based biosensors .GoldBull. 2010, 43, 29–41.[CrossRef]
- [121] Vidotti,M.;Carvalho,R.F.;Mendes,R.K.;Ferreira,D.C.M.;Kubota,L.T.Biosensors based on gold nanostructures.J.Braz.Chem.Soc.2011,22,3–20.
- [122] Pandit, S.; Dassgupta,D.; Dewan, N.;Ahmed, P. Nanotechnology-based biosensors and its application.Pharm.Innov.J.2016, 5,18–25.
- [123] Vashist,S.K.;Venkatesh,A.G.;Mitsakakis,K.;Czilwik,G.;Roth,G.;VonStetten,F.;Zeng erle,R.Nanotechnology based biosensors and diagnostics: Technology push versus industrial / health care requirements .Bionanoscience2012,2,115–126.
- [124] Ma,F.;Li,C.C.;Zhang,C.Y.Development of quantum dot-based biosensors: Principles and applications.J.Mater.Chem.B2018, 6,6173–6190.
- [125] Kim, H.M.;Park, J.H.;Lee, S.K. Fiber optic sensor based on ZnO nanowires decorated by Au nanoparticles for improved plasmonic biosensor.Sci.Rep.2019,9,15605.
- [126] Ramanathan,K.;Bangar,M.A.;Yun,M.;Chen,W.;Myung,N.V.;Mulchandani,A.Bi o affinity sensing using biologically functionalized conducting polymer nanowire.J.Am.Chem.Soc.2005,127,496–497.
- [127] Patolsky,F.;Zheng,G.;Lieber,C.M.Nanowire-based biosensors. Anal. Chem. 2006, 78, 4260–4269.
- [128] Cao,J.;Sun,T.;Grattan,K.T.V.Goldnanorod-based localized surface plasmonresonanc ebiosensors:Areview.Sens.ActuatorsB Chem.2014,195,332–351.
- [129] Ibupoto,Z.H.;Ali,S.M.U.;Khun,L.;Chey,C.O.;Nur,O.;Willander,M.ZnOnanor ods based enzymatic biosensor for selective determination of penicill in. Biosensors2011,1,153–163.
- [130] Liu,G.;Feng,D.Q.;Qian,Y.;Wang,W.;Zhu,J.J. Construction of FRET biosensor for off-on detection of lead ions based on carbon dots and gold nanorods. Talanta 2019,201,90–95.
- [131] Singh,R.P. Prospects of nano biomaterials for biosensing. Int. J. Electrochem. 2011, 2011, 125487.

- [132] Simon, J.; Flahaut, E.; Golzio, M. Overview of carbon nanotubes for biomedical applications. *Materials* 2019, 12, 624.
- [133] Sireesha, M.; Babu, J. V.; Kiran, A. S. K.; Ramakrishna, S. A review on carbon nanotubes in biosensors or devices and their applications in medicine. *Nanocomposites* 2018, 4, 36–57.
- [134] Luo, X.; Shi, W.; Yu, H.; Xie, Z.; Li, K.; Cui, Y. Wearable carbon nano tube-based biosensors on gloves for lactate. *Sensors* 2018, 18, 3398.
- [135] Janssen, J.; Lambeta, M.; White, P.; Byagowi, A. Carbon nano tube-based electrochemical biosensor for label-free protein detection. *Biosensors* 2019, 9, 144.
- [136] Xiaowu Tang, X.; Bansaruntip, S.; Nakayama, N.; Yenilmez, E.; Chang, Y. L.; Wang, Q. Carbon nano tube DNA sensor and sensing mechanism. *NanoLett.* 2006, 6, 1632–1636.
- [137] Kim, B.; Lee, J.; Namgung, S.; Kim, J.; Park, J. Y.; Lee, M. S.; Hong, S. DNA sensors based on CNT-FET with floating electrodes. *Sens. Actuators B Chem.* 2012, 169, 182–187.
- [138] Lee, B. Y.; Seo, S. M.; Lee, D. J.; Lee, M.; Lee, J.; Cheon, J. H.; Cho, E.; Lee, H.; Chung, I. Y.; Park, Y. J.; et al. Biosensor system-on-a-chip including CMOS-based signal processing circuits and 64 carbon nanotube-based sensors for the detection of a neurotransmitter. *Lab Chip* 2010, 10, 894–898.
- [139] Abbasi, E.; Aval, S. F.; Akbarzadeh, A.; Milani, M.; Nasrabadi, H. T.; Joo, S. W.; Hanifehpour, Y.; Koshki, K. N.; Asl, R. P. Dendrimers: Synthesis, applications, and properties. *Nanoscale Res. Lett.* 2014, 9, 247.
- [140] Zheng, Y.; Li, S.; Weng, Z.; Gao, C. Hyperbranched polymers: Advances for synthesis and applications. *Chem. Soc. Rev.* 2015, 44, 4091–4130.
- [141] Yanez, C. S.; Rodriguez, C. C. Dendrimers: Amazing platform for bioactive molecule delivery system. *Materials* 2020, 13, 570.
- [142] Satija, J.; Sai, V. V. R.; Muherji, S. Dendrimers in biosensors: Concept and applications. *J. Mater. Chem.* 2011, 21, 14367–14386.
- [143] Caminade, A. M.; Turrin, C. O. Dendrimers for drug delivery. *J. Mater. Chem. B* 2014, 2, 4055–4066.
- [144] A. Uhler, I. Uhler, “Historical perspective on discovery of Porous Silicon”, *Physic Status Solidi C Current Topics*, no. 9, pp. 3185–3187. 2005. DOI: 3185-3187/pssc.200461100.
- [145] L. T. Canham, “Silicon quantum wire array fabrication by electrochemical and chemical dissolution of wafers”, *Applied Physics letters*, vol. 57, no. 10, pp. 1046–1048, 1990.
- [146] H. A. Hadi, T. H. Abood, A. T. Mohi, M. S. Karim, “Impact of the etching time and current density on Capacitance-Voltage characteristics of P-type of porous silicon,” *World Scientific News*, vol. 67, no. 2, pp. 149–160, 2017.
- [147] M. J. Hussein, W. M. M. Yunus, H. M. Kamari, A. Zakaria, H. F. Oleiw, “Effect of current density and etching time on photoluminescence and energy band gap of p-type porous silicon,” *optical and quantum electronics*, vol. 48, no. 194, pp. 2–8, 2016.
- [148] M. H. F. Suhaimi, M. Rusop, S. Abdullah, “Porosity and thickness effect of porous silicon layer on photoluminescence spectra,” *International Conference on Technology, Informatics, Management, Engineering & Environment*, 2013.
- [149] A. Mortezaali, S. R. Sani, F. J. Jooni, “Correlation between porosity of porous silicon and optoelectronic properties,” vol. 1, no. 3, pp. 293–299, 2009.
- [150] S. J. Kim, B. H. Jeon, K. S. Choi, N. K. Min, “Capacitive porous silicon sensors for measurement of low alcohol gas concentration at room temperature,” *J Solid State Electrochem*, vol. 4, pp. 363–366, 2000.
- [151] D. Basu, T. Sarkar, K. Sen, S. M. Hossain, J. Das, “Multi-parametric Optical Glucose Sensor based on Surface Functionalized nano-Porous Silicon,” *IEEE Sensors Journal*, vol. 18, no. 24, 2018.
- [152] R. C. Anderson, R. S. Muller, C. W. Tobias, “Investigations of the Electrical Properties of Porous Silicon,” *J. Electrochem. Soc.*, vol. 138, no. 11, pp. 3406–3411, 1991.
- [153] H. Saha, S. K. Dutta, S. M. Hossain, S. Chakarborty, A. Saha, “Mechanism and Control of Formation of Porous Silicon on p-Type Si,” *Bull. Mater. Sci.*, vol. 21, no. 3, pp. 195–201, 1998.

- [154] T. Sarkar, D. Basu, N. Mukherjee, J. Das, "Comparison of Glucose Sensitivity of Nano and Macro Porous Silicon," *Materials today proceedings.*, vol. 5, no. 3, pp. 9798-9803, 2018.
- [155] X. Yang, F. Xi, X. Chen, S. Li, X. Wan, W. Ma, P. Dong, J. Duan, Y. Chang, "Porous Silicon Fabrication and Surface Cracking Behavior Research Based on Anodic Electrochemical Etching," *FUEL CELLS* 00, vol. 0000, no. 0, pp. 1-6, 2020.
- [156] H. Foell, M. Christophersen, J. Carstensen, G. Hasse, "Formation and Application of Porous Silicon," *Materials Science and Engineering R Reports*, vol. 39, no. 4, pp. 93-141, 2002.
- [157] P. Sarafis, E. Hourdakakis, A. G. Nassiopoulou, "Dielectric Permittivity of Porous Si for Use as Substrate Material in Si-Integrated RF Devices," *IEEE transactions on electron devices*, vol. 60, no. 4, pp. 1436-1443, 2013.
- [158] F. A. Harraz, A. A. Ismail, M. Faisal, S. A. Al-Hajry, M. S. Al-Assiri, "Organic analytes sensitivity in meso-porous silicon electrical sensor with frontside and backside contact," *Arabian Journal of Chemistry*, DOI: <http://dx.doi.org/10.1016/j.arabjc.2017.05.015>, 2017.
- [159] F. A. Harraz, "Porous Silicon Chemical Sensor and Bio Sensor: A Review," *Sensors and Actuators B: Chemical*, vol. 202, pp. 897-912, 2014.
- [160] E. A. Kabaa, S. A. Abdulateef, N. M. Ahmed, Z. Hassan, F. A. Sabah, "A Novel Porous Silicon Multi-ions Selective Electrode Based Extended Field Effect Transistor for Sodium, Potassium, Calcium and Magnesium Sensor," *Applied Physics AMaterial Science and Processing*, vol. 125, no. 753, 2019.
- [161] G. N. Tovar, D. R. García, A. W. Arce, G. Palestino, S. R. Mendoza, "Mesoporous Silicon Particles Favor the Induction of Long-Lived Humoral Responses in Mice to a Peptide-Based Vaccine," *Materials*, vol. 11, no. 1083, 2018.
- [162] Y. M. Spivak, S. V. Mjakin, V. A. Moshnikov, M. F. Panov, A. O. Belorus, A. A. Bobkov, "Surface Functionality Features of Porous Silicon Prepared and Treated in Different Conditions," *Journal of Nanomaterials*, vol. 2016, DOI: <http://dx.doi.org/10.1155/2016/2629582>, 2016.
- [163] Z. Gaburro, N. Dalldossoh, L. Pavasi, "Porous Silicon", *Encyclopedia of Condensed Matter Physics*, Elsevier, pp. 391-401, 2005.
- [164] P. Kumar, P. Huber, "Effect of Etching Parameter on Pore Size and Porosity of Electrochemically Formed Nanoporous Silicon," *Journal of Nanomaterials*, vol. 2007, DOI: 10.1155/2007/89718, 2007.
- [165] A. Ramizy, I. M. Ibrahim, M. A. Hammadi, "The Effect of Etching Current Density on Porous Silicon Fabricated by Electrochemical Etching Process," *International Journal of Scientific & Engineering Research*, vol. 7, no. 4, pp. 717-722, 2016.
- [166] C. Baratto, G. Faglia, E. Comini, G. Sberveglieri, A. Taroni, V. L. Ferrara, L. Quercia, G. D. Francia, "A novel Porous Silicon sensor for detection of sub-ppm NO<sub>2</sub> concentrations", *sensors and actuators B*, vol. 77, pp. 62-63, 2001.
- [167] C. Barillaro, A. Nannini, F. Pieri, "APSFET: a new, Porous Silicon based gas sensing device", *Sensors and Actuators B*, vol. 93(1-3), pp. 263-270, 2003.
- [168] P. A. Snow, E. K. Squire, P. St. J. Russell, L. T. Canham, "Vapour sensing using the optical properties of porous silicon bragg's mirror", *Journal of Applied Physics*, vol. 86, pp. 1781-1784, 1999.
- [169] Z. M. Rittersman, A. Splinter, A. Bodecker, W. Benecke, "A novel surface micromachined capacitive porous silicon humidity sensor", *Sensors and Actuators B*, vol. 68, pp. 210-217, 2000.
- [170] J. Das, S. M. Hossain, S. Chakraborty, H. Saha, "Role of parasitic in humidity sensing by porous silicon", *Sensors and Actuators A*, vol. 94, pp. 44-52, 2001.
- [171] M. Archer, M. Christopherson, P. M. Fauchet, "Electrical porous silicon chemical sensor for detection of organic solvents", *Sensors and Actuators B: chemical*, vol. 106(1), pp. 347-357, 2005.
- [172] P. N. Patel, V. Mishra, A. K. "Nano porous silicon microcavity optical biosensor device for glucose detection", *Digest journal of nanomaterials and biosensors*, vol. 7(3), pp. 973-982, 2012.
- [173] M. Aeche, P. M. Fauchet, "Electrical sensing of DNA hybridized in porous silicon layers", *Physica Status Solidi (A)*, vol. 198(2), pp. 503-507, 2003.

- [174] H. A. Hadi, T. H. Abood, A. T. Mohi, M. S. Karim, "Impact of the etching time and current density on Capacitance-Voltage characteristics of P-type of porous silicon," *World Scientific News*, vol. 67, no. 2, pp. 149-160, 2017.
- [175] M. J. Hussein, W. M. M. Yunus, H. M. Kamari, A. Zakaria, H. F. Oleiw, "Effect of current density and etching time on photoluminescence and energy band gap of p-type porous silicon," *optical and quantum electronics*, vol. 48, no. 194, pp.2-8, 2016.
- [176] M. H. F. Suhaimi, M. Rusop, S. Abdullah, "Porosity and thickness effect of porous silicon layer on photoluminescence spectra," *International Conference on Technology, Informatics, Management, Engineering & Environment*, 2013.
- [177] A. Mortezaali, S. R. Sani, F. J. Jooni, "Correlation between porosity of porous silicon and optoelectronic properties," vol. 1, no. 3, pp. 293-299, 2009.
- [178] S. J. Kim, B. H. Jeon, K. S. Choi, N. K. Min, "Capacitive porous silicon sensors for measurement of low alcohol gas concentration at room temperature," *J Solid State Electrochem*, vol. 4, pp. 363-366, 2000.
- [179] D. Basu, T. Sarkar, K. Sen, S. M. Hossain, J. Das, "Multi-parametric Optical Glucose Sensor based on Surface Functionalized nano-Porous Silicon," *IEEE Sensors Journal*, vol. 18, no. 24, 2018.
- [180] R. C. Anderson, R. S. Muller, C. W. Tobias, "Investigations of the Electrical Properties of Porous Silicon," *J. Electrochem. Soc.*, vol. 138, no. 11, pp. 3406-3411, 1991.
- [181] H. Saha, S. K. Dutta, S. M. Hossain, S. Chakarborty, A. Saha, "Mechanism and Control of Formation of Porous Silicon on p- Type Si," *Bull. Mater. Sci.*, vol. 21, no. 3, pp. 195-201, 1998.
- [182] T. Sarkar, D. Basu, N. Mukherjee, J. Das, "Comparison of Glucose Sensitivity of Nano and Macro Porous Silicon," *Materials today proceedings.*, vol. 5, no. 3, pp. 9798-9803, 2018.
- [183] X. Yang, F. Xi, X. Chen, S. Li1, X.Wan, W.Ma, P. Dong, J. Duan, Y. Chang, "Porous Silicon Fabrication and Surface Cracking Behavior Research Based on Anodic Electrochemical Etching," *FUEL CELLS 00*, vol.0000, no. 0, pp. 1-6, 2020.
- [184] H. Foell, M. Christophersen, J. Carstensen, G. Hasse, "Formation and Application of Porous Silicon," *Materials Science and Engineering R Reports*, vol. 39, no. 4, pp. 93-141, 2002.
- [185] P. Sarafis, E. Hourdakis, A. G. Nassiopoulou, "Dielectric Permittivity of Porous Si for Use as Substrate Material in Si-Integrated RF Devices," *IEEE transactions on electron devices*, vol. 60, no. 4, pp. 1436-1443, 2013.
- [186] F. A. Harraz, A. A. Ismail, M. Faisal, S. A. Al-Hajry, M. S. Al-Assiri, "Organic analytes sensitivity in meso-porous silicon electrical sensor with frontside and backside contact," *Arabian Journal of Chemistry*, DOI: <http://dx.doi.org/10.1016/j.arabjc.2017.05.015>, 2017.
- [187] F. A. Harraz, "Porous Silicon Chemical Sensor and Bio Sensor: A Review," *Sensors and Actuators B:Chemical*, vol. 202, pp. 897-912, 2014.
- [188] E. A. Kabaa, S. A. Abdulateef, N. M. Ahmed, Z. Hassan, F. A. Sabah, "A Novel Porous Silicon Multi-ions Selective Electrode Based Extended Field Effect Transistor for Sodium, Potassium, Calcium and Magnesium Sensor," *Applied Physics AMterial Science and Processing*, vol. 125, no. 753, 2019.
- [189] G. N. Tovar, D. R. García, A. W. Arce, G. Palestino, S. R. Mendoza, "Mesoporous Silicon Particles Favor the Induction of Long-Lived Humoral Responses in Mice to a Peptide-Based Vaccine," *Materials*, vol. 11, no. 1083, 2018.
- [190] Y. M. Spivak, S. V. Mjakin, V. A. Moshnikov, M. F. Panov, A. O. Belorus, A. A. Bobkov, "Surface Functionality Features of Porous Silicon Prepared and Treated in Different Conditions," *Journal of Nanomaterials*, vol. 2016, DOI: <http://dx.doi.org/10.1155/2016/2629582>, 2016.
- [191] S. Jang, "Chemical and Physical Properties of Porous Silicon", *Journal of Chosun Natural Science*, vol. 4, no. 1, pp. 1-6, 2011.
- [192] Y. Arita, K. Kato, and T. Sudo, "The n+-IPOS scheme and its applications to IC's", *IEEE T. Electron Dev.*, Vol. 24, p. 757, 1977.
- [193] T. Unagami and K. Kato, "Study of the Injection Type IPOS Scheme", *Jpn. J. Appl. Phys.*, Vol. 16, p. 1635, 1977.
- [194] K. Imai, "A new dielectric isolation method using porous silicon", *Solid State Electron*, Vol. 24, p. 159, 1981.

- [195] F. Otoi, K. Anzai, H. Kitabayashi, K. Uchiho, and Y. Mizokami, "Fabrication of high speed 1 micron FIPOS/CMOS", J. Electrochem. Soc., Vol. 131, p. C319, 1984
- [196] L. T. Canham, "Silicon quantum wire array fabrication by electrochemical and chemical dissolution of wafers", Appl. Phys. Lett., Vol. 57, p. 1046, 1990.
- [197] A. G. Cullis and L. T. Canham, "Visible light emission due to quantum size effects in highly porous crystalline silicon", Nature, Vol. 353, p. 335, 1991.
- [198] Z. Sui, P. P. Leong, I. P. Herman, G. S. Higashi, and H. Temkin, "Raman analysis of light-emitting porous silicon", Appl. Phys. Lett., Vol. 60, p. 2086, 1992.
- [199] C. Delerue, G. Allan, and M. Lannoo, "Theoretical aspects of the luminescence of porous silicon", Phys. Rev. B, Vol. 48, p. 11024, 1993.
- [200] F. Koch, V. Petrova-koch, T. Muschik, A. nikolov, and V. Gavrilenko, "Fast Photoluminescence from Porous Silicon", Mater. Res. Soc. Symp. Proc., Vol. 298, p. 319, 1993.
- [201] A. Richter, P. steiner, F. Kozlowski, and W. Lang, "Current induced light emission from a porous silicon device", IEEE Electron Device Lett., Vol. 12, p. 691, 1991.
- [202] K. D. Hirschmann, L. Tsybeskov, S. P. Duttagupta, and P. M. Fauchet, "Silicon-based visible light-emitting devices integrated into microelectronic circuits", Nature, Vol. 384, p. 338, 1996.
- [203] C. Mazzoleni and L. Pavesi, "Application to optical components of dielectric porous silicon multilayers", Appl. Phys. Lett., Vol. 67, p. 2983, 1995.
- [204] J. M. Lauerhaas and M. J. Sailor, "Chemical Modification of the Photoluminescence Quenching of Porous Silicon", Science, Vol. 261, p. 1567, 1993.
- [205] H. Sohn, S. Letant, M. J. Sailor, and C. Trogler, "Detection of Fluorophosphonate Chemical Warfare Agents by Catalytic Hydrolysis with a Porous Silicon Interferometer", J. Am. Chem. Soc., Vol. 122, p. 5399, 2000.
- [206] S. Letant and M. J. Sailor, "Molecular Identification by Time-Resolved Interferometry in a Porous Silicon Film", Adv. Mater., Vol. 13, p. 355, 2001.
- [207] S. Chan, S. R. Horner, P. M. Fauchet, and B. L. Miller, "Identification of Gram Negative Bacteria Using Nanoscale Silicon Microcavities", J. Am. Chem. Soc., Vol. 123, p. 11797, 2001.
- [208] H. Sohn, R. M. Calhoun, M. J. Sailor, and W. C. Trogler, "Detection of TNT and Picric Acid on Surfaces and in Seawater by Using Photoluminescent Polysiloles", Angew. Chem. Int. Ed., Vol. 40, p. 2104, 2001.
- [209] H. Sohn, M. J. Sailor, D. magde, and W. C. Trogler, "Detection of Nitroaromatic Explosives Based on Photoluminescent Polymers Containing Metalloles", J. Am. Chem. Soc., Vol. 125, p. 3821, 2003.
- [210] X. Li, J. L. Coffer, Y. D. Chen, R. F. Pinizzotto, J. Newey, and L. T. Canham, "Transition Metal Complex-Doped Hydroxyapatite Layers on Porous Silicon", J. Am. Chem. Soc., Vol. 120, p. 1
- [211] T. E. Bell, P. T. J. Gennissen, D. Demunter, and M. Kuhl, "Porous silicon as a sacrificial material", J. Micromech. Microeng., Vol. 6, p. 361, 1996.
- [212] V. P. Parkhutik, E. Matveeva, R. Perez, J. Alamo, and D. Beltraan, "Mechanism of large oscillations of anodic potential during anodization of silicon in H<sub>3</sub>PO<sub>4</sub>/HF solutions", Mater. Sci. Engn. B, Vol. 69- 70, p. 53, 2000.
- [213] L.T. Canham. "Tunable Properties of Porous Silcon. In: CANham L. (eds), Handbook of Porous Silicon, springer, 2014.
- [214] A. G. Cullis, L.T. Cunhan, P. D. J. Calcott. "The structural and Luminescence properties of Porous Silcon", Journal of Applied Physics, vol. 82, no. 909, 1997.
- [215] W.Theib, "Optical Properties of Porous Siliocn", SurafceSience reports, vol. 29, pp. 91-192, 1997.
- [216] S. M. Prokes, O. J. Glembocki, V. M. Bremudez, R. Kaplan, L.E. Friedersdorf, P.C. Searson, " SiH x Excitation: An alternate mechanism of Porous Si photoluminescence", Physical review B vol. 45, no. 23, 1992.
- [217] M. S. Brandt, H. D. Fuchs, M. Stutmann, J. Weber, M. Cardona, " The origin of visible luminescence from "Porous Silicon", Solid State Communication, vol. 81, no. 4, pp. 307-312, 1992.
- [218] T. Sarkar, N. Mukherjee, J. Das, "Studies on conductivity of surface functionalized nano Porous silicon for detection of hypo and hyper glycemia", Material Research Express, vol. 6, 2019.



- [219] S. Kim, J. W. Park, D. Kim, D. Kim, I. Lee, S. Jon, "Bioinspired Colorimetric Detection of Calcium(II) Ions in Serum Using Calsequestrin-Functionalized Gold Nanoparticles," *Angew. Chem. Int.*, vol. 48, pp. 4138-4141, 2009.
- [220] M. S. Eom, W. Jang, Y. S. Lee, G. Choi, Y. Kwon, M. S. Han, "A bi-ligand co-functionalized gold nanoparticles-based calcium ion probe and its application to the detection of calcium ions in serum," *Chem. Comm.*, vol. 48, pp.5566-5568, 2012.
- [221] T. Atanasijevic, M. Shusteff, P. Fam, A. Jasanoff, "Calcium-sensitive MRI contrast agents based on superparamagnetic iron oxide nanoparticles and calmodulin," *Pnas*, vol. 103, no. 40, pp. 14707-14712, 2006.
- [222] S.J. Kim, J. Blumling, M. C. Davidson, H. Saad, S.Y. Eun, G. A. Silva, "Calcium and EDTA Induced Folding and Unfolding of Calmodulin on Functionalized Quantum Dot Surfaces," *Journal of Nanoneuroscience*, vol. 2, pp. 1-7, 2012.
- [223] S. A. Razavi, L. Hoghooghirad, H. Golab-Ghadaksaz, M. Hedayati, "Calcium Determination in EDTA Treated Plasma by Colorimetric Method and Microplate Reading Format," *Zahedan J. Res. Med. Sci.*, vol. 17, no. 2, pp. 7-10, 2015.
- [224] Y. Guo, X. Tong, L. Ji, Z. Wang, H. Wang, J. Hu, R. Pei, "Visual detection of Ca<sup>2+</sup> based on aggregation-induced emission of Au(I)–Cys complexes with superb selectivity," *Chem. Commun.*, vol. 51, pp. 596-598, 2015.
- [225] M. Zhang, C. Abrams, L. Wang, A. Gizzi, L. He, R. Lin, Y. Chen, P. J. Loll, J. M. Pascal, J. Zhang, "Structural basis for calmodulin as a dynamic calcium sensor," *Structure*, vol. 20, no. 5, pp.911-923, 2012.
- [226] D. Chin, A. R. Means, "Calmodulin: a prototypical calcium sensor," *trends in Cell Biology*, vol. 10, pp.322-328, 2000.
- [227] T. W. Lin, P.J. Hsieh, C.L. Lin, Y.Y. Fang, J.X. Yang, C. C. Tsai, P. L. Chiang, C. Y. Pan, Y. T. Chen, "Label-free detection of protein-protein interactions using a calmodulin-modified nanowire transistor," *PNAS*, vol. 107, no. 3, pp. 1047-1052, 2010.
- [228] W. Hall, J. Modica, J. Anker, Y. Lin, M. Mrksich, R.P.V. Duyne, "Biosensing with a Calmodulin-Functionalized Plasmonic Switch," *Nano Lett.*, vol. 11, no. 3, pp. 1098-1105, 2011.



# Chapter-2

# Chapter 2: Design and Development of Multi-parametric Finger Clubbing Monitor

---

Digital clubbing is an important clinical symptom. Characterized by the bulbous appearance of the finger tips, digital clubbing is often associated to a number of cardio-pulmonary disorders namely lung cancer, chronic obstructive pulmonary disorder, cyanotic congenital heart disease, idiopathic pulmonary fibrosis and numerous other medical conditions [1-3]. Caused due to platelet derived growth factors and vascular endothelial growth factors, diagnosis of digital clubbing plays predominant role in early detection of many cardio-pulmonary conditions [1-3]. Qualitative tests provides insufficiently for the conclusive diagnosis of digital clubbing. Profile axis angle determination of human finger can be treated as an effective indicator for quantitative measurement of digital clubbing. This work proposes the development of an automated instrument; designer for precise measurement of profile axis angle and the Distal Phalangeal Depth (DPD), Inter Phalangeal Depth (IPD) ratio of human fingers for quantitative and cost effective diagnosis of digital clubbing.

## 2.1A BRIEF INTRODUCTION

Finger clubbing is a clinical condition characterized by the drumstick or bulbous appearance of fingers. It causes the structural change in the appearance of the finger which results in the increase in antero-posterior and lateral diameter of the nails [1]. Finger clubbing was first diagnosed, many centuries ago by Hippocrates as a sign of underlying disorder [1-5]. Since then finger clubbing has been associated with a number of diseases namely lung cancer, bronchiectasis, cyanotic congenital heart disease, idiopathic pulmonary fibrosis, cirrhosis of liver, cystic fibrosis, mesothelioma, inflammatory bowel disease and hepatic cirrhosis [1,3,6-9]. Hence finger clubbing is very common in cardiopulmonary disorders [10]. Moreover the association of finger clubbing has also been confirmed with intra-thoracic tumors and Crohn's disease [4]. Finger clubbing is caused due to unfragmented platelets

precursor in the pulmonary circulation which accumulates in peripheral vasculature, releasing platelet derived growth factor resulting in digital clubbing [6]. Finger clubbing occurs in steps [1,11]. Initially the nail bed softens, giving it a spongy appearance. Second steps results in the increase of lovi-bond angle, which is the angle between the nail plate and the proximal nail fold. The lovi-bond angle increases from its normal measure of nearly  $170^0$  to greater values, indicating first order finger clubbing [2,4,6,8-10,12-13]. Eventually, the depth of distal phalanx increases compared to depth of inter phalanx, thus disruption of distal and inter phalange depth ratio occurs, indicating second order finger clubbing [1]. Finally the nail appears shinny [1]. Qualitative method for detection of finger clubbing includes Schamroth's window test [1,6,9,14], and visual methods. Distal phalange depth (DPD) and inter phalange depth (IPD) ratio together with the lovi-bond angle measure provides important parameters for quantitative diagnosis of finger clubbing [2,6,8,10-21]. This work presents the design and development of an automated instrument based on software development in MATLAB programing environment that endorses image processing technique and laser-photo-detector technique. This technique developed here is capable of explicit measurement of profile axis angle and DPD-IPD ratio of adult human finger, effective in automated and quantified diagnosis of digital clubbing.

## **2.2 INSTRUMENT DESIGN**

Two techniques, namely image processing technique and laser-photo-detector technique are undertaken for the development of the multi-parametric finger clubbing monitor. Both the techniques utilizes MATLAB programming environment for the development of software capable of precise and accurate detection of finger clubbing in human adults.

### **❖ Instrument for Image Acquisition**

For the purpose of image acquisition a double walled box is constructed (fig.2.1 a), with the inner-wall translucent white and the outer wall opaque provided with two holes. The first bigger hole serves the purpose of finger insertion and the second small hole for camera mounting. The outer dimension of the box is 14cm X 10cm X 12 cm.

Between the walls of the box LEDs are fitted to facilitate silhouette image of the finger. The camera is at right angle to the finger. Distance of the finger insertion hole from the translucent white screen is 2.5cm, whereas the distance of the camera from the finger insertion hole is 8.5cm. The image is obtained up to the inter phalange of the finger, that both the distal phalange and the inter phalange are in view. Image of the designed instrument and the image obtained with it are shown in fig 2.1 a and b respectively.

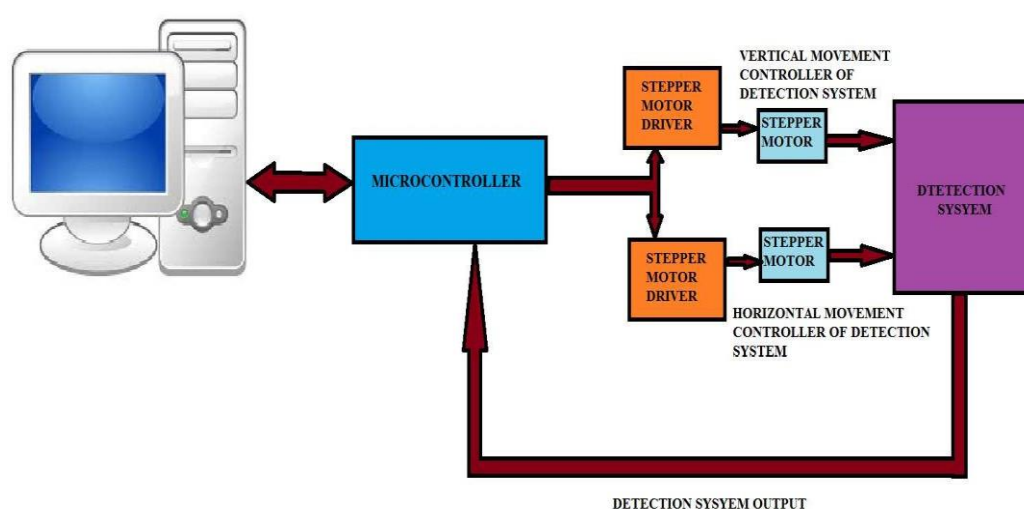


**Fig 2.1 (a) Image being captured by the developed instrument. (b) The image obtained by the monitor.**

#### ❖ **Instrument for Laser-Photo-Detector Technique**

The instrument is designed for quantitative determination of profile axis angle of an adult human finger for accurate diagnosis of finger clubbing. The design of the instrument is represented in form of block diagram in figure 2.1. The instrument works on the principle of laser photo detection and obliteration technique for determination of finger profile axis angle. Consisting of an 'N' shaped laser-photo-detector arrangement, the instrument consists of bi-motor system to bring about horizontal and vertical movement of the 'N' shaped arrangement. The 'n' shaped arrangement is designed to slide vertically and horizontally about a bench, upon which the diagnosing finger is rested. The measure of vertical and horizontal movement of the laser-photo-detector arrangement is used to determine the finger contour over the nail plate and the proximal nail fold for the determination of the finger profile axis angle which is the angle between the nail plate and the proximal

nail fold. Similar technique is utilized for determination of DPD-IPD ratio [18, 19]. The vertical-horizontal simultaneous movement of the laser-photo-detector arrangement about the finger resting platform is brought about for the determination of the finger depth ratio. This entire system is computer interfaced by an interfacing microprocessor. The schematic block diagram of the instrument is shown in fig2.2. The data thus obtained is supplied to the developed program for precise and quantified calculation of finger profile axis angle.



**Fig 2.2.The schematic block diagram of the instrument developed.**

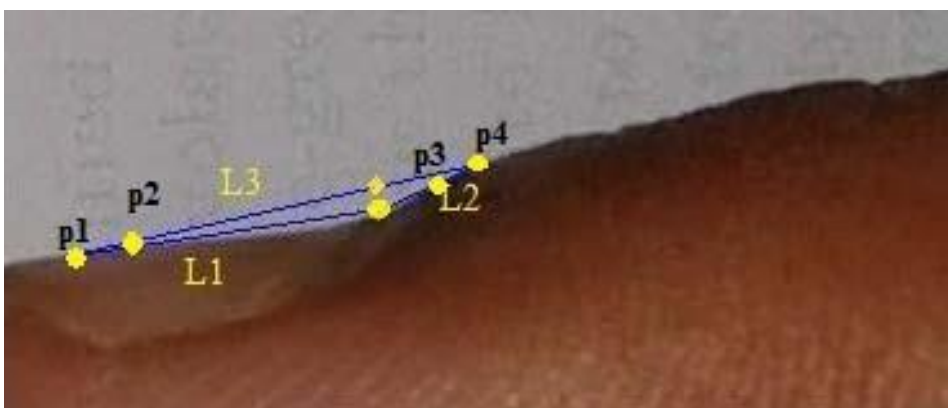
## 2.3 MECHANISM OF DETECTION

As stated before, the detection of the finger clubbing is carried out by two techniques, the image processing technique and the laser-photo-detector technique. The results of both the techniques are used for accurate determination of profile axis angle and the DPD-IPD ratio of human finger, the two important markers of finger clubbing.

### ❖ Mechanism of Detection using Image Processing Technique

For the determination of profile axis angle using image processing, Software has been developed in MATLAB to compute the lovi-bond angle of adult human finger. The software is designed on image

processing technique. The software binaries the image and detect four points on the finger image, two points on the nail plate (P1, P2) (fig.2.3) and the other two on the proximal nail fold (P3,P4) (fig.2.3).The software developed for the purpose, treats a binary image to be a matrix of rows and columns consisting of values corresponding to the pixel intensity at the given point on the image. Thus, in the case of binary image the matrix consists of 0 and 1.The software developed, chooses the above mentioned points on the image for a particular column value for which the corresponding row value displays a transition from 0 to 1.This is essentially a point upon the finger. The first column value for point P1 is so chosen that the point P1 lies on the edge on the nail plate, as shown in fig.2.3 The column value for obtaining P2 is chosen as close to P1 as possible (fig.2.3).The column value to obtain P3 is chosen so that the pointP3 lies at the edge of the proximal nail fold, as shown infig.2.3 and the point P4 is obtained as close to P3 as possible (fig.2.3). This is done for better accuracy. Next the software is programmed to compute the angle between the two linesL1, L2 (fig. 2.3), formed by joining the points P1, P2 and points P3, P4 respectively. This angle thus obtained is the lovi-bond angle for the finger [18, 19].



**Fig.2.3.**Image depicting lines L1 between points (P1,P2) and L2 between points (P3, P4)

In order to determine DPD-IPD ratio, the software developed is so programmed that it firstly rotates the image obtained to a vertical image. Secondly it binaries the image so the image matrix consists of only 0 and 1.The software is then programmed to

count the number of 0 in each row of the image matrix. By this process the width of the finger that corresponds to the number of 0 in a particular row is calculated. This process is continuous for the entire length of the finger image (the image is obtained up to the interphalange of the finger. So both the distal phalange and the interphalange are in view). The characteristic of the width profile is monitored by the software to compute the tendency of DPD-IPD ratio, which serves as an ideal marker for finger clubbing detection. The binarised image and the image matrix is shown in fig 2.4 (a) and (b) respectively.



**Fig.2.4.(a) Binary image of the finger. (b) Image matrix of the finger.**

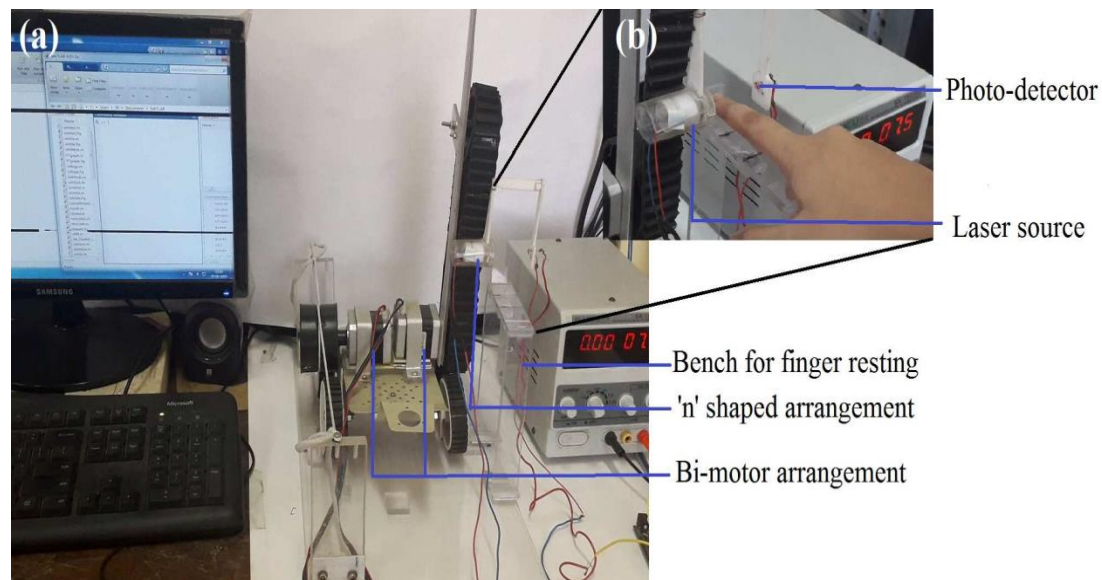
#### ❖ Mechanism of Detection using Laser-Photo-Detector Technique

For the determination of profile axis angle using laser and photo-detector arrangement, the diagnosing finger is placed upon the resting bench. The bench is so placed that it lies within the cavity of the 'N' shaped arrangement, such that the laser lies on one side of the resting bench and the photo-detector lies on the other. The system is programmed to bring about the vertical movement of the 'N' shaped laser-photo-detector arrangement in the region of the nail plate, from a fixed home position. Next the program measures the vertical distance moved by the 'N' shaped arrangement, before the laser photons falling upon the photo-detector, is just obliterated by the nail plate. The arrangement is moved to another point of the nail plate and the vertical distance measurement routine is repeated. This determines the nail-



plate contour. The same routine is repeated for two points upon the proximal nail fold to obtain the proximal nail fold contour. The contours thus obtained are next tallied with the algorithm developed for different finger shapes and the profile axis angle for the finger is accurately determined by the program.

For the determination of the DPD-IPD ratio, the finger is placed on the resting bench, between the laser and photo-detector exactly same as before. In this case, the system is programed to bring about vertical displacement of the 'N' shaped laser-photo-detector arrangement and the programed is designed to measure the vertical distance moved by the 'N' shaped arrangement with the laser beam, which were falling upon the photo-detector is obliterated by the finger placed on the resting bench. This effectively gives the finger width at that particular point. The software designed in this work is programed to follow this routine starting from the finger-tip to the proximal nail fold, at various points and determine the finger width profile as we move from the finger-tip towards the nail fold to determine the DPD-IPD ratio, thus providing a perfect marker for the diagnosis of finger clubbing. The image of the developed instrument is depicted in fig 2.5 (a) and (b).





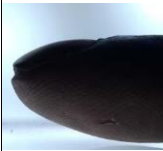




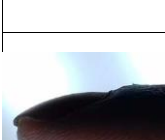

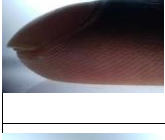



**Fig.2.(a) The overview of the instrument developed. (b) Enlarged view of laser-photo-detector arrangement while diagnosing.**

## 2.4 REAL TIME APPLICATION OF THE INSTRUMENTS

The instruments developed in this work are used upon patients of cardio-pulmonary and chest department of a local hospital. The ability of the instruments for precise measurement of profile axis angle and DPD-IPD ratio of finger is tested and the result obtained is tabulated in table 2.1.

**TABLE 2.1. Output of Instruments for the determination of profile axis angle and width profile.**

Image of finger	Diagnosis of patients	INSTRUMENT OUTPUT- IMAGE PROCESSING TECHNIQUE		INSTRUMENT OUTPUT- LASER-PHOTO-DETECTOR TECHNIQUE	
		Program output for profile axis angle (in degrees)	Program output for DPD-IPD measurement	Profile axis angle measured by the instrument developed (in degrees)	DPD-IPD Ratio measurement by the instrument developed
	(Male) Chronic obstructive pulmonary disease.	205 >170 Finger may be clubbed, 1 <sup>st</sup> order	IPD > DPD The finger may be clubbed, 2 <sup>nd</sup> order	205.0028	IPD > DPD The finger may be clubbed
	(Male) Smoker for 20 years. Chronic obstructive pulmonary disease.	190 >170 Finger may be clubbed, 1 <sup>st</sup> order	IPD < DPD , The Finger may be clubbed, 2 <sup>nd</sup> order	190.1244	IPD < DPD , The Finger may be clubbed
	(Male) Suspected lung carcinoma or lung mass.	190 >170 Finger may be clubbed, 1 <sup>st</sup> order	IPD < DPD , The Finger may be clubbed, 2 <sup>nd</sup> order	189.7106	IPD < DPD , The Finger may be clubbed
	(Male) Suspected chronic obstructive pulmonary disease.	187 >170 Finger may be clubbed, 1 <sup>st</sup> order	IPD < DPD , The Finger may be clubbed, 2 <sup>nd</sup> order	187.0199	IPD < DPD , The Finger may be clubbed
	(Male) Suspected squamous cell carcinoma.	198 >170 Finger may be clubbed, 1 <sup>st</sup> order	IPD < DPD , The Finger may be clubbed, 2 <sup>nd</sup> order	198.9638	IPD < DPD , The Finger may be clubbed

	(Male) Mass found in lungs, suspected lung carcinoma.	194 >170 Finger may be clubbed , 1st order	IPD<DPD , The Finger may be clubbed, 2nd order	194.400 7	IPD<DPD , The Finger may be clubbed
	(Male) Chronic obstructive pulmonary disease.	189 >170 Finger may be clubbed , 1st order	IPD>DPD , The Finger may not be clubbed	187.74 29	IPD>DPD , The Finger may not be clubbed
	(Male) Chronic obstructive pulmonary disease, chronic bronchitis phenotype, complaint Of haemoptysis. Suspected lung carcinoma.	202 >170 Finger may be clubbed, 1st order	IPD<DPD , The Finger may be clubbed, 2nd order	203.198 6 201.30 30	IPD<DPD , The Finger may be clubbed
	(Male) Idiopathic cause	217 >170 Finger may be clubbed, 1st order	IPD<DPD , The Finger may be clubbed, 2nd order	212.220 8	IPD<DPD , The Finger may be clubbed
	(Male) Smoker for 15 years. Suspected rheumatic heart disease	181 >170 Finger may be clubbed , 1st order	IPD<DPD , The Finger may be clubbed, 2nd order	182.848 2	IPD<DPD , The Finger may be clubbed
	(Male) Complaint of chest pain, suggestive of chronic lung disease.	176 >170 Finger may be clubbed, 1st order	IPD<DPD , The finger may be clubbed, 2nd order	174.56 70	IPD<DPD , The finger may be clubbed
	(Female) Pleural effusion.	180 >170 Finger may be clubbed, 1st order	IPD<DPD , The finger may be clubbed, 2nd order	180.543 2	IPD<DPD , The finger may be clubbed
	Normal (Male ) (Control experiment)	162 <170 Finger may not be clubbed	IPD>DPD , The finger may not be clubbed	162.786 5	IPD>DPD , The finger may not be clubbed

## 2.5 CONCLUSION AND FUTURE SCOPE

It is well established from the above data that digital clubbing finds association in numerous cardio pulmonary conditions. Almost all the patients, complaining or diagnosed with any chest or heart related disorder have moderate to severe digital clubbing. The effectiveness of the instruments developed is also revealed by the above data. The measure of the profile axis angle and DPD-IPD ratio, determined by the instruments in order to diagnose finger clubbing is found to be quite accurate and give a clear quantitative idea of the degree of finger clubbing present in a patient.

Evidently, the early detection of any cardio-pulmonary condition plays an important role in the prognosis of any such disorders. Importantly, in case of lung cancer, early detection of the disease plays a vital role in reduction of the death risks. Thus the instruments developed in this work is effective in early, quantified, automated, accurate, non-invasive and cost-effective diagnosis of finger clubbing that may lead to early treatment for all the mentioned medical conditions, including lung cancer. Since earlier methods employed for the detection of finger clubbing were mostly qualitative and not automated, the instruments developed in this work has a distinct advantage over the other previously applied methods. Installation of the device in hospitals and medical clinics will lead to an advantageous and early detection of digital clubbing inpatients.

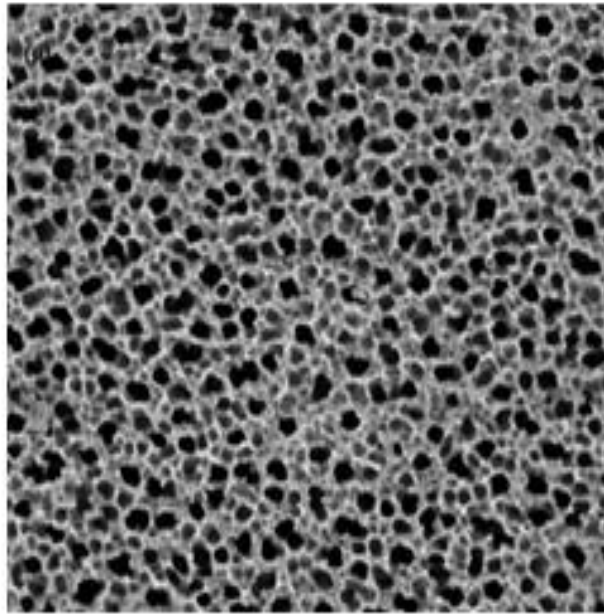
The instruments developed in this work, determines finger clubbing by only the determination of profile axis angle and DPD-IPD ratio, the accuracy of the instrument can be increased by quantified determination of other parameters like Crug's angle which can add quite significantly toward the accuracy of the instruments. Moreover, since finger clubbing is not a conclusive parameter for the diagnosis of serious cardio-pulmonary malfunctioning, there is further room for investigation into the topic in search of more conclusive parameters like serum calcium detection for early and undeniable diagnosis of cardio-pulmonary disorders to enable early management and better prognosis in the following chapters.

## Reference

- [1] MalaySarkar, D.M.Mahesh, and Irappa Madabhavi,“Digital clubbing”, Lung India, vol. 29(4), pp. 354-362, (2012).M. Young, The Technical Writer’s Handbook. Mill Valley, CA:University Science,1989.
- [2] Daniela Husarik, Stephan R. Vavricka, Michael Mark, Andreas Schaffner, Roland B. Walter,"Assessment of digital clubbing in medical inpatients by digital photography and computerized analysis",SwissMedicalWeekly,vol.132,pp.132-138,2002.
- [3] Kerith E. Spicknall, BA, Matthew J. Zirwas, MD, and Joseph C. EnglishIII,MD,"Clubbing: An update on diagnosis, differential diagnosis, pathophysiology, and clinical relevance",Journal of the American Academy of Dermatology, vol. 52(6),pp.1020-1028,2005.
- [4] G. Kitis, H Thompson, R H Allan,"Finger clubbing in inflammatory bowel disease: its prevalence and pathogenesis." British Medical Journal, vol.2(6194),pp.825–828,(October1979).
- [5] Dickinson CJ, “Lung disease associated with digital clubbing”, Clin Exp Rheumatol,10(7),pp.23-25,1992.
- [6] Motswaledi MH, Mayayise MC,” Nail changes in systemic diseases”,South African Family Practice, vol.52(5),pp.409-413,2010.
- [7] X.Vandemergel, B. Rennboog,“Prevalence, aetiologies and significance of clubbing in a department of general internal medicine”, European Journal of Internal Medicine, vol.19(5), pp.325-329, 2008.
- [8] Chun Wai Chan,” Evaluation of digital clubbing”, Australian Family Physician, vol.44(3),pp.113-116,2015.
- [9] Archana Singal, Rahul Arora,“Nail as a window of systemic diseases”, Indian Dermatology online journal,vol.6(2),pp.67-74,2015.
- [10] Gurcharan Singh, Nayeem Sadath Haneef, Uday A,” Nail changes and disorders among the elderly”, Indian Journal Of Dermatology, Venereology and Leprology, vol.71(6 ), pp.386-392,2005.
- [11] R D Djodibroto, MD, P T Thomas, MD ,Kamarudin T Kana, MD, Hla Myint, MBBS,"Finger Clubbing: Do We Require Digital Index Quantitator?", Med J Malaysia, vol. 69(2),pp.60-63, April,2014.
- [12] Kathryn A Mayers, Donald R. E. Farquhar, "Does this patient have clubbing?",The rational clinical examination, vol. 286(3),pp. 341-347,July182001.
- [13] T J Pitts-Tucker, M G Miller, and J M Littlewood, “Finger clubbing incystic fibrosis”, Archives of Disease in Childhood, vol. 61, pp. 576-579,1986.
- [14] Bernard Kernath, "Digital clubbing: As sign of underlying disease",Hospital Physician, vol.39(9),pp.25-27,2003.
- [15] Homagni Sikha Roy, Zhigang Wang, Haitao Ran et.al., “Diagnosis ofdigitalclubbinghigh-frequency ultrasound imaging”.International Journal of Dermatology, vol. 52(1),pp.1-5,2012.
- [16] James Y. Paton, Daisy B. Bautista, Michael W. Stabile et.al., “Digitalclubbing and pulmonary function abnormalities in children withlungdisease”,Pediatricpulmonology, vol.10(1),pp.25-29,1991.
- [17] José da Silva Moreira, Marlene Hass, Ana Luiza Schneider Moreira,James de Freitas Fleck, José de Jesus Peixoto Camargo ,” Reversal of digital clubbing in surgically treated lung cancer patients”, Jornal Brasileiro de pneumologia, vol.34(7),pp.481-489,2008.
- [18] Kaustav Sen, Arnesh Sen, Deeparati Basu ,Syed Minhaz Hossain, JayotiDas, “Automated technique based on image processing for accurate diagnosis of finger clubbing”.IEEE sensors conference, DOI.10.1109/ICSENS.2018.8589695,pp.1-4, 2018.
- [19] Kaustav sen, deeparati Basu, Aarnesh Sen, Syed Minhaz Hossain, Jayoti Das, “ Automated detection of profile axis angle of human finger for quantitative digital clubbing diagnosis”,

10<sup>th</sup>ICCCNT, DOI. 10.1109/ICCCNT45670.2019.8944519, 2019.

- [20] S. M. W. Masra<sup>1</sup>, K. L. Goh, J. S. Henry, M. S. Muhammad, R. D.Djojodibroto and R. Sapawi, "Development of Finger Clubbing Meter", Conference: UNIMASSTEM Engineering Conference 2015, At Kuching, Sarawak, 833, Masra, Masniah. (2015). Development of Finger Clubbing Meter..10.4028/www.scientific.net/AMM.833.190.
- [21] Donald Bentley, Angela Moore, Harry Shwachman, "Finger clubbing: aquantitative survey by analysis of the shadowgraph ". The Lancet, vol.2(7978), pp. 164-167, 1976.



# chapter-3

# Chapter 3: Porous Silicon: Synthesis and Characterization

---

Due to some tremendously interesting properties of Porous silicon (PSi), it has gained huge application in the field of micro-electronics [1]. Due to the quantum-confinement exhibited by PSi that results in its wide and direct band-gap, PSi has found use as an ideal candidate for applications as sensors [1]. Due to porous nature, PSi provides huge surface area for bio- molecular interaction and absorption [2-4]. Moreover PSi exhibits the phenomena of photoluminescence that provides application in the field of optical sensors [5-7]. The surface morphology of PSi is easily adjustable, that makes it an ideal choice for bio-sensing applications [6, 8-12]. Being a bio-compatible material, PSi finds application as bio-vehicle for high targeted delivery of drugs [13-14]. Due to its high loading capacity, PSi has gained huge importance as bio-sensors, chemical-sensors and ionic-sensors [15-17]. Application of PSi Based ionic sensors has gained a lot of importance lately that finds use in food industry, scientific laboratories and most importantly in clinical diagnosis. Moreover, the surface morphology, namely pore size, porosity and pore structure of PSi is highly dependent on fabrication condition such as electrolytic composition and concentration, wafer resistivity, current density, dopant type and electro-chemical etching time [18,19]. Porous silicon based calcium detectors has gained prominence in recent years.

## 3.1 POROUS SILICON FABRICATION PROCESS

Various techniques are in use for the fabrication of PSi. The First and the most widely used technique among them being the anodic etching technique also known as electro-chemical etching technique [20]. Except electro-chemical etching, many other techniques were formulated over the years for the fabrication of PSi, they are:

Stain etching, where the solution of Hydrofluoric (HF) acid and concentrated Nitric acid caused the formation of PSi by the appearance of stain on Si wafer surface [20]. Photoetching is yet another method for the preparation of PSi, where Silicon wafer immersed in HF solution is illuminated by coherent source of light like



He-Ne laser leading to the formation of mesoporous Silicon [20]. Fabrication of PSi is also observed to be possible by spraying solar cell surface by HF solution resulting in slow dissolution of Si atom by low velocity HF, the process later established as vapour etching technique [20]. Spark erosion is another physical technique for PSi fabrication, not involving dissolution of Si atoms in any chemical. In this method the Si Surface is exposed to spark tip and the surface is eroded for hours for pore formation on the surface [20]. Laser-induced plasma erosion is yet another physical method introduced for PSi formation that involves air optical breakdown plasma to be targeted upon a silicon surface for porosification [20]. Ion implantation method of PSi fabrication involves high-dose, low energy silver ions into mono-crystalline Silicon for Pore formation [20].

In this work Electrochemical etching method has been applied for effective fabrication of PSi and has been discussed in details in this chapter.

### **3.1.1. Electrochemical Etching Process of Fabrication of Porous Silicon.**

Nano and macro PSi has been fabricated in this work, the fabrication process can be sub-divided into two major steps, namely wafer cleaning and electro-chemical etching. The steps are elaborated here.

#### **3.1.1.1 Cleaning of Silicon Wafers.**

Si wafers, that are single end acid polished, consisting of <100> orientation and P-type (Boron doped) are cut into dimensions of 1.5×1.5 cm are chosen for the fabrication process. The resistivities of the wafers are as follows:

1-10Ωcm for nano samples and 10-20Ωcm for macro samples.

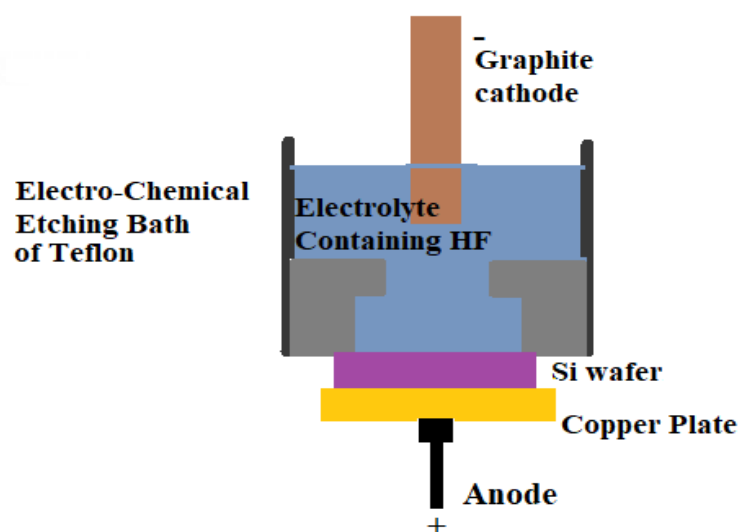
The wafers are dipped in acetone solution and heated to 42°C for 10min. The heated wafer in acetone solution are then sonicated in ultrasonic cleaner for 10min. The sonicated wafers are then dipped in methanol for 3min, after which they are thoroughly rinsed with deionized (DI) water, multiple times. This steps cleanses the wafer of any grease or oil particle present on its surface. Next a solution of 30% GR grade of hydrogen per oxide (H<sub>2</sub>O<sub>2</sub>) and 98% GR grade of sulphuric acid (H<sub>2</sub>SO<sub>4</sub>) are prepared in the ratio 1:1 and the wafers are dipped in the solution for about 30min or rather till the

vigorous agitation reaction stops. The wafers are again rinsed thoroughly in running DI water, multiple times. This steps cleanses the wafer of any heavy metal particle present upon the wafer surface. Lastly a solution of 20ml DI water and 5ml HF is prepared and the wafers are dipped into it for 2min, which cleanses the wafer of nascent oxides present on the wafer surface. The wafers are finally washed multiple times with DI water and are made ready for back metallic contact, which is done by vapour deposition of Aluminium on the unpolished wafer surface. This metal deposition established the Ohmic contact required during anodic etching of the Si wafer for PSi fabrication.

### **3.1.1.2 Electro-Chemical Etching method for PSi Fabrication.**

Three types of Cell configuration are available for electro-chemical etching of Si for effective PSi formation. They are namely lateral cell, single cell and double cell [20]. In lateral cell configuration the Si wafer, acting as anode and platinum or any other HF resistant material like graphite, acting as cathode are held laterally to each other in the electrolytic bath. The cell configuration, though simple poses certain disadvantages like non-uniform porosity being the major among them. In Double cell configuration the electrolytic bath consists of two half cells one containing the cathode and the other consisting of the anode, while the Si wafer is held in between the electrodes and the electric current passes through the Si wafer. Uniform porosity being one of the major advantage of this arrangement while complex setup is the major disadvantage accounting for not so frequent use of the arrangement for PSi fabrication. The single cell arrangement consist of vertical arrangement of the cathode and the anode. The Si wafer acting as anode has one side sealed to the electrolyte causing PSi formation on single surface. This method is the most common method employed for porosification of Si wafers [20]. This method provides acceptable uniformity in porosity of the PSi and its simple arrangement adds to its acceptability for the most frequent method employed for PSi fabrication [20]. In this work the single cell arrangement has been used for effective PSi fabrication.

Fig 3.1 schematically depicts the single cell configuration structure of the etching chamber or the electrolytic bath where the PSi is fabricated. The chamber is basically made of acid resistant materials like Teflon. Si wafer acts as anode, which is further provided with a copper plate contact to facilitate uniform porosity. Graphite is used as cathode. The wafer is so placed that only a single surface of it is exposed to the electrolyte, upon which porosification is done. The diameter of the graphite cathode is nearly equal to the exposed diameter of the wafer to facilitate uniform current density.

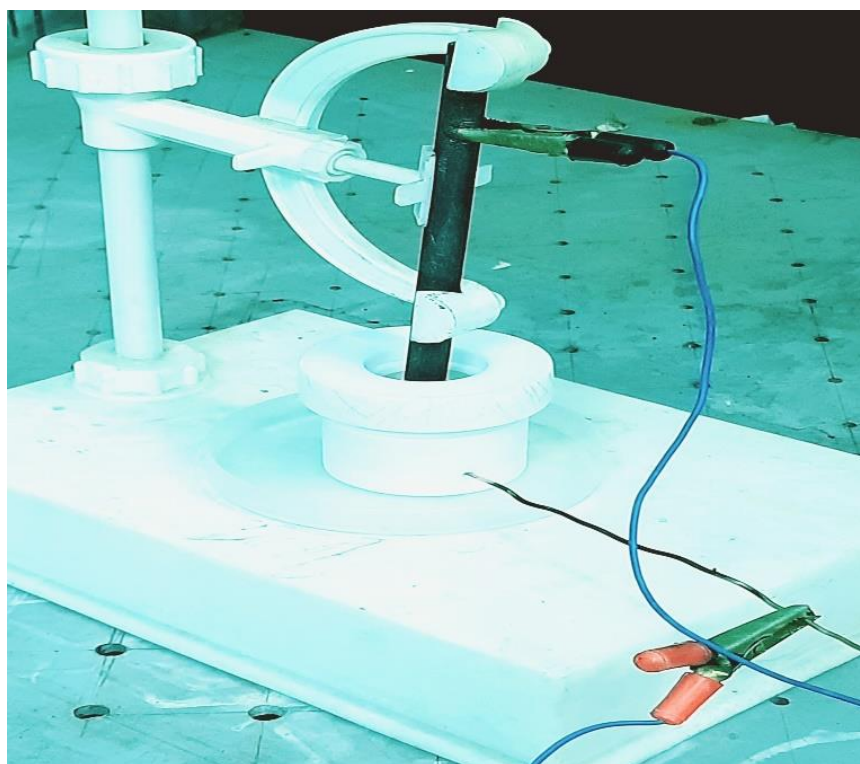


**Fig 3.1. Schematic diagram of the Electro-Chemical Etching Cell.**

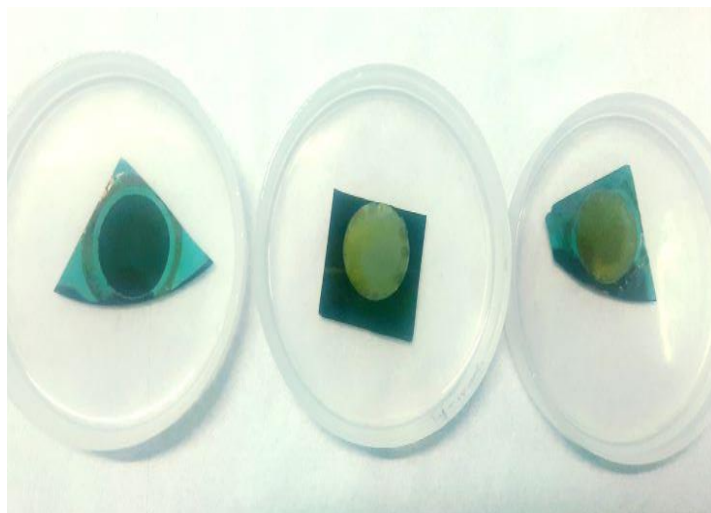
Boron doped silicon wafers (P-type)<100>of both resistivities (1-10 $\Omega$ cm and 10-20 $\Omega$ cm) were laser cut into dimension 1.5 $\times$ 1.5cm. The wafers were acid polished, washed multiple times with DI water and completely dried at room temperature. Metal (Aluminum) is deposited on the lower surface of the wafers by vapour deposition technique, to facilitate ohmic contact during electrochemical etching. The cleaning and metal contact were done according to steps mentioned previously. After metal deposition, the wafers were rinsed multiple times with absolute ethanol and completely dried at room temperature and prepared for electrochemical etching process.

The electrochemical etching process is carried out in an acid resistant bath with graphite rod and silicon wafer acting as cathode and anode respectively, as describe above. Rinsed and dried silicon wafers of

resistivity 1-10 $\Omega$ cm were used for the preparation of nano-PSi. For the preparation of nano-PSi, the electrolyte solution consist of ethanol (>99.9%) and HF (48%) mixed in the ratio of 1:1. The etching was carried out under ambient environmental conditions, at room temperature. Current density of 15mA/cm<sup>2</sup> is maintained throughout the process. For the macro-PSi sample preparation, wafers of resistivity 10-20 $\Omega$ cm was taken and the electrolyte solution of DMF (99.8%) and HF (48%) in the ratio 3:1 or 1:1 (as required) was prepared. Again, ambient environmental conditions were maintained during the etching process. Constant current density of 15mA/cm<sup>2</sup> was maintained. The prepared PSi samples were rinsed multiple times in absolute ethanol and DI water, dried completely at room temperature and heat treated for stabilization of the PSi structure. The picture of the electrochemical bath and the prepared PSi are shown in fig 3.2 and 3.3 respectively.



**Fig 3.2. Photograph of the electrochemical bath used for PSi fabrication**

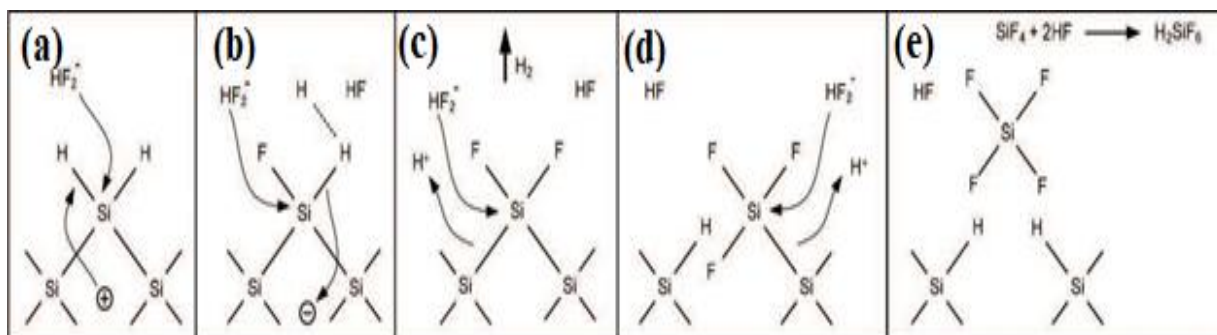


**Fig 3.3. Photograph of fabricated macro and nano-PSi**

### **3.2 MECHANISM OF PSi FORMATION**

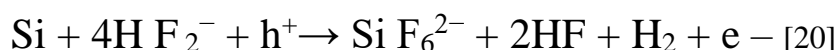
The silicon atom dissolution in the anodic etching mechanism can be controlled by current or the voltage of the cell [20]. Generally the process involves liberation of  $H_2$  bubbles that generally gates attached to the surface of the Si wafer that prevents the electro-active species to have any action on the surface. This makes the addition of surfactants like methanol, ethanol or DMF absolutely necessary as these surfactants allows electrolyte to penetrate into the pores by minimization of  $H_2$  bubble liberation.

The removal of silicon atom from the wafer surface is a charge transfer mechanism that can take place in two regimes, namely tetravalent regime that leads to electro-polishing and the divalent regime that leads to porosification. The divalent regime is depicted in fig 3.4.



**Fig 3.4. Divalent regime of dissolution of Si atom in HF based electrolyte [59].**

A silicon sample surface, immersed in HF based electrolyte is generally passivated by Si-H bonds [20]. And since the Si-F bond is much stronger than Si-H bond, any surface silicon atom attached to F is immediately removed from the surface and the surface is again passivated by H atom [20]. A hole, within the silicon material, travelling to the interface of the silicon and HF based electrolyte onsets the dissolution of the surface atom. Since Si-H bond are unpolarised due to close electronegativity values for Si and H, the  $\text{HF}_2^-$  ion present in the HF based electrolyte is not able to attack the Si-H bonds on the wafer surface. The presence of a hole makes  $\text{HF}_2^-$  ion attack the Si-H bond and replace it with Si-F bond. The Si-F bond being highly polarised due to huge electronegativity difference of Si and F, another  $\text{HF}_2^-$  ion attacks the Si atom and releases a  $\text{H}_2$  molecule. The polarization effect of the Si-H bond lowers significantly the electron density of the Si back bond and causes the dissolution of the loosely bounded Si atom by the HF based electrolyte. On removal of Si atom from a flat wafer surface introduces a small micro-rough area in otherwise smooth wafer surface. This micro-rough area changes the electric field distribution on the surface and increases the probability of the presence of hole in this rough area leading to more dissolution of Si atom in this area in comparison to other smooth areas, leading to pore formation. The chemical equation depicting the PSi formation is shown below.



### 3.3 CHARACTERIAZATION

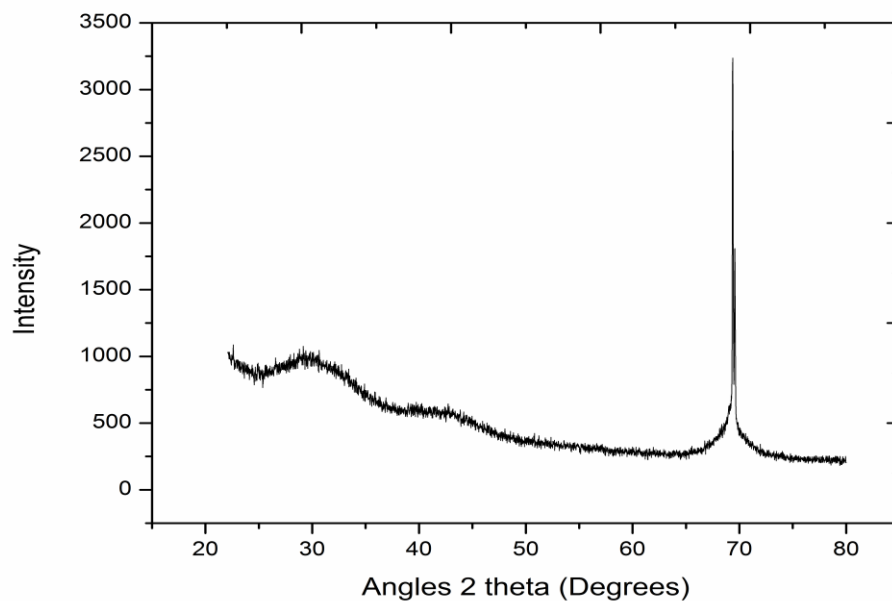
The structural and morphological analysis of the sample prepared were done in this work using XRD (Bruker, D8 Advance Diffractometer), FE-SEM (FEI, INSPECT F50). Both nano and macro PSi samples were prepared in this work and a

short discussion on the comparison of the morphological difference between the two structures is done.

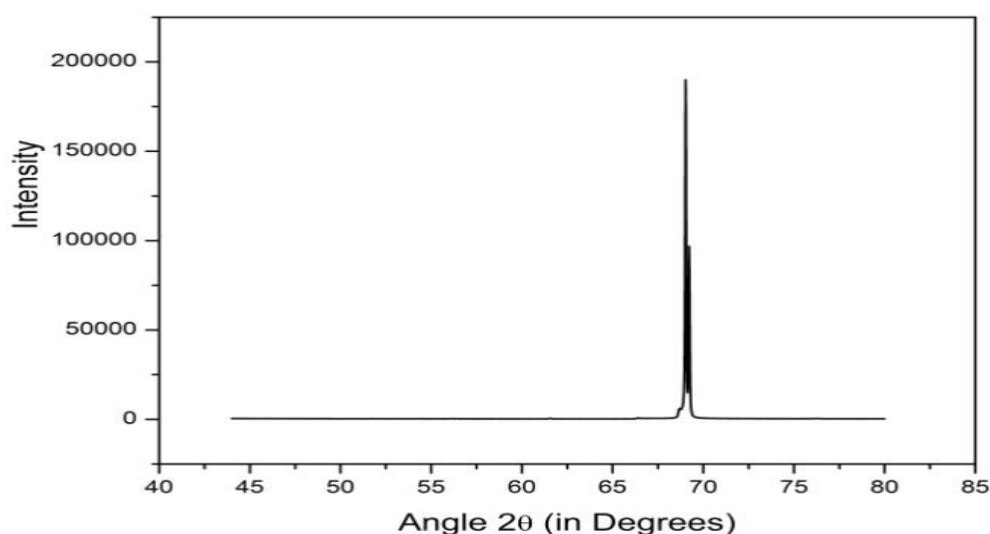
### 3.3.1 XRD

To perform the XRD, the  $2\theta$  value of the sample is varied from angle of  $20^\circ$  to  $80^\circ$  for nano PSi samples and from  $45^\circ$  to  $80^\circ$  for macro PSi samples. Step-size of  $0.02^\circ$  together with a scan-speed of 0.1s is used for the experiment. Source used for XRD is  $\text{CuK}\alpha$  ( $\lambda=1.5418\text{\AA}$ ), while the experiment was performed maintaining generating parameters of 40KV and 40mA.

For nano-PSi and macro-PSi sample, the characteristic peak, at angle  $\sim 69.9^\circ$  is observed as can be seen in fig 3.5 and 3.6 respectively, which is characteristics of P-type Si material of  $\langle 100 \rangle$  orientation [21]. On further analysis of the XRD graphs of nano and macro-PSi samples a more drastic and higher peak is observed for macro samples in comparison to the nano samples. Thus more crystalline characteristics in the case of macro-PSi samples relative to nano-PSi samples can be inferred from this observation. Moreover a prominent amorphous hump is observed in the XRD graph of nano-PSi sample at an angle around  $27^\circ$  owing to nano hillock like structures (later revealed by the FESEM image). Such humps are not observed in the XRD data of macro-PSi samples.



**Fig 3.5. X-Ray diffraction pattern for nano-PSi sample**



**Fig 3.6. X-Ray diffraction patter for macro-PSi sample**

### 3.3.2 FESEM

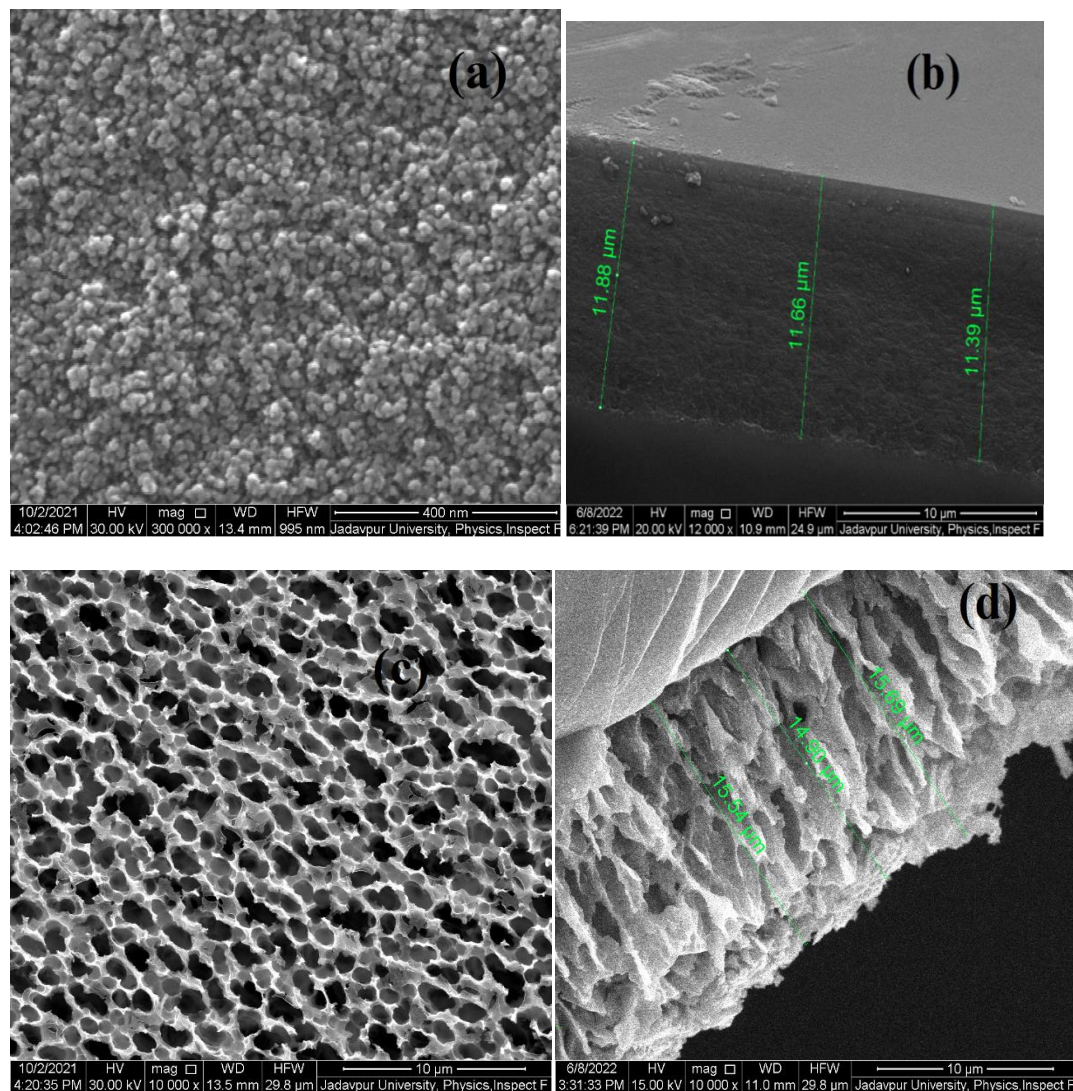
The cross-sectional and top view FESEM of both nano and macro PSi samples were carried out, for different etching time (as per requirement), keeping the current density of each sample constant. A striking difference in morphology of nano and macro PSi samples was observed with varying etching time, which is discussed later in this work. In this chapter the basic morphological difference of macro and nano-PSi samples are concentrated upon.

Fig 3.7 shows the top view and cross-sectional FESEM images of both nano and macro PSi samples.

For the top surface view of the prepared nano-PSi samples, as observed from the FESEM images in fig 3.7 (a), “hillock-like” nano structures can be clearly seen. The top surface morphology for macro-PSi samples are observed to be much different from that of nano-PSi samples, as can be seen in fig 3.7 (c). The porous structure of the macro-PSi samples is seen to be increased many-folds and much more prominent in comparison to nano-PSi, with well-formed pores and definite edges being clearly visible in the case of macro-PSi. Many-fold increase in the porous structure is evident in macro-PSi samples in comparison to nano-PSi samples, as observed from fig 3.7.



The comparison of cross-sectional FESEM images of nano and macro-PSi shows striking difference. The layer thickness for macro sample is observed to be much more than that for nano samples, prepared under same fabrication parameters and same etching time. The layer thickness for nano sample is in the range of 11-12 $\mu\text{m}$ , whereas that for macro samples are observed to be in the range of 15-16 $\mu\text{m}$ , as shown in fig 3.7 (b) and (d) respectively. Moreover, in case of macro PSi samples well form pour tunnels are distinctly visible in the cross-sectional FESEM image while no such well-formed structures are visible in case of nano-PSi samples.



**Fig 3.7. (a) FESEM Top View Image of Nano-PSi of etching time 30min. (b) cross-sectional view of Nano-PSi of etching time 30min. (c) FESEM Top View Image of Macro-PSi of etching time 30min. (d) Cross-sectional view of Macro-PSi of etching time 30min.**

### 3.4 APPLICATIONS OF POROUS SILICON

PSi has gained immense scientific attention on discovery of photoluminescence, as previously discussed. Since then PSi has found profound and diverse applications in the field of optics and optoelectronics, Electronics as well as in the field of medicine and diagnostics [20]. Even though previously optical applications of PSi has predominated its area of research and applications, but in later years the material has also found applications in areas of diagnostics, medicine, cosmetics and nutrition [20]. In-fact, instead of the conventional chip based structure of PSi, independent structures like PSi powders has been put into applications [20]. This section deals with certain prominent applications of PSi and PSi based structures.

As said before, unlike bulk silicon, which have indirect band-gap, quantum confinement effect of PSi makes possible radiative transition that finds use of PSi in the fabrication of light emitting devices, working throughout infra-red, visible and ultra-violet spectrum. In-fact success has been achieved in fabrication of integrated PSi LEDs [20]. PSi also finds use in fabrication of optical wave-guides with low porosity and high-porosity layers. In such structures the low porosity layer traps the light owing to its higher refractive index in comparison to low refractive index of high porosity layer [20]. Depending upon the variation of porosities of different layers multiple propagation modes can be made possible in such PSi based structures.

Some major electronic application of PSi involves its use as gas-sensing material, anti-reflection coating in solar cells, it finds use as component in lithium-ion batteries and as a gettering agent [20]. Owing to its huge surface area for absorption, PSi provides a great material for gas sensing. In-fact PSi has been used to sense more than fifty chemical species, by alteration of its electrical and optical properties. Due to its tuneable refractive-index, PSi is used as anti-reflection coatings in solar cells. PSi acts as anode in lithium-ion batteries and together with providing more capacity in comparison to other conventional anodes, it provides mechanical stability by accommodating the stress due to expansion and contraction. Again due to its huge

surface area, PSi is used for the removal of impurities from active regions of electronic devices.

Wafer based PSi as well as PSi based independent materials finds use in medical and diagnostics applications of PSi [20]. Due to its immensely high loading capacity and biocompatibility, PSi finds use in the field of biosensors for the sensing of multiple enzymes, proteins and antibodies [20]. Its tuneable porosity, loading capacity and biocompatibility makes it a natural choice as a delivery agent in effective drug delivery [20]. Moreover desirable properties of PSi as natural biodegradable materials find use in the field of tissue engineering [20].

### **3.6. CONCLUSION**

PSi synthesis process and formation mechanism has been elaborated on and the process of electro-chemical etching, used in this work for effective fabrication of PSi has been discussed. Next the characterization of the sample is carried out using XRD and FESEM for obtaining both top view and cross-sectional images of the both nano and macro-PSi samples. Later, owing to some interesting properties exhibited by PSi, some important applications of PSi and PSi based structures have been discussed.

On analysis of the XRD data, it was found that a more crystalline nature of the remanent skeleton silicon structure of macro-PSi sample is present which is depicted by its sharper peaks in comparison to nano PSi samples, that in spite of being basically crystalline, shows an amorphous hump in its XRD values. The FESEM images reveal a striking difference in the morphology of nano and macro-PSi samples. Hillocks like nano structures are clearly visible in nano PSi top view FESEM image, while well-formed pores can be seen in FESEM image of macro PSi. In cross-sectional view well-formed porous channels in macro samples are in sharp contrast to the cross-sectional view of nanoPSi.

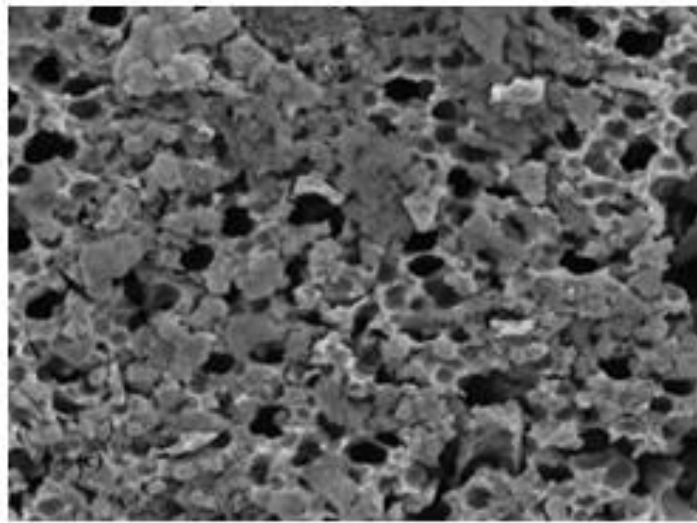
This chapter establishes PSi as a great sensing material. Its huge loading capacity, biocompatibility, exhibition of wide band of photoluminescence, together with other interesting optical and electrical properties makes it a natural choice for fabrication of huge variety of sensors, including great biosensing abilities. Moreover easily

tuneable porosity, pore size and hence the loading capacity of PSi making sensing mechanism by it flexible as a sensing and transducing material.

# Reference

1. H. A. Hadi, T. H. Abood, A. T. Mohi, M. S. Karim, "Impact of the etching time and current density on Capacitance-Voltage characteristics of P-type of porous silicon," *World Scientific News*, vol. 67, no. 2, pp. 149-160, 2017.
2. S. J. Kim, B. H. Jeon, K. S. Choi, N. K. Min, "Capacitive porous silicon sensors for measurement of low alcohol gas concentration at room temperature," *J Solid State Electrochem*, vol. 4, pp. 363-366, 2000.
3. D. Basu, T. Sarkar, K. Sen, S. M. Hossain, J. Das, "Multi-parametric Optical Glucose Sensor based on Surface Functionalized nano-Porous Silicon," *IEEE Sensors Journal*, vol. 18, no. 24, 2018.
4. R. C. Anderson, R. S. Muller, C. W. Tobias, "Investigations of the Electrical Properties of Porous Silicon," *J. Electrochem. Soc.*, vol. 138, no. 11, pp. 3406-3411, 1991.
5. M. J. Hussein, W. M. M. Yunus, H. M. Kamari, A. Zakaria, H. F. Oleiw, "Effect of current density and etching time on photoluminescence and energy band gap of p-type porous silicon," *optical and quantum electronics*, vol. 48, no. 194, pp.2-8, 2016.
6. M. H. F. Suhaimi, M. Rusop, S. Abdullah, "Porosity and thickness effect of porous silicon layer on photoluminescence spectra," *International Conference on Technology, Informatics, Management, Engineering & Environment*, 2013.
7. A. Mortezaali, S. R. Sani, F. J. Jooni, "Correlation between porosity of porous silicon and optoelectronic properties," vol. 1, no. 3, pp. 293-299, 2009.
8. H. Saha, S. K. Dutta, S. M. Hossain, S. Chakarborty, A. Saha, "Mechanism and Control of Formation of Porous Silicon on p- Type Si," *Bull. Mater. Sci.*, vol. 21, no. 3, pp. 195-201, 1998.
9. T. Sarkar, D. Basu, N. Mukherjee, J. Das, "Comparison of Glucose Sensitivity of Nano and Macro Porous Silicon," *Materials today proceedings.*, vol. 5, no. 3, pp. 9798-9803, 2018.
10. X. Yang, F. Xi, X. Chen, S. Li1, X.Wan, W.Ma, P. Dong, J. Duan, Y. Chang, "Porous Silicon Fabrication and Surface Cracking Behavior Research Based on Anodic Electrochemical Etching," *FUEL CELLS 00*, vol.0000, no. 0, pp. 1-6, 2020.
11. H. Foell, M. Christophersen, J. Carstensen, G. Hasse, "Formation and Application of Porous Silicon," *Materials Science and Engineering R Reports*, vol. 39, no. 4, pp. 93-141, 2002.
12. P. Sarafis, E. Hourdakakis, A. G. Nassiopoulou, "Dielectric Permittivity of Porous Si for Use as Substrate Material in Si-Integrated RF Devices," *IEEE transactions on electron devices*, vol. 60, no. 4, pp. 1436-1443, 2013.
13. G. N. Tovar, D. R. García, A. W. Arce, G. Palestino, S. R. Mendoza, "Mesoporous Silicon Particles Favor the Induction of Long-Lived Humoral Responses in Mice to a Peptide-Based Vaccine," *Materials*, vol. 11, no. 1083, 2018.
14. Y .M. Spivak, S. V. Mjakin, V. A. Moshnikov, M. F. Panov, A. O. Belorus, A. A. Bobkov, "Surface Functionality Features of Porous Silicon Prepared and Treated in Different Conditions," *Journal of Nanomaterials*, vol. 2016, DOI: <http://dx.doi.org/10.1155/2016/2629582>, 2016.
15. F. A. Harraz, A. A. Ismail, M. Faisal, S. A. Al-Hajry, M. S. Al-Assiri, "Organic analytes sensitivity in meso-porous silicon electrical sensor with frontside and backside contact," *Arabian Journal of Chemistry*, DOI: <http://dx.doi.org/10.1016/j.arabjc.2017.05.015>, 2017.
16. F. A. Harraz, "Porous Silicon Chemical Sensor and Bio Sensor: A Review," *Sensors and Actuators B:Chemical*, vol. 202, pp. 897-912, 2014.
17. E. A. Kabaa, S. A. Abdulateef, N. M. Ahmed, Z. Hassan, F. A. Sabah, "A Novel Porous Silicon Multi-ions Selective Electrode Based Extended Field Effect Transistor for Sodium, Potassium, Calcium and Magnesium Sensor," *Applied Physics AMterial Science and Processing*, vol. 125, no. 753, 2019.
18. P. Kumar, P. Huber, "Effect of Etching Parameter on Pore Size and Porosity of Electrochemically Formed Nanoporous Silicon," *Journal of Nanomaterials*, vol. 2007, DOI: 10.1155/2007/89718, 2007.
19. A. Ramizy, I. M. Ibrahim, M. A. Hammadi,"The Effect of Etching Current Density on Porous Silicon Fabricated by Electrochemical Etching Process," *International Journal of Scientific & Engineering Research*, vol. 7, no. 4, pp. 717-722, 2016.

20. F. Karbassian, "Porous Silicon", Intech Open, Chapter-1, 2018.  
<http://dx.doi.org/10.5772/intechopen.72910>.
21. W. S. Yan, D. Y. Wei, S. Xu, H.P. Ahou, " Highly doped P-Type nanocrystalline silicon thin films fabricated by low-frequency inductively coupled plasma without H<sub>2</sub> dilution." Journal of applied Ohysics, vol. 110, np. 6, 2011.



# Chapter-4

## **Chapter 4: Calmodulin Surface-Functionalized Porous Silicon based Calcium Detector**

---

Mineral ions in suitable concentration is essential for proper maintenance of life functioning. Calcium ion among them plays a very vital role. Calcium ion is the second most abundant ion and plays an essential role in cellular signaling process [1-4]. Moreover calcium regulates numerous cellular processes like skeletal and cardiac muscle excitation, blood coagulation and neurotransmission [5-6]. Abnormal calcium ion concentration in human serum is a clear indicator of numerous diseases. Increase in serum calcium level or hyper-calcemia, primarily indicates hyperthyroidism, hyperparathyroidism but mostly is found in case of malignancies [7]. Association of hyper-calcemia with lung cancer is quiet common; in fact it is the most prevalent metabolic anomaly accompanying malignancies [7-11]. In that case detection of calcium becomes vital for better prognosis of patients. Calcium detection techniques developed so far are chromatography technique [12], electrochemical technique [13,14], potentiometric technique [15-17] and spectroscopic techniques [18-21]. These processes though effective are costly and require complex instrumentations.

Calmodulin is prototypical calcium sensing protein [22-25]. Present in all eukaryotic cells, calmodulin regulates essential cellular processes [22,23]. Having the capability of calcium detection in biologically relevant concentration range, calmodulin also shows additional discrimination towards calcium ions [22-24]. Thus calmodulin surface functionalized porous silicon structure is effective in calcium binding.

As discussed previously, Porous silicon (PSi), being a promising new material has unique properties which find use in microelectronics [26]. Since the structure is porous, it provides huge surface area to volume ratio effective for absorption [27-29]. Due to quantum confinement effect exhibited by porous silicon, its direct and wide band gap finds huge utility as a sensor material [26]. Moreover the porosity and the pore size of PSi can easily be manipulated together with its easy and cheap process



of fabrication [28,30-34]. Furthermore the large surface area of PSi provides huge area of interaction for bio-molecules [35].

This chapter deals with the fabrication of macro porous silicon structure by electrochemical etching process [24,26-27]. Calmodulin protein is surface functionalized upon it by physisorption method [24]. Porous silicon facilitates huge increase in surface area for calcium absorption while calmodulin provides effective calcium binding sites. Besides being robust, the detector shows effective changes in optical parameters for calcium ions. The sensor thus fabricated was applied to different and composite cation solutions of physiologically relevant concentrations and several optical parameters such as reflectance, scattering loss, absorption loss and electrical parameters like current change with changing voltage, capacitance versus input voltage frequency were measured. The detector was found to exhibit significant change in the mentioned optical parameters for calcium ion, while remaining diminished responsive or unresponsive for other di-valent and mono-valent cations. Later a comparative study of the optical and electrical responses of is conducted, that may facilitate multi-parametric approach, providing enhanced sensitivity for any future work in this field.

## **4.1 SAMPLE PREPARATION**

### **4.1.1 Materials Used**

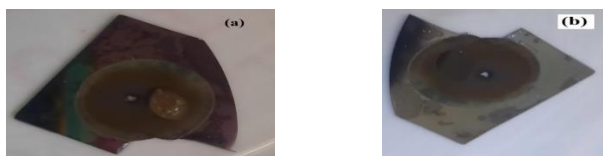
Silicon wafer (P-Type, <100>, resistivity(10-20 $\Omega$ cm), Hydrofluoric acid (HF, 48%), sulphuric acid (H<sub>2</sub>SO<sub>4</sub>, 98%), Ethanol (C<sub>2</sub>H<sub>5</sub>OH, 99.9%), Calmodulin (CaM) Bovine (Lyophilized powder,  $\geq$ 98%), 2-Amino-2 (Hydroxymethyl)-1,3-Propanediol (Tris buffered saline (TBS)), Calcium Chloride (CaCl<sub>2</sub>, 99.9%), Magnesium Chloride (MgCl<sub>2</sub>, 99.9%), Sodium Chloride (NaCl, 99.5%), Manganese Chloride (MnCl<sub>2</sub>, 99.9%), Potassium Chloride (KCl, 99%), Ultrapure water (deionized (DI) water  $\sim$ 18M $\Omega$ cm resistivity) (Milipore Co.). The silicon wafer was obtained from Macwin. The chemicals were obtained from Sigma-Aldrich. India. Distilled water was also used.

#### 4.1.2 Fabrication of Surface-Functionalized Detecting Platform

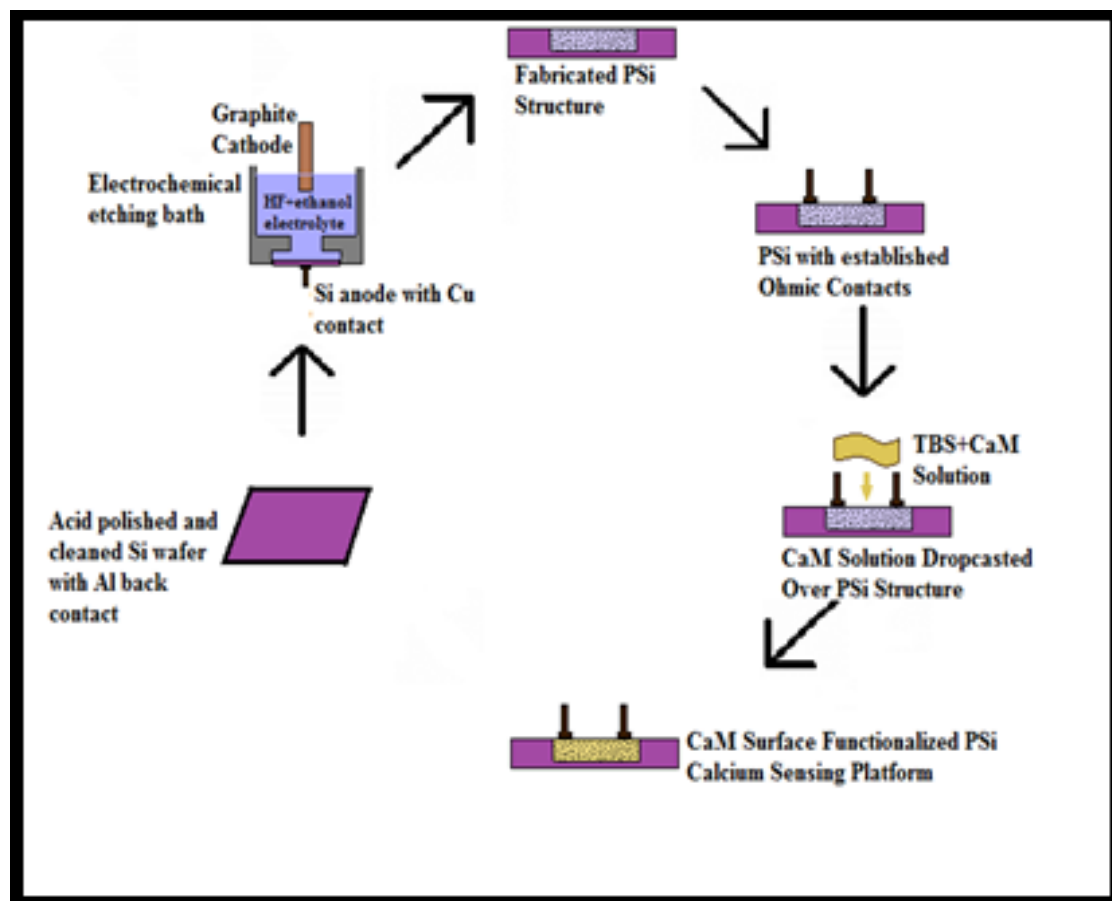
As discussed in the previous chapter, porous silicon (PSi) structure was fabricated upon single crystalline P-type <100> silicon wafers of resistivity 10-20 $\Omega$ cm. The wafers are cut into the dimension of 1.5 $\times$ 1.5 cm<sup>2</sup>, ohmic contact was then established with aluminium on the dorsal surface. Electrochemical etching of these silicon wafers is performed in any HF resistant cell such as Teflon with graphite acting as cathode and the silicon wafer itself as anode. Electrolyte of 48% HF and >99% N, N Dimethyl formamide (DMF) in the ratio 1:1 is used. A constant current density of 15mA/cm<sup>2</sup> is used for 20 minutes to perform the etching process. The PSi sample thus prepared is washed multiple times with deionized water and dried at room temperature. The prepared PSi is then subjected to heat treatment, for thermal stabilization of the structure, by annealing in a furnace at 450<sup>0</sup>C for 45 to 50 seconds. A detailed process analysis, together with the photograph and schematic representation of the etching cell has been discussed in the previous chapter.

Preparation of calmodulin (CaM) solution is performed by diluting in Tris-buffered saline (TBS) solution. CaM solution of 1mg in 1ml of TBS solution was prepared by use of magnetic stirring at 1900 rpm for 10 minutes. The pH of the CaM solution is maintained at 7.6. This solution is drop casted upon the PSi detector surface. CaM immobilization on the sensor surface is done by physisorption method. The sensor is incubated at 4<sup>o</sup>C for 18 hours for complete CaM absorption by the PSi structure. Image of drop-casted CaM solution upon PSi detector surface is shown in figure 4.1. The sensor is then rinsed with deionized water to remove excess CaM from its surface; it is then dried at room temperature. The schematic representation of the fabrication and surface functionalization process is depicted in figure 4.2.

0.1mM solution of Ca<sup>2+</sup>, Mg<sup>2+</sup>, Mn<sup>2+</sup>, Na<sup>+</sup> and K<sup>+</sup> ions were prepared in 0.05M TBS solution by magnetic stirring at 1900 rpm for 10 minutes. The pH was maintained at 7.6.



**Fig 4.1. Photograph of PSi surface (a) after CaM dropcasting. (b) After incubation for 20hrs.**



**Fig 4.2. Schematic diagram of the fabrication steps of CaM-Functionalized PSi Calcium detecting platform.**

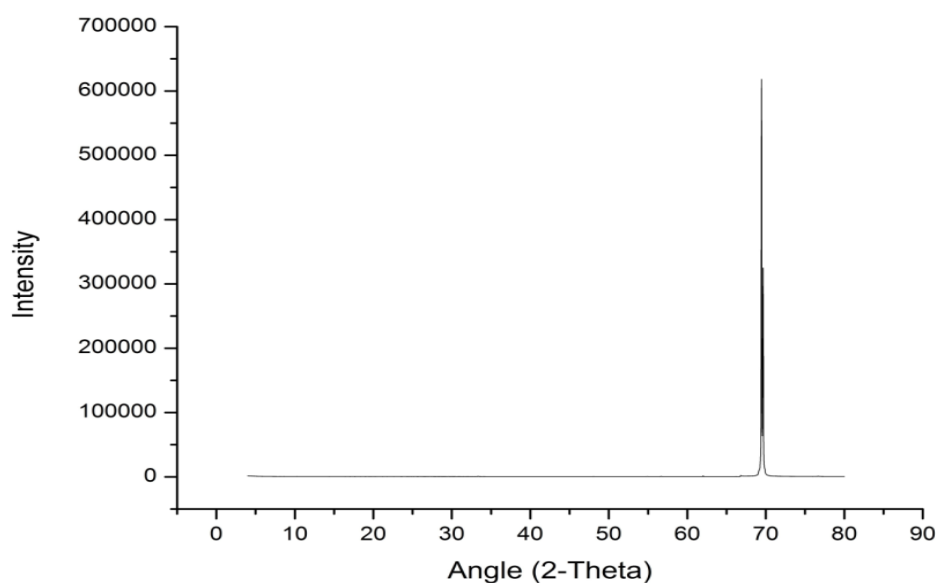
## 4.2 STRUCTURAL CHARACTERIAZATION

The structural characterization of the CaM surface-functionalized PSi based calcium detector sample is done by performing XRD study, FESEM imaging and FTIR spectroscopy, to establish successful attachment of CaM on PSi surface.

### 4.2.1 XRD.

To perform the structural investigation of the sensor prepared detector platfoerm, XRD (Bruker D8 Advance Diffractometer) was performed of the sensor by varying  $2\theta$  value for the sample within an angle limit of  $10^0$  to  $85^0$ , using a step size of  $0.02^0$  and at a scan speed of 0.1s. Source of  $\text{CuK}\alpha$  ( $\lambda=1.5418\text{\AA}$ ) is used for

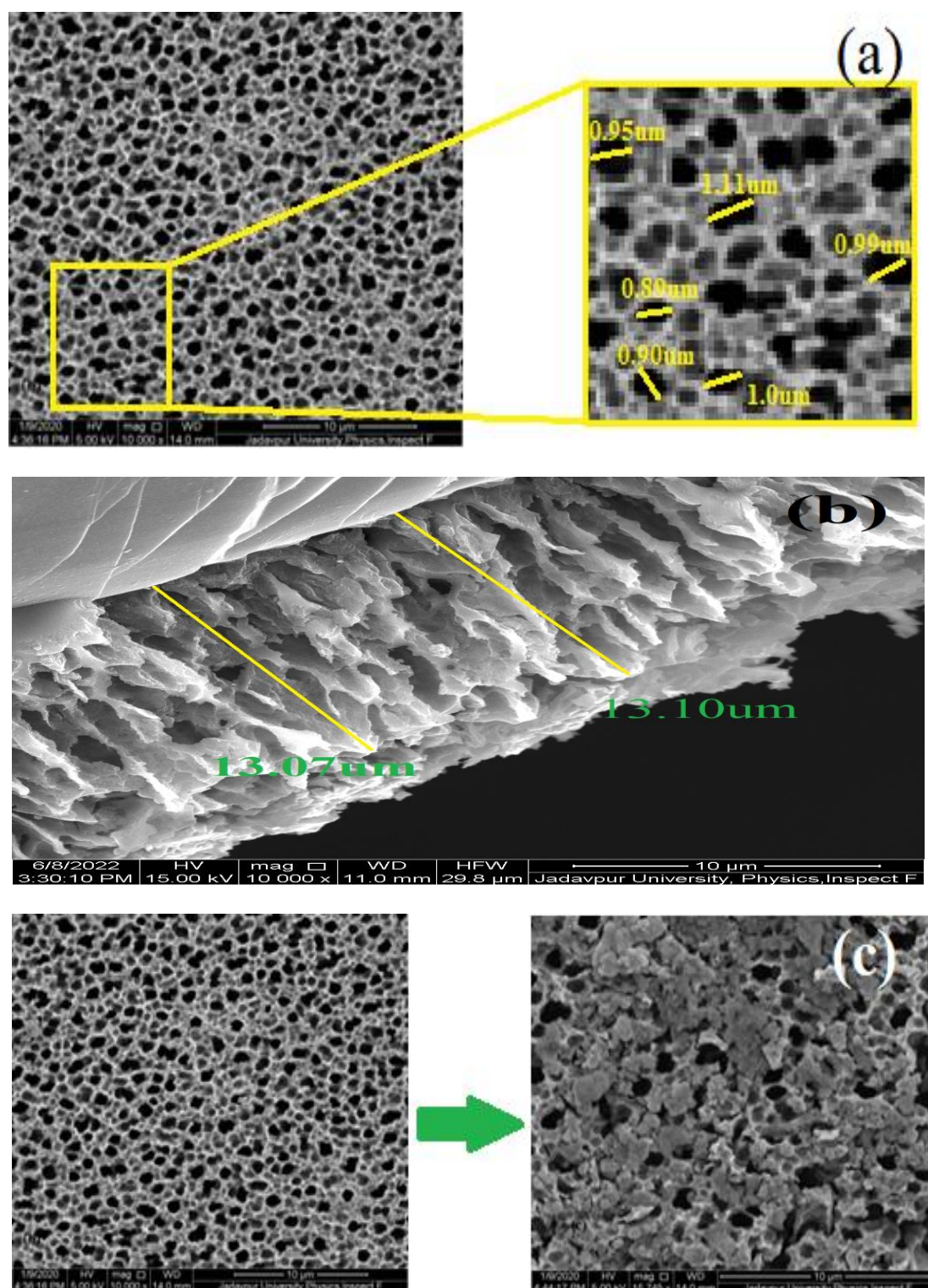
XRD and the generating parameters of 40KV and 40mA were used. As shown in Fig 4.3, the peaks were found at  $\sim 69.9^\circ$ , characteristic of silicon samples, as discussed in details in the preceding chapter. As for macro-PSi samples, a very sharp peak is observed which proves that after porosification, the skeleton silicon structure retains the crystalline nature.



**Fig 4.3. X-Ray Diffraction pattern for macro PSi.**

#### 4.2.2 FESEM

The morphology of the sample prepared was investigated by FESEM (FEI INSPECT F50). Figure 4.4 (a) focuses on the pore diameter range of the macro-PSi sample prepared and the diameters were found to be within the range of 0.89-1.11 $\mu\text{m}$ . The overall morphology of the macro PSi sample prepared shows well defined pore formation within remnant skeleton silicon structure. A cross-section FESEM imaging of the sample shown in figure 4.4 (b) shows the cross-sectional view of the prepared PSi layer to be around 13.10 $\mu\text{m}$ . Figure 4.4 (c) shows the PSi surface before and after CaM surface-functionalization and absorption. Clustered CaM molecules can be seen attached to the macro PSi sensor surface.



**Fig 4.4. (a) The focused FESEM image showing pore diameter of the macro-PSi sample. (b) Cross-sectional FESEM image of prepared macro-PSi. (c) Macro-PSi sample surface, before and after CaM absorption.**

### 4.2.3 FTIR Spectroscopy

The FTIR spectra of the CaM surface functionalized PSi surface is shown in figure 4.5. Since CaM consists of amide I and amide II regions [36], sample shows absorption due to amide, depicted in peak centered at  $1644\text{cm}^{-1}$  [36-38]. Absorption peak at  $1465\text{cm}^{-1}$  is due to C-H bending of the alkane group present in CaM molecule [37]. In side PSi structure, numerous Si-O bridges are formed, owing to the stretching of oxygen atom within the bridge structure peak is observed at  $1056\text{ cm}^{-1}$  [39]. A peak shift to  $1060\text{ cm}^{-1}$  is possible with increase in oxygen content [39]. Moreover, the absorption band of range between  $800\text{-}1260\text{ cm}^{-1}$  depicts different peaks due to  $\text{SiO}_2$  and peaks due to residual organic groups [40]

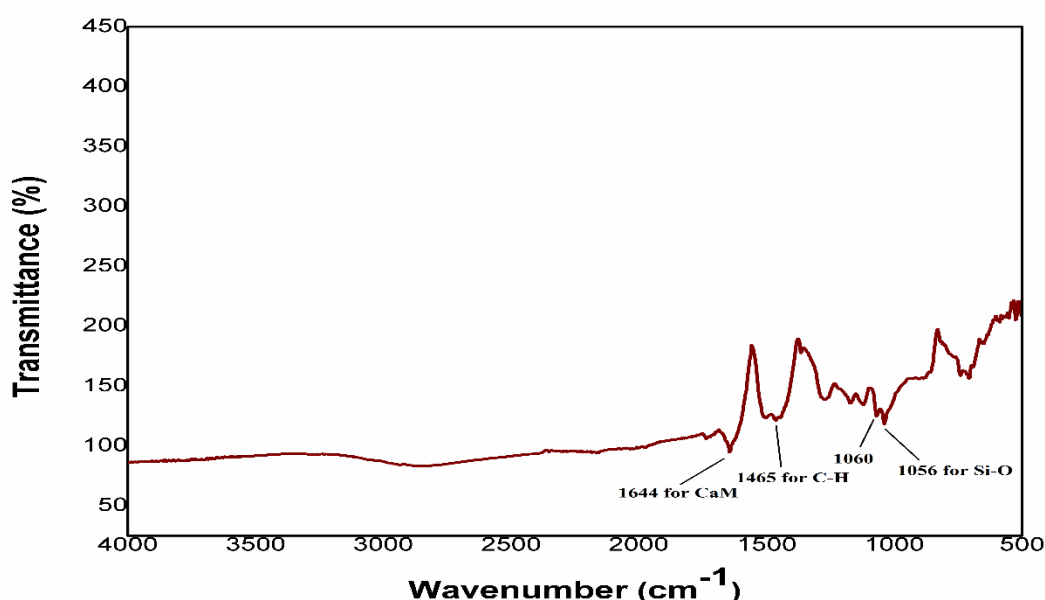


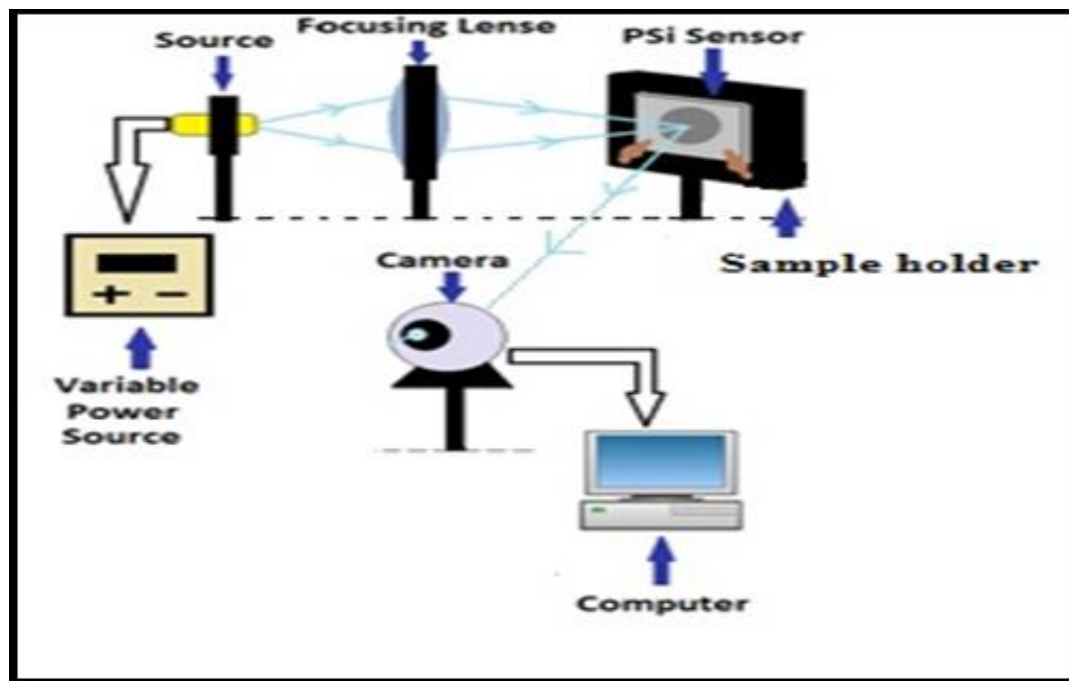
Fig 4.5. FTIR spectra of CaM functionalized macro PSi sample.

## 4.3 OPTICAL DATA ACQUISITION SETUP

The optical data is obtained from an optical breadboard arrangement as shown in figure 4.6. White light (commercially available) together with a variable power supply has been used as the source. The power supply to the light source is varied to a fixed intensity which is maintained throughout the experiment. Convex lens arrangement has been used to maintain a spot size of approximately  $0.4\text{cm}^2$ . The sensor is mounted on a holder at an angle of  $30^\circ$  to the incident beam, while the reflected beam from the sensor is obtained on a screen. A commercially available



standard webcam is employed to obtain the image of the reflected spot. Image processing software is then used on the acquired image to measure the different optical parameters namely reflected intensity, scattering loss and absorption loss.



**Fig 4.6. Schematic diagram of optical data acquisition setup.**

#### 4.4 OBTAINING AND PROCESSING OPTICAL DATA

The CaM surface functionalized detector is mounted on the holder, white light is made to fall on the detector surface and image of the reflected spot is obtained, without any ionic solution incubation. This reading is treated as the basal or control reading for the experiment. The sensor is then incubated in turn in Calcium ( $\text{Ca}^{2+}$ ), magnesium ( $\text{Mg}^{2+}$ ), manganese ( $\text{Mn}^{2+}$ ), sodium ( $\text{Na}^+$ ), potassium ( $\text{K}^+$ ) and composite ionic solutions (the composite ionic solution consisting of 0.1mM solution of  $\text{Ca}^{2+}$ ,  $\text{Mg}^{2+}$ ,  $\text{Mn}^{2+}$ ,  $\text{Na}^+$  and  $\text{K}^+$  ions mixed together in 0.05M TBS solution) and the reflected ray image from the detector for different ionic solutions were processed by the image processing software to calculate the change in the optical parameters. The data acquisition is done in ambient conditions.

The ionic solution incubation of the detector platform is done by drop casting 40 $\mu\text{L}$  of the respective ionic solution on the s detector surface. The ionic

solution is left for absorption on the detector platform for 30min after which the excess ionic solution is washed thoroughly using de-ionized water. The detector platform is then dried at ambient temperature for one hour and the completely dried sensor is mounted on the optical data acquisition arrangement for optical data recording. After every ionic solution incubation and data recording, the detector is rinsed with calcium chelating solution to remove calcium which is attached (if any in the case of other ionic solution incubation) to the detector surface, after which it is again washed with de-ionized water and dried at room temperature. The detector is then reused for the next reading.

The images of the reflected beam for different ionic solution incubation of the detector surface are processed by a software developed under MATLAB image processing environment to obtain the image intensity distribution matrix (IIDM). Change in the central peak intensity of the IIDM of the ionic solution incubated detector with respect to the control reading gives the change in specular reflectance. The mathematical expression for response due to change in specular reflectance is given by the following equations:

$$S_1 = ((I_0 - I_w) / I_0) \times 100 \% \dots\dots\dots(1)$$

Here,  $I_0 > I_w$ .

$I_0$  = Central peak intensity without ion incubation.

$I_w$  = Central peak intensity with ion incubation.

The full wave with at half maxima (FWHM) of the surface plots of IIDM is used to obtain the change in diffused reflectance which is attributed due to scattering of the reflected beam from the detector surface. Change in FWHM of the ionic solution incubated detector with respect to the control reading gives the scattering response. The mathematical expression for the same is given by the following equation:

$$S_2 = ((D_w - D_0) / D_0) \times 100 \% \dots\dots\dots(2)$$

Here,  $D_w > D_0$ .

$D_0$  = FWHM value without ion incubation.

$D_w$  = FWHM value with ion incubation.



The change in integral reflectance is obtained from the decrease in the volume of the 3D Gaussian model curve, obtained from IIDMs. The decrease in the volume under the curve, signifying the decrease in integral reflectance is due to the ion absorption by the detector surface. The mathematical expression for which is given by the following equation:

$$S_3 = ((A_o - A_w) / A_o) \times 100 \% \dots\dots\dots(3)$$

Here,  $A_o > A_w$

$A_o$  = Volume of the curve without ion incubation.

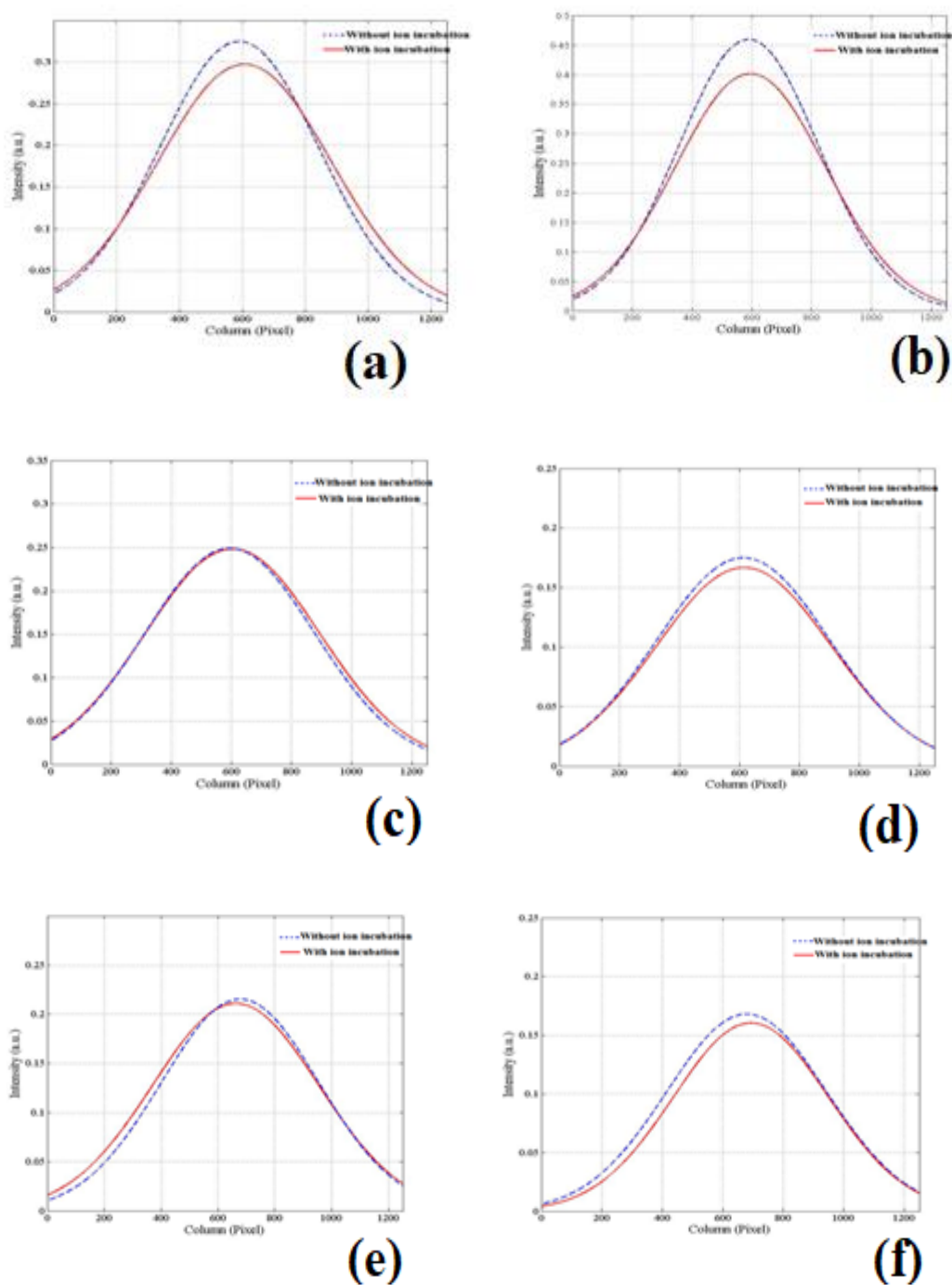
$A_w$  = Volume of the curve with ion incubation.

Thus the total response of the detector is given by:

$$S = S_1 \times S_2 \times S_3 \dots\dots\dots(4)$$

#### 4.5 OPTICAL RESPONSE

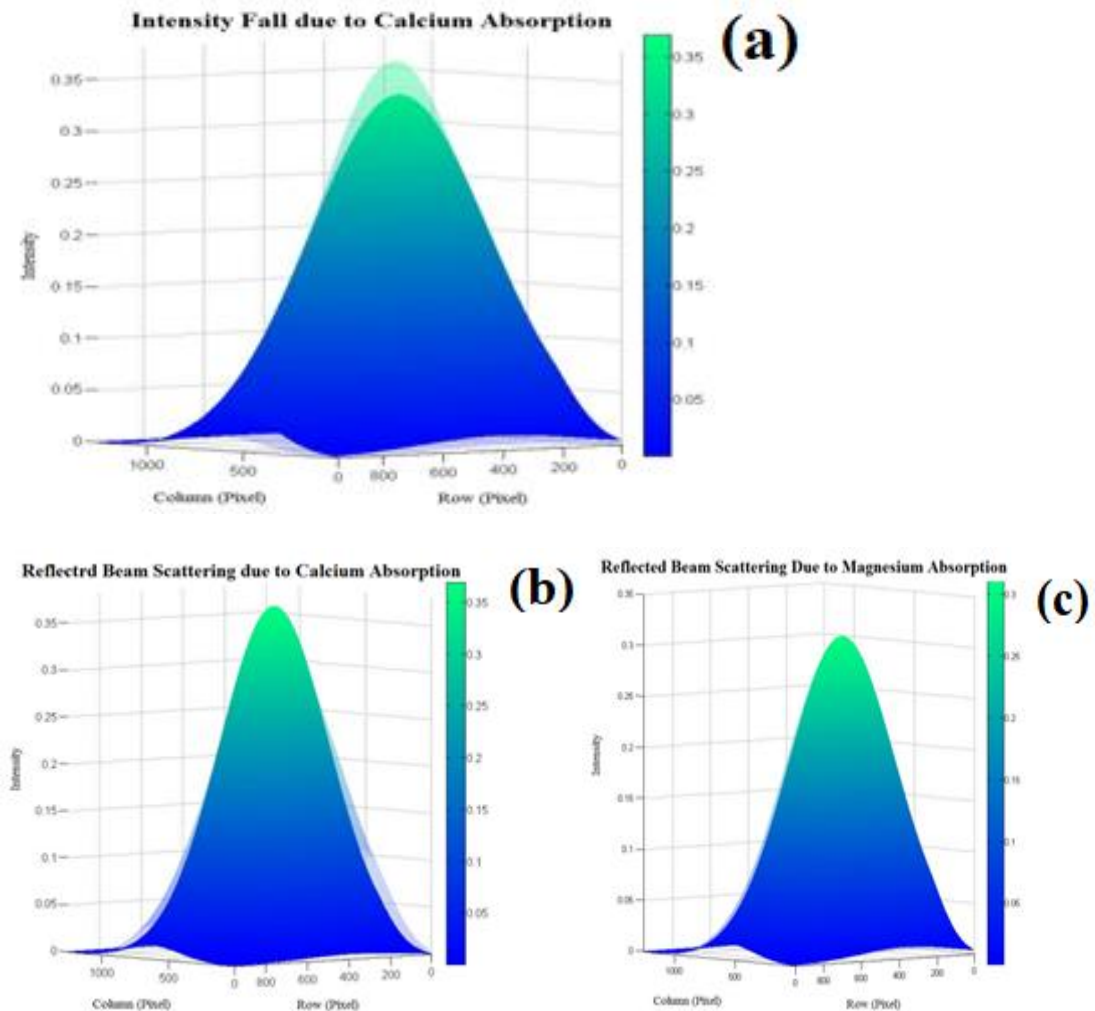
As mentioned previously, the detector surface was incubated with different bi-valent and mono-valent ionic solutions. White incident beam was made to fall upon the sensor surface and multiple optical parameters like specular reflectance, scattering loss and absorption loss were investigated. The detailed analysis of the reflected beam shows significant fall in reflected peak intensity for  $Ca^{2+}$  incubated detector surface, which is closely mimicked by the result for composite salt incubated detector surface, as evident from the difference of IIDMs values for incubated and non-incubated samples as shown in fig 4.7(a-b), whereas, negligible change is visible for the same when the detector is investigated with other ionic solutions as evident for fig.4.7 (c-f). The evident fall in intensity patterns as shown in Fig. 4.7 (a), as obtained from the 2-D Gaussian model of the IIDMs, the fall in peak intensity of the reflected beam for  $Ca^{2+}$  incubated detector surface is clearly manifested. The blue line representing non-incubated sample while the red one representing the incubated sample. Fig. 4.7 (c-f) also shows insignificant change in peak intensity of reflected beam when the detector is tested with other ionic solution.



**Fig 4.7. 2D Gaussian plots of IIDMs for (a)  $\text{Ca}^{2+}$ , (b) composite ionic solution, (c)  $\text{Mg}^{2+}$ , (d)  $\text{Mn}^{2+}$ , (e)  $\text{K}^+$  and (f)  $\text{Na}^+$**

A significant rise in the beam scattering or FWHM is observed in case of detector incubated with  $\text{Ca}^{2+}$  ionic solution, in comparison with other ionic solution incubation. Fig.4.8(a), (b) and (c) represent the 3-D Gaussian of the IIDMs.

Fig.4.8(a) represents a significant decrease in peak intensity for the detector incubated with  $\text{Ca}^{2+}$  ion. The shaded curve representing the detector output without ion incubation, while the solid one representing the output with ion incubation. Fig.4.8 (b) shows the increase in FWHM value, hence scattering for the detector with  $\text{Ca}^{2+}$  ion incubation, in comparison to the sensor's FWHM value when incubated with  $\text{Mg}^{2+}$  ion is depicted in Fig.4.8 (c). For Fig.4.8 (b) and (c) the solid curve represents the sensor output without ion incubation and the shaded one represents the output with ion incubation. As mentioned, the detector shows an appreciable amount of increase in scattering for  $\text{Ca}^{2+}$  ion incubation while showing almost negligible change for the same in case of  $\text{Mg}^{2+}$  ion and other bi-valent or mono valent ion incubation.



**Fig 4.8. (a) 3D Gaussian plots of Reflected beam intensity pattern before and after Calcium absorption, 3D Gaussian plot of beam scattering due to (b) Calcium ion absorption and (c) Magnesium ion absorption.**

The increase in incident beam absorption is calculated from the decrease in the integrated reflectance value which is the volume under the 3-D Gaussians. The decrease in integrated reflectance was found to be significant in case of  $\text{Ca}^{2+}$ , whereas, almost no change is observed for other ions. The response of the detector for composite ion incubation closely mimics the observation as seen for the  $\text{Ca}^{2+}$  ion incubation.

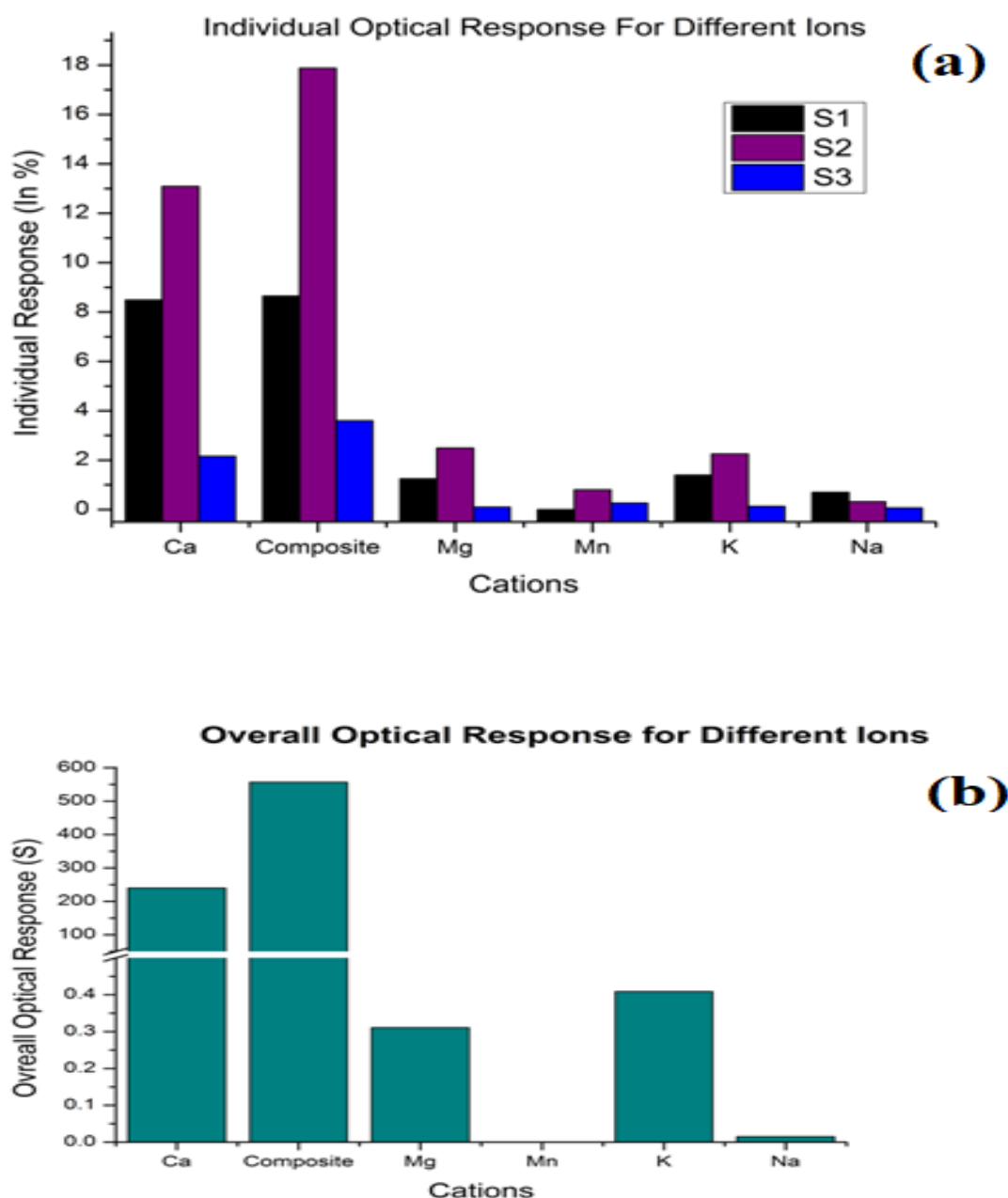
#### 4.6 DISCUSSION ON OPTICAL RESPONSE

The response parameters namely S1, S2, S3 are plotted individually along with the overall response of the detector towards individual ions, are shown in Fig 4.9(a), to depict the response of the detector for calcium ions in comparison with other ions. The overall response of the detector, which is the product of the individual responses, is shown in Fig 4.9(b). The plot shows significant selectivity of the detecting platform towards calcium ion in comparison with other mono-valent and bi-valent ions.

Effects such as absorption, specular and diffused reflectance affect the intensity and divergence of a reflected beam for a surface. For a composite detector surface the effective reflectance depends upon the contribution of individual reflectance of different components as shown in Bruggeman's approach [41]. Since the macro porous silicon detector surface is surface functionalized by CaM, we expect a relative increase in refractive index of the detector surface owing to the fact that the previously air filled pores of the macro porous silicon is now filled with CaM. Further, with calcium ion absorption the effective refractive index of the detector surface is expected to increase even more thus an increase in specular reflectance value is expected. This trend is valid for smooth reflecting surfaces.

In this work a decline in the specular reflectance value and an increase in diffused reflectance is noted. This is attributed to roughness of the detector surface. Porous silicon has in build surface roughness [28], which further increases with CaM surface functionalization. Moreover, selective calcium attachment to the detector surface increases the surface roughness even more and since for a rough surface, specular reflectance value decreases for any incident angle [28,42,43], a decrement

is observed in the specular reflectance which is due to multiple reflection, effect of shadowing or obscuring due to the roughness of surface [28, 43]. As divergence increases in the reflected beam with increase in surface roughness, scattering increases, thus increasing the diffuse reflectance value, which in turn increases the diffusion loss. Absorption loss is also observed to increase due to multiple reflections on a rough detector surface.

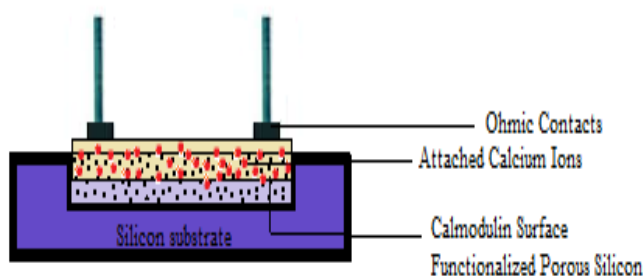


**Fig 4.9. Calibrated histogram plot depicting (a) individual response for the ions and (b) the overall response**

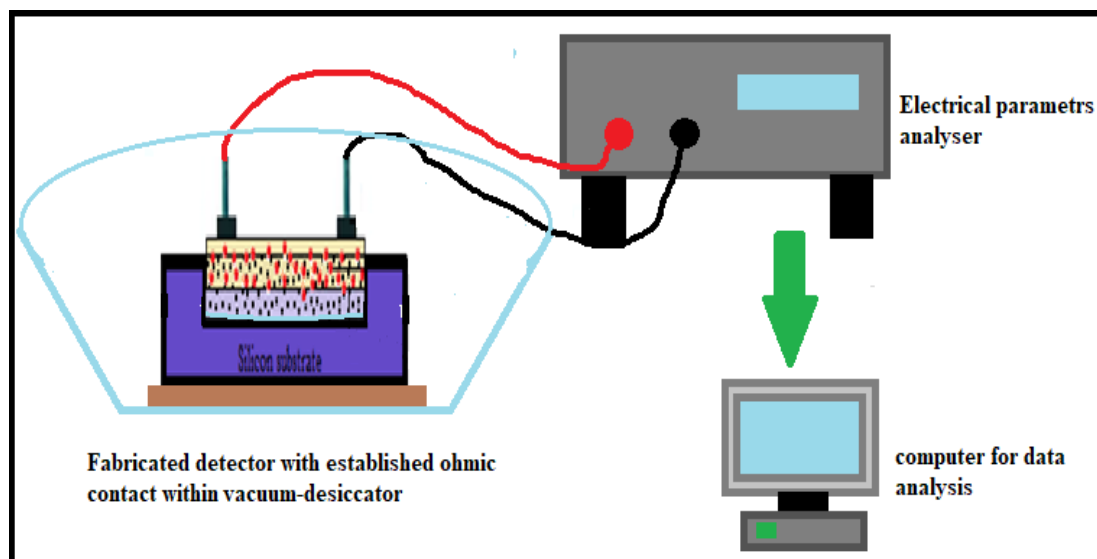
#### 4.7 ELECTRICAL DATA ACQUISITION SETUP AND PROCESSING

For the calibration of the electrical parameters of the fabricated detector sample. Ohmic contacts are established on the sample surface. For the establishment of ohmic contact on the detector surface, Silver-nitrite paste is applied on the detector surface, dried for 12 hrs at room temperature and then heat treated at 450°C for 45-50 seconds for stabilization of the PSi structure as well as for the stabilization of the ohmic contact established. Electrical continuity is checked multiple times over the ohmic contacts to ensure error free connection.

The electrical properties, namely conductive and capacitive property of the detector are performed using an electrical parameter analyzer (kethley) and a capacitive parameter analyzer under air- ambient condition. Two ohmic contacts were established upon the detector surface and the electrical parameter data were collected using a data acquisition system. The sensitivity of the detector is tested by monitoring the change in current (I) of the detector surface against increasing voltage (V) applied across the detector surface. The voltage was applied across the established ohmic contacts while the detector surface is incubated with respective cationic solution. The frequency (f) versus capacitance (C) data of the detector is monitored by applying voltage of varying frequency across the detector surface and respective capacitive readings were monitored, while the detector surface is incubated with respective cationic solutions. Both the electrical parameters were measured using ionic solutions of concentrations mentioned previously that is biologically relevant. The detector surface is also tested with the mixture ionic solution and the results were tallied accordingly. The fabricated detector with established ohmic contacts is shown in fig 4.10 and the electrical data acquiring arrangement is depicted in fig 4.11.



**Fig 4.10. Schematic representation of the fabricated detecting platform.**



**Fig 4.11. Schematic representaion of the electrical parameter analysing setup.**

The electrical response of the detector developed in this work is that of the I-V response and the C-F response of the detector for different cations. Mathematically the I-V response of the detector is obtained by using the following formula:

$$R_i = (I_i - I_{wi}) / (I_{wi}) \times 100\% \dots \dots \dots (5)$$

For the C-F response of the detector:

$$R_c = (C_i - C_{wi}) / (C_{wi}) \times 100\% \dots \dots \dots (6)$$

Where,  $I_i$  = Current value at 5V with ion incubation,

$I_{wi}$  = Current value at 5V without ion incubation.

$C_i$  = Capacitance value at min frequency with ion incubation,

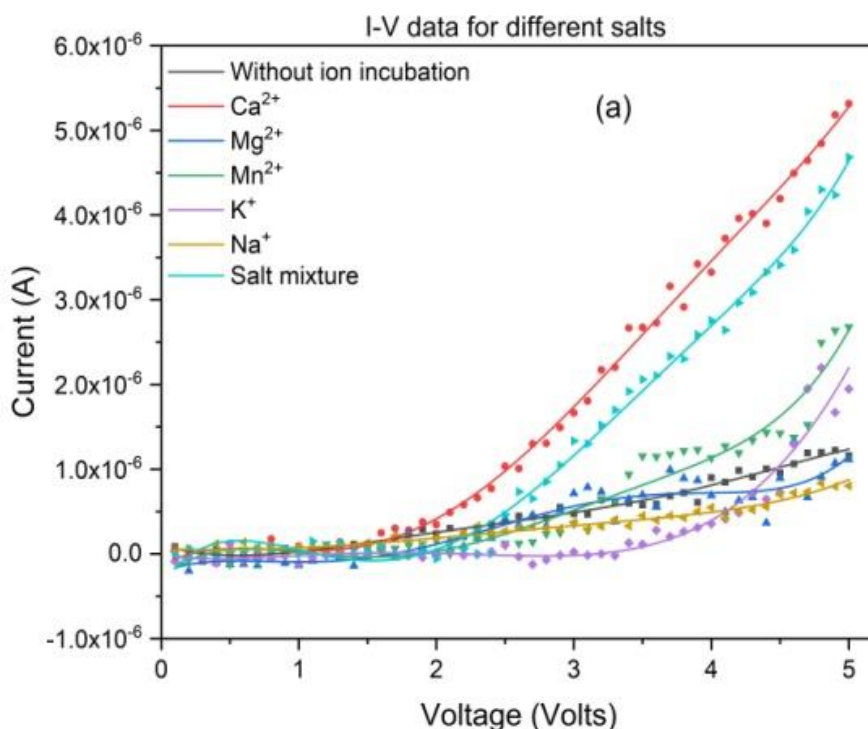
$C_{wi}$  = Capacitance value at min frequency without ion incubation.

#### 4.8 ELECTRICAL CHARACTERIZATION

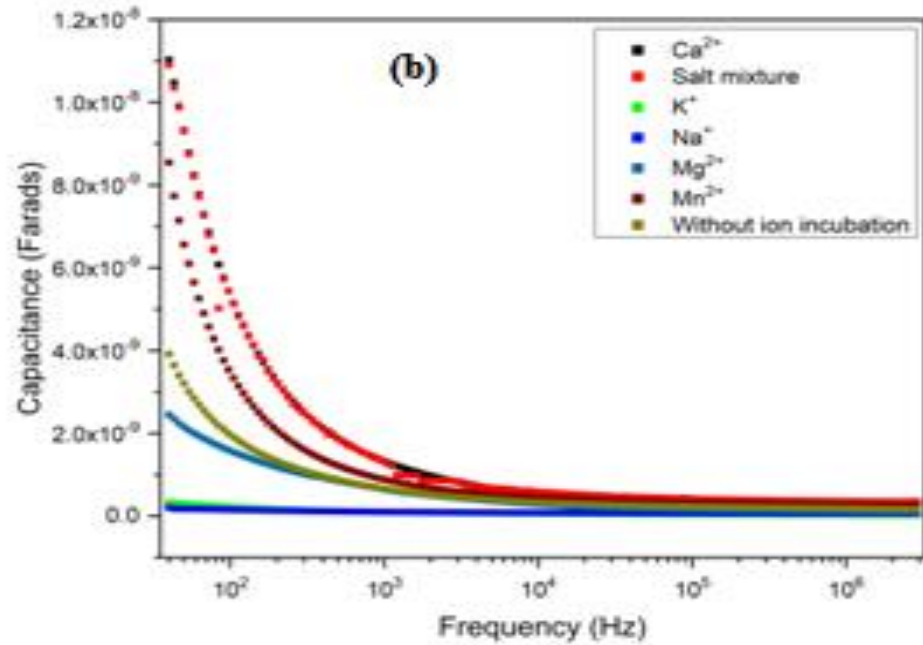
The electrical response of the detector is tested with and without  $\text{Ca}^{2+}$  ion incubation of the detecting platform. The current (I) response of the detecting platform is calibrated by simultaneous variation of the applied voltage (V) across it, within a fixed voltage range. As shown in fig 4.12 (a), the detector's current response is seen to be almost exponential, when the platform is incubated with  $\text{Ca}^{2+}$  ion, in the voltage range of 2.5-5V, clearly visible by the red line in the graph, in comparison to the response for the detector without ion incubation, depicted by the black line in the

same graph. The detector's selectivity towards  $\text{Ca}^{2+}$  ion is further tested by the current versus voltage characteristics of the detector for other bi-valent and mono-valent cations such as  $\text{Mg}^{2+}$ ,  $\text{Mn}^{2+}$ ,  $\text{Na}^+$  and  $\text{K}^+$  ions (those which are commonly present in human body). Fig 4.12 (a) shows no drastic current change of the detector for other ions. For the mixture ion solution, the detector's response closely mimics its response in the case of  $\text{Ca}^{2+}$  ion, as shown by the turquoise line in fig 4.12 (a).

The change in capacitance value for changing input voltage frequency is calibrated for the detector. As shown in fig 4.12 (b), the detector shows high capacitive response for  $\text{Ca}^{2+}$  ion incubation at low input voltage frequency, in comparisons to other ions. The Capacitance value however diminishes with increase in voltage frequency. For the mixture salt incubation the capacitance response of the detector closely mimics the response for  $\text{Ca}^{2+}$  ion, once again demonstrating the high selectivity of the detector towards  $\text{Ca}^{2+}$  ion among all the other ions under consideration.







**Fig 4.12. (a) Current (I) Vs Voltage (V) response of the sensing platform for different ion incubation and (b) Capacitance Vs Input voltage frequency response of the sensor for different ion incubation.**

#### 4.9 DISCUSSION ON ELECTRICAL RESPONSE

As discussed in the previous chapter, in disordered solids like PSi surface states and dangling bonds are inherently created during its fabrication [44]. As such the carrier transport can be explained through several mechanism such as hopping, Poole-Frenkle (P-F) and Trap-Assisted-Tunnelling (TAT) and in many cases all the mechanism attributes towards charge transport in such solids [44]. As stated in the previous chapter that conduction mechanism in PSi at lower field range (upto 1.5V) occurs due to hopping of thermally excited carriers between isolated defect states give an ohmic region in the conduction curve of PSi [44], this is exactly what is observed in fig 4.12 (a). As in higher electric field region P-F mechanism is dominant that suggest conductance of PSi to be proportional to  $V^{0.5}$  that occurs due to induced electric field that thermally excites carriers from their trap states that now takes part in conduction mechanism [44]. Moreover in higher electric field region, two level TAT mechanism predominates for carrier conduction [44]. Thus the

substantial increment in the current is attributed to the binding of the  $\text{Ca}^{2+}$  ion to CaM functionalized PSi detecting platform. Due to the binding affinity of CaM towards  $\text{Ca}^{2+}$  ion,  $\text{Ca}^{2+}$  ion gets attached to the detecting platform, which creates numerous more carriers to get trapped in the defect states of the PSi structure and on application of electric field these carriers conducts following the above mentioned mechanism, causing resistance to decrease drastically resulting in the exponential rise in the current value as shown in fig 4.12 (a). As extra carriers due to other ions are not being able to attach to the PSi based detector platform, the current value for other ions remains low unlike the case for  $\text{Ca}^{2+}$  [45]

The change in capacitance value in lower frequency range ( $10\text{-}10^5$  Hz) can be attributed to differential polarization effect [46, 47]. In lower frequency range of the input voltage the space-charge polarization and orientational polarization results in the change of dielectric constant, characteristics for nano-structured materials that leads to the change in the capacitance value [47, 48]. A nano-structured material like PSi possess a large number of interfaces and numerous defects within these interfaces. On application of external electric field, the change in the positive and negative space charge region that occurs through these defects produces dipole moment. The developed dipole moment is termed as space-charge polarization. The rotation of these dipole on application of external electric field results in orientational polarization, effecting the dielectric constant of the material, hence the capacitance value gets effected [46, 49]. In frequencies greater than  $10^5$ , the dipoles are unable to orient themselves as rapidly as the externally applied electric field changes, resulting in the nullification of the orientational polarization effect. At higher frequency only space charge polarization effect is present, which too saturates at even higher frequencies that explains the behaviour of the frequency versus capacitance graph in higher input voltage frequency range.

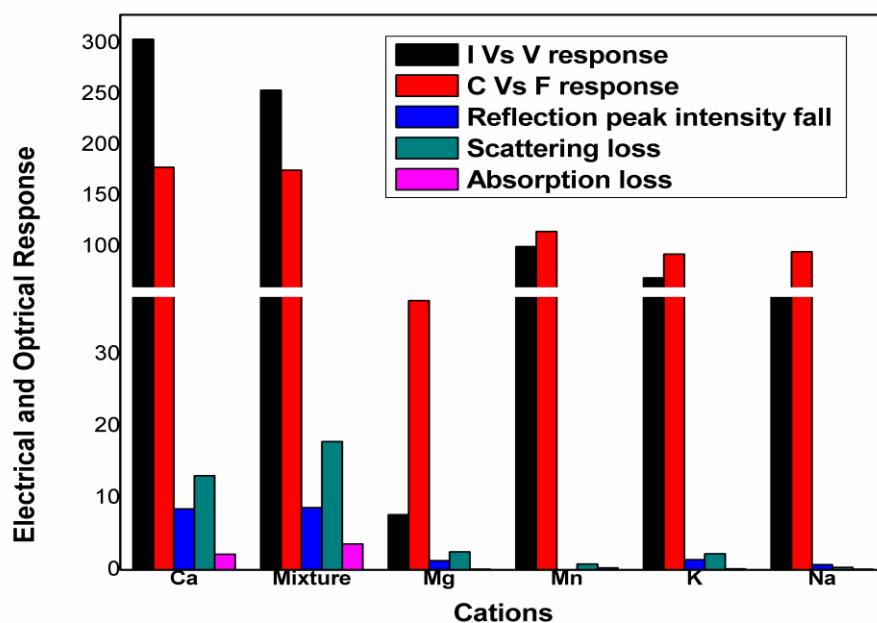
#### **4.10 COMPARATIVE STUDY OF OPTICAL AND ELECTRICAL RESPONSE**

In the Optical calcium detector the fall in reflection peak intensity, absorption loss and the scattering loss of the detector platform were under taken as parameters to study the response of the detector platform. The detector showed appreciable response and selectivity towards calcium ion. In the mentioned optical detector the

optical response, namely reflection peak intensity fall, scattering loss and absorption loss of the detecting platform was found to be 8.49%, 13.09% and 2.16% for calcium ion, 8.65%, 17.88% and 3.60% for mixture ion solution, 1.25%, 2.49% and 0.10% for Magnesium, 0%, 0.80% and 0.26% for Manganese, 1.40%, 2.25% and 0.13% for Potassium and 0.76%, 0.32% and 0.07% for sodium respectively.

The electrical response of the detector is obtained by calibrating the change in the I Vs V response of the detector as well as the C Vs F change of the detecting platform. The I-V response of the detector is found to be 303.84% for calcium ion, 253.84% for mixture ion solution, 7.69% for magnesium, 100% for manganese, 69.3% for potassium and 42.3% for sodium. The C Vs F response of the detector shows a response of 178% for calcium ion, 175% for mixture ion solution, 37.5% for magnesium, 115% for manganese, 92.55% for potassium and 95% for sodium. Thus both the electrical response is observed to be highest for calcium ion and mixture ion solution in comparison to all the other ions. It is clearly visible from the response obtained from the electrical and optical parameters that the detector developed in this work shows appreciable discrimination towards calcium ion, that is more evidently established when the electrical and optical calcium detecting platform is tested with mixture ion solution and the response being consistent with the response of the electrical and optical detector for calcium ion only, as depicted in fig 4.13. Both the electrical and optical parameter response of the detector shows highest response for calcium ion and for mixture ion solution, showing evidence of the selectivity of the detector towards calcium ion.

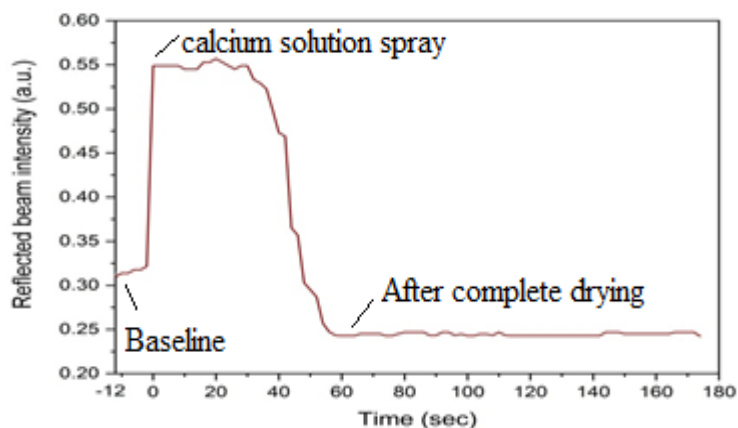
Comparing the optical response with the electrical response of detector developed here, the electrical response of the detector surface is found to be more profound and appreciably consistent with the response of the optical detector, as clearly visible in fig 4.13. The electrical detector developed shows considerably selective towards calcium ion as in the case of the previously developed optical detector. Though, in comparison the selectivity of optical detector towards calcium is better to that for electrical detector as data reveals, both the detectors shows discriminatory response towards  $\text{Ca}^{2+}$  ion, at biologically relevant concentration. This may find use in the designing of multi-parametric calcium sensor with better selectivity and sensitivity.



**Fig 4.13. Individual Electrical response and Optical response of the CaM functionalized PSi Calcium detector.**

#### 4.11 TRANSIENT RESPONSE AND RESPONE TIME OF THE DETECTOR

The transient response of the prepared detector surface was observed in order to measure the response time of the CaM surface-functionalized PSi detector. 0.01mM calcium salt dissolved in 0.5M solvent (TBS) is used for the measurement. The transient response is shown in fig 4.14.

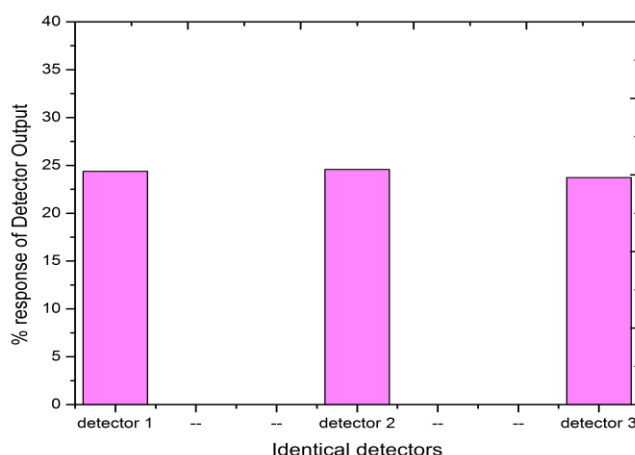


**Fig 4.14. Transient response of the PSi based detector.**

The peak intensity fall of the reflected beam was observed with time for obtaining the transient response data. Specular reflectance value for CaM surface-functionalized sample surface, without calcium incubation is treated as base-line value. On spraying the detector surface with calcium ion solution, a sharp rise in the reflected beam intensity is observed which is due to the lensing effect produced by the water layer upon the recently ion solution sprayed sample surface, as can be observed at time = 0sec in fig 4.14. As drying mechanism sets in, there is again a drastic decrease observed in reflected beam intensity at time = 44s and finally the value saturates at around 60s. This indicates complete drying of the detector surface. The saturated value is less than the baseline value for the detector platform, as observed in previous optical data analysis. As response time by definition is the time required by the detector surface to reach 90% of its steady state value. The response time of the detector platform fabricated in this work is approximately found to be 54s.

#### 4.12 REPRODUCIBILITY OF THE DETECTOR

The reproducibility of the detector has been observed for 3 detectors prepared under same etching conditions. All the detectors were surface functionalized with 20 $\mu$ l of 1:1 CaM-TBS solution and incubated at 4<sup>0</sup>C for 20hours. Exactly same concentration of calcium ion solution that is, 0.01mM calcium salt dissolved in 0.5M solvent (TBS) is prepared and 60 $\mu$ l of the same is sprayed over the detector surface.



**Fig 4.15. Reproducibility study of the developed detector.**

The decrease in specular reflected light intensity is used as the determining parameter for observing the reproducibility of the detectors under consideration. Fig 4.15 shows the response of all the detectors, towards calcium ion, observed while keeping all the fabrication and incubation parameters unaltered. The fabricated detectors shows appreciable reproducibility with response for three detectors of unaltered detection conditions to be within the range of 0.84%.

#### 4.13 CONCLUSION

In this chapter the fabrication of CaM surface-functionalized PSi based calcium detector is discussed. Observations have been made from the structural characterization of the prepared detector. The optical and electrical response of the detector towards calcium ion at a biologically relevant concentration has been shown. Moreover as the response of the detector has been tested for other mono-valent and di-valent cations (commonly present during clinical analysis). The selectivity of the detector towards calcium ion has been considerably established.

Multiple optical parameters investigated show significant changes in specular reflectance, scattering loss and absorption loss for the detector platform in case of calcium ion incubation. The two electrical parameters taken under consideration for the detection of calcium ion shows appreciable response towards calcium ion in comparison to other ions with which the detector is tested in turn. The comparative study establishes that both the responses of the detector surface, namely the overall optical and the electrical response exhibits high level of consistency with each other.

Thus the detector shows remarkable selectivity towards calcium. Moreover the detector exhibits improved response due to multi-parametric approach and is capable of detecting calcium in biologically relevant concentrations. In addition, the detector is cost-effective, robust and exhibits high affinity towards calcium, providing an effective sensor capable of calcium sensing in water, food as well as in biological/clinical samples. In-fact one of the major application of the detector can be in the field of clinical diagnosis of

serum calcium. Since serum calcium level is an eminent marker for a lot of health conditions such as lung cancer, the detector may provide early detection and better prognosis for numerous health conditions and play a key role in early treatment of such diseases.

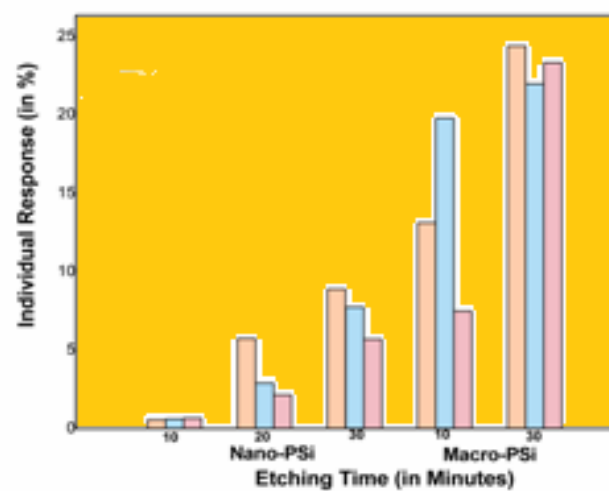
## Reference

1. S. Kim, J. W. Park, D. Kim, D. Kim, I. Lee, S. Jon, "Bioinspired Colorimetric Detection of Calcium(II) Ions in Serum Using Calsequestrin-Functionalized Gold Nanoparticles," *Angew. Chem. Int.*, vol. 48, pp. 4138-4141, 2009.
2. M. S. Eom, W. Jang, Y. S. Lee, G. Choi, Y. Kwon, M. S. Han, "A bi-ligand co-functionalized gold nanoparticles-based calcium ion probe and its application to the detection of calcium ions in serum," *Chem. Comm.*, vol. 48, pp. 5566-5568, 2012.
3. T. Atanasijevic, M. Shusteff, P. Fam, A. Jasanoff, "Calcium-sensitive MRI contrast agents based on superparamagnetic iron oxide nanoparticles and calmodulin," *Pnas*, vol. 103, no. 40, pp. 14707-14712, 2006.
4. S.J. Kim, J. Blumling, M. C. Davidson, H. Saad, S.Y. Eun, G. A. Silva, "Calcium and EDTA Induced Folding and Unfolding of Calmodulin on Functionalized Quantum Dot Surfaces," *Journal of Nanoneuroscience*, vol. 2, pp. 1-7, 2012.
5. S. A. Razavi, L. Hoghooghi, H. Golab-Ghadaksaz, M. Hedayati, "Calcium Determination in EDTA Treated Plasma by Colorimetric Method and Microplate Reading Format," *Zahedan J. Res. Med. Sci.*, vol. 17, no. 2, pp. 7-10, 2015.
6. Y. Guo, X. Tong, L. Ji, Z. Wang, H. Wang, J. Hu, R. Pei, "Visual detection of  $\text{Ca}^{2+}$  based on aggregation-induced emission of Au(I)-Cys complexes with superb selectivity," *Chem. Commun.*, vol. 51, pp. 596-598, 2015.
7. J. Matsumoto, T. Kojima, T. Shimizu, S. Kitashiro, K. Konishi, Y. Matsumura, Y. Kawarada, H. Ikeda, T. Yoshiki, "A Case of Lung Cancer with Hypercalcemia which was Incidentally Complicated with Primary Hyperparathyroidism due to Parathyroid Adenoma," *Ann Thorac Cardiovasc Surg*, vol. 8, no. 3, pp. 151-153, 2002.
8. D. Seccareccia, "Cancer-related hypercalcemia," *Can Fam Physician*, vol. 56, no. 3, pp. 244-246, 2010.
9. W. Goldner, "Cancer-Related Hypercalcemia," *Journal of Oncology Practice*, vol. 12, no. 5, pp. 426-432, 2016.
10. S. Nemr, S. Alluri, D. Sundaramurthy, D. Landry, G. Braden, "Hypercalcemia in Lung Cancer due to Simultaneously Elevated PTHrP and Ectopic Calcitriol Production: First Case Report," *Case Reports in Oncological Medicine*, vol. 2017, pp. 1-3, 2017.
11. J. Zagzag, M. I. Hu, S. B. Fisher, N. D. Perrier, "Hypercalcemia and Cancer: Differential Diagnosis and Treatment," *CA: A Cancer Journal for Clinicians*, vol. 68, pp. 377-386, 2018.
12. G. P. Cartoni, F. Coccioli, "Characterization of Mineral Waters by High-performance Liquid Chromatography," *J. Chromatogr. A*, vol. 360, pp. 225-230, 1986.
13. M. J. A. Shiddiky, A. A. J. Torriero, "Application of ionic liquids in electrochemical sensing systems," *Biosens. Bioelectron.*, vol. 26, pp. 1775-1787, 2011.
14. A. H. Ismail, C. Schafer, A. Heiss, M. Walter, W. Jahnen-Dechent, S. Leonhardt, "An Electrochemical Impedance Spectroscopy (EIS) Assay Measuring the Calcification Inhibition Capacity in Biological Fluids," *Biosens. Bioelectron.*, vol. 26, pp. 4702-4707, 2011.
15. R. Ahmad, N. Tripathy, M. S. Ahn, J. Y. Yoo, Y. B. Hahn, "Preparation of a Highly Conductive Seed Layer for Calcium Sensor Fabrication with Enhanced Sensing Performance," *Acs Sensors*, vol. 3, pp. 772-778, 2018.
16. S. Y. Lin, S. W. Liu, C. M. Lin, C. H. Chen, "Recognition of Potassium Ion in Water by 15-crown-5 Functionalized Gold Nanoparticles," *Anal. Chem.*, vol. 74, pp. 330-335, 2002.
17. P. J. Greenawalt, S. Amemiya, "Voltammetric Mechanism of Multiion Detection with Thin Ionophore-Based Polymeric Membrane," *Anal. Chem.*, vol. 88, pp. 5827-5834, 2016.
18. M. Moirangthem, R. Arts, M. Merkx, A. P. H. J. Schenning, "An Optical Sensor Based on a Photonic Polymer Film to Detect Calcium in Serum," *Advanced Functional Materials*, vol. 26, pp. 1154-1160, 2016.
19. X. Hun, Z. Zhang, "Preparation of a novel fluorescence nanosensor based on calcein-doped silica nanoparticles, and its application to the determination of calcium in blood serum," *Microchim Acta*, vol. 159, pp. 255-261, 2007.
20. H. Buening-Pfaue, "Analysis of Water in Food by Near Infrared Spectroscopy," *Food Chem.*, vol. 82, pp. 107-115, 2003.
21. V. K. Johns, P. K. Patel, S. Hassett, P. Calvo-Marzal, Y. Qin, K. Y. Chumbimuni-Torres, "Visible Light Activated Ion Sensing Using a Photoacid Polymer for Calcium Detection," *Anal. Chem.*, vol. 86, pp. 6184-6187, 2014.



22. M. Zhang, C. Abrams, L. Wang, A. Gizzi, L. He, R. Lin, Y. Chen, P. J. Loll, J. M. Pascal, J. Zhang, "Structural basis for calmodulin as a dynamic calcium sensor," *Structure*, vol. 20, no. 5, pp.911-923, 2012.
23. D. Chin, A. R. Means, "Calmodulin: a prototypical calcium sensor," *trends in Cell Biology*, vol. 10, pp.322-328, 2000.
24. T. W. Lin, P.J. Hsieh, C.L. Lin, Y.Y. Fang, J.X. Yang, C. C. Tsai, P. L. Chiang, C. Y. Pan, Y. T. Chen, "Label-free detection of protein-protein interactions using a calmodulin-modified nanowire transistor'," *PNAS*, vol. 107, no. 3, pp. 1047-1052, 2010.
25. W. Hall, J. Modica, J. Anker, Y. Lin, M. Mrksich, R.P.V. Duyne, "Biosensing with a Calmodulin-Functionalized Plasmonic Switch," *Nano Lett.*, vol. 11, no. 3, pp. 1098-1105, 2011.
26. H. A. Hadi, T. H. Abood, A. T. Mohi, M. S. Karim, "Impact of the etching time and current density on Capacitance-Voltage characteristics of P-type of porous silicon," *World Scientific News*, vol. 67, no. 2, pp. 149-160, 2017.
27. S. J. Kim, B. H. Jeon, K. S. Choi, N. K. Min, "Capacitive porous silicon sensors for measurement of low alcohol gas concentration at room temperature," *J Solid State Electrochem*, vol. 4, pp. 363-366, 2000.
28. D. Basu, T. Sarkar, K. Sen, S. M. Hossain, J. Das, "Multi-parametric Optical Glucose Sensor based on Surface Functionalized nano-Porous Silicon," *IEEE Sensors Journal*, vol. 18, no. 24, 2018.
29. R. C. Anderson, R. S. Muller, C. W. Tobias, "Investigations of the Electrical Properties of Porous Silicon," *J. Electrochem. Soc.*, vol. 138, no. 11, pp. 3406-3411, 1991.
30. H. Saha, S. K. Dutta, S. M. Hossain, S. Chakarborty, A. Saha, "Mechanism and Control of Formation of Porous Silicon on p- Type Si," *Bull. Mater. Sci.*, vol. 21, no. 3, pp. 195-201, 1998.
31. T. Sarkar, D. Basu, N. Mukherjee, J. Das, "Comparison of Glucose Sensitivity of Nano and Macro Porous Silicon," *Materials today proceedings.*, vol. 5, no. 3, pp. 9798-9803, 2018.
32. X. Yang, F. Xi, X. Chen, S. Li1, X.Wan, W.Ma, P. Dong, J. Duan, Y. Chang, "Porous Silicon Fabrication and Surface Cracking Behavior Research Based on Anodic Electrochemical Etching," *FUEL CELLS 00*, vol.0000, no. 0, pp. 1-6, 2020.
33. H. Foell, M. Christophersen, J. Carstensen, G. Hasse, "Formation and Application of Porous Silicon," *Materials Science and Engineering R Reports*, vol. 39, no. 4, pp. 93-141, 2002.
34. P. Sarafis, E. Hourdakis, A. G. Nassiopoulou, "Dielectric Permittivity of Porous Si for Use as Substrate Material in Si-Integrated RF Devices," *IEEE transactions on electron devices*, vol. 60, no. 4, pp. 1436-1443, 2013.
35. M. Hiraoui, M. Guendouz, N. Lorrain, A. Moadhen, L. Haji, M. Oueslati, "Spectroscopy studies of functionalized oxidized porous silicon surface for biosensing applications," *Materials Chemistry and Physics*, vol. 128, pp. 151-156, 2011.
36. W. J. Royea, R. L. Amey, "Ftir Analysis of Al(III) Binding to Calmodulin", *Main group Metal Chemistry*, vol. 17, no. 6, 1994.
37. S. Cinar, C. Czeslik, "Inhibitor and Peptide binding to Calmodulin Characterized by high pressure Fourier Transform Infrared spectroscopy and Froster resonance Energy Transfer", *BBA - Proteins and Proteomics*, vol. 1866, pp. 617-623, 2018.
38. S. C. Edington, A. Gonzalez, T. R. Middendorf, D. B. Halling, R. W. Aldrich, C. R. Baiz, "Coordination to Lanthanide ions distorts binding site in Calmodulin", *PANS*, vol. 115, no. 14, 2018.
39. S. M Iftiqar, " Structural studies in semiconducting hydrogenated amorphous silicon oxide films.", *High Temperature Material Processes: An International quarterly of High Technology Plasma processes*, vol. 6, no. 1, 2002.
40. A. Beganskiene, V. Sirutkaitis, M. Kurtinaitiene, R. Juskenas, A. Kareiva. "FTIR, TEM and NMR Investigation of Stober Silica Nanoparticles," *Mater Sci.* vol. 10, pp. 287-290, 2004.
41. M. Khardani, M. Bouaïcha, B. Bessaïs, "Bruggeman effective medium approach for modelling optical properties of porous silicon: comparison with experiment," *Physica Status Solidi C*, vol. 4, no. 6, pp. 1986-1990, 2007.
42. K. Zaki, A. Neureuther, "Scattering from a perfectly conducting surface with a sinusoidal height profile: TE polarization," *IEEE Transactions on antennas and propagation*, vol. 19, no. 2, pp. 208-214, Mar. 1971.
43. Kaustav Sen, Deeparati Basu, Syed Minhaz Hossain & Jayoti Das. "Calcium selective optical sensor based on calmodulin functionalized porous silicon". *Applied Physics: A* 127, no. 10 (2021): 1-8. DOI: <https://doi.org/10.1007/s00339-021-04869-z>

44. T. Sarkar, N. Mukherjee, J. Das, “Studies on conductivity of surface functionalized nano Porous silicon for detection of hypo and hyper glycemia”, *Material Research Express*, vol. 6, 2019.
45. Kaustav Sen, Tanusree Sarkar, Deeparati Basu, Syed Minhaz Hossain & Jayoti Das. “Calmodulin Functionalized Porous Silicon Based Electrical Calcium Detector and its Comparison with Optical Detector”. *Silicon*. (2022) DOI: 10.1007/s12633-022-02265-7
46. P. Venkaterwarlu, A. Laha, S.B. Krupanidhi, “AC properties of laser ablated La-modified lead titanate thin films,” *Thin solid Films*, vol. 474, pp. 1–9, 2005
47. T. Sarkar, N. Mukherjee, J. Das, “Studies on dielectric constant and AC conductivity of nano porous silicon layer for efficient glucose sensing,” *Journal of Material Science: Materials in Electronics*, vol. 31, no. 21, 2020.
48. B. Tareev, “Dielectric Behavior of Some Vinyl Polymers/Montmorillonite Nanocomposites on the Way to Apply Them as Semiconducting Materials,” *Physics of Dielectric Materials*, Mir Publications, Moscow, 1979.
49. A.A. Hendi, “Structure, Electrical Conductivity and Dielectric properties of bulk, 2-amino-(4,5- diphenylfuran-3-carbonitrile),” *Life Sci. J*, vol. 8, no. 3, pp. 554-559, 2011.



# Chapter-5



## Chapter 5: Effect of Etching time on Detector Response

---

In the previous chapter calmodilin (CaM) surface-functionalized, Porous silicon (PSi) based calcium detector has been fabricated. The optical and electrical response of the detector have been studied and the selectivity of the detector is establish by the comparison of the detectors response towards calcium ions among other bi-valent and mono-valent cations. As sated before, CaM becomes a great choice as a surface-functionalization material owing to its high affinity towards calcium ion [1-4]. Having said that, CaM is a common protein in eukaryotic cell whichis an effective calcium binder [1-4]. So, surface-functionalization of CaM on PSi based detector surface makes it effectively calcium selective. Moreover, as discussed in lengths earlier, many attractive properties of PSi makes it a natural choice as biosensing material. Namely, The phenomena of photoluminescence exhibited by PSi, unlike crystalline silicon, due to its indirect band-gap, owing to quantum-confinement effect [5], found wide range use in optical sensor applications [6-8].The exceptionally high surface area of PSi makes it a perfect material for absorption and interaction of bio-molecules [9-11].With the help of its high loading capacity, PSi finds wide-spread use in arena of chemical sensors, bio-sensors, ionic-sensors, to name a few [12-14]. Due to its biocompatibility and high absorption capacity, PSi finds use as bio-vehicles for highly targeted drug delivery [15, 16]. One of the major advantage of PSi as a sensing material is its easily adjustable surface morphology and porosity, which makes PSi a popular choice for bio- sensors [10, 17-22]. This property of PSi adds immensely towards its applicational dynamicity as a sensing material.

As the porosity, pore size, structure and morphology of PSi are dependent on the factors like anodization condition, electrolytic composition, wafer resistivity and dopant type [23, 24]. In this work, the electrochemical etching time is altered to study the change in optical and electrical response of nano and macro PSi based calcium detectors. Three nano-porous and two macro-porous PSi samples were fabricated with altered etching times while all the other anodization and fabrication conditions like current density, electrolytic composition, concentration of CaM

surface fictionalization and the physical environmental conditions were kept unaltered. Both the optical and electrical response data of the calcium detectors were obtained for equal calcium concentration incubations in unaltered physical conditions, for all the samples. The observations show noticeable change in the detector response data for the samples for varying etching time, in case of both nano and macro porous samples. Optical data, like reflected light intensity, scattering and absorption loss and electrical data like current versus voltage response were taken under consideration to mark the change observed in various samples. The changes observed were evident, even for calcium concentration within the physiologically relevant range. Thus this study provides significant incite in fabrication of PSi based calcium sensors or any other ionic, chemical and bio sensors for the optimization of fabrication condition in order to achieve enhanced sensitivity and response, which may find application in clinical diagnosis, food and drug industry and in scientific studies.

## **5.1 FABRICATION OF NANO AND MACRO POROUS SILICON**

The fabrication of nano and macro PSi requires wafers of different resistivities and different electrolytes. Though, the fabrication process basically remains almost the same, as discussed in the previous chapter for macro-PSi preparation. The discussion on the fabrication process is repeated here in order to mark distinctly the difference in the preparation process of macro and nano PSi samples.

### **5.1.1 Chemicals Required**

Hydrofluoric acid (HF, 48%), N, N-Dimethylformamide (DMF) ( $\text{HCON}(\text{CH}_3)_2$ , 99.8%), Silicon wafer (P-Type, <100>, resistivities 10-20 $\Omega\text{cm}$  and 1-10 $\Omega\text{cm}$ ), Ethanol ( $\text{C}_2\text{H}_5\text{OH}$ , 99.9%), Sulphuric acid ( $\text{H}_2\text{SO}_4$ , 98%), 2-Amino-2 (Hydroxymethyl)-1,3-Propanediol (Tris buffered saline (TBS)), Calcium Chloride ( $\text{CaCl}_2$ , 99.9%), Calmodulin (CaM) Bovine (Lyophilized powder,  $\geq 98\%$ ), Distill water, Ultrapure water (deionized (DI) water  $\sim 18\text{M}\Omega\text{cm}$  resistivity) (Milipore Co.). The silicon wafer was obtained from Macwin India. The chemicals were obtained from Sigma-Aldrich.

### 5.1.2 Fabrication of CaM Surface-Functionalized Nano and Macro PSi with Varying Etching Time

Boron doped silicon wafers (P-type) <100> of both resistivities (1-10 $\Omega$ cm and 10-20 $\Omega$ cm) were laser cut into dimension 1.5 $\times$ 1.5cm. The wafers were acid polished, washed multiple times with DI water and completely dried at room temperature. Metal (Aluminum) is deposited on the back surface of the wafers by vapour deposition technique, to establish ohmic contact during electrochemical etching. After metal deposition, the wafers were annealed at 750 $^{\circ}$ C for 45sec. The wafers were then rinsed multiple times with absolute ethanol and completely dried at room temperature and prepared for electrochemical etching process.

The electrochemical etching process is carried out in an acid resistant bath with graphite rod and silicon wafer acting as cathode and anode respectively. Rinsed and dried silicon wafers of resistivity 1-10 $\Omega$ cm were used for the preparation of nano-PSi. For the preparation of nano-PSi, the electrolyte solution consist of ethanol (>99.9%) and HF (48%) mixed in the ratio of 1:1. The etching was carried out under ambient environmental conditions, at room temperature. Current density of 15mA/cm $^2$  is maintained throughout the process, while the etching time was varied to be kept at 10min, 20min and 30min for the three different nano-PSi samples.

For the macro-PSi sample preparation, wafers of resistivity 10-20 $\Omega$ cm was taken and the electrolyte solution of Di-methyl Formamide (DMF) (99.8%) and HF (48%) in the ratio 1:1 was prepared. Again, ambient environmental conditions were maintained same during the etching process. Constant current density of 15mA/cm $^2$  was maintained, while etching time was varied and maintained at 10min and 30min for the two macro-PSi samples prepared. The prepared PSi samples were rinsed multiple times in absolute ethanol and DI water, dried completely at room temperature and heat treated (450 $^{\circ}$ C for 15 sec) for stabilization of the PSi structure.

As already discussed, for the preparation of CaM solution, CaM is diluted in Trizma-Base (TBS) solution in 1:1 ratio, this is done by dissolution of CaM in TBS by the process of magnetic stirring at 1500rpm for 10min. The pH of the solution prepared is maintained at 7.1. Finally, all the calcium detector surfaces (all the nano and macro PSi of varying etching times) are prepared by drop-casting CaM solution upon the PSi surfaces. This is done by the help of spin-coater. 20 $\mu$ l of CaM solution is measured by a micro-pipette and drop casted upon the PSi substrate while the PSi

is rotated by a spin-coater at 900rpm. This ensures uniform distribution of the CaM solution upon the PSi surface. This process is repeated for both the nano and macro-PSi samples. The detectors are then incubated at 4°C for 18-20 hours for complete physisorption of the CaM solution by the PSi surface. 60µL of the calcium solution (preparation discussed in previous chapter) is drop-casted upon the CaM functionalized PSi surfaces. 30 min incubation time was provided for all the detectors, under ambient pressure and temperature conditions for complete attachment of the calcium ions. The detectors were then completely dried at room temperature and prepared for acquisition of optical and electrical data. Table 5.1 depicts a tabular representation of difference in fabrication conditions for macro and nano PSi samples.

**TABLE 5.1: Fabrication conditions for the preparation of nano and macro-PSi samples.**

	<b>Doping</b>	<b>Resistivity</b>	<b>Electrolyte</b>	<b>Photo-luminescence</b>
<b>NANO-PSi</b>	Boron doped (P-Type)	1-10Ωcm	1:1=HF:Ethanol	Bright luminescence observed
<b>MACRO-PSi</b>	Boron doped (P-Type)	10-20Ωcm	1:1=HF:DMF	Faint luminescence observed

## 5.2 STRUCTURAL CHARACTERIZATION OF NANO AND MACRO PSi WITH CHANGING ETCHING TIME

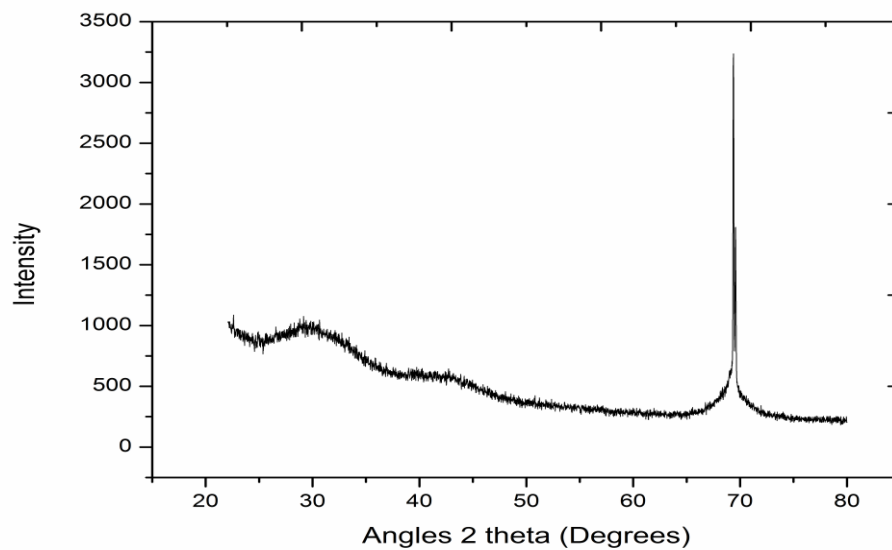
The Sample prepared in this work have been structurally investigated by performing X-Ray diffraction (XRD) spectroscopy (Bruker D8 Advance Diffractometer) and the surface morphological investigation of the samples were done by Field Emission Scanning Electron Microscope (FESEM) (FEI INSPECT F50). Both the cross-sectional and top surface images of the samples were obtained



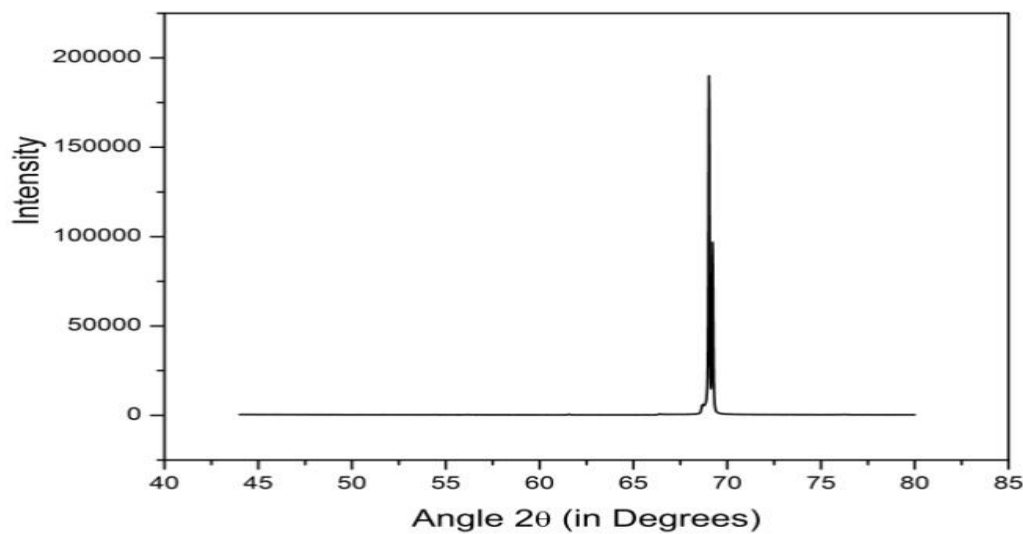
from FESEM. To perform the XRD, the  $2\theta$  value of the sample is varied from angle of  $20^\circ$  to  $80^\circ$ , for nano-PSi samples and  $45^\circ$  to  $80^\circ$  in case of macro-PSi. Step-size of  $0.02^\circ$  together with a scan-speed of 0.1s are used for the experiment. Source used for XRD is  $\text{CuK}\alpha$  ( $\lambda=1.5418\text{\AA}$ ), while the experiment was performed maintaining generating parameters of 40KV and 40mA.

### 5.2.1 XRD of Nano and Macro PSi with Varying Etching Time

As per the observations and discussions made before, for nano-PSi and macro-PSi sample, the characteristic peak of silicon sample, at angle  $\sim 69.9^\circ$  is observed as can be seen in fig 5.1 and fig 5.2. On further analysis of the XRD graphs of nano and macro-PSi samples a more drastic and higher peak is observed for macro samples in comparison to the nano samples. Thus more crystalline characteristics in the case of macro-PSi samples relative to nano-PSi samples can be inferred from this observation. In-fact a prominent amorphous hump is observed in the XRD graph of nano-PSi sample at an angle around  $27^\circ$  owing to nano hillock like structures (later revealed by the FESEM image) [25]. Such humps are not observed in the XRD data of macro-PSi samples. No change in XRD pattern is observed with changing etching time for both nano and macro PSi samples as stated in fig 5.1 and 5.2. This is owing to the fact that the basic crystalline nature of PSi is not affected with changing etching time of sample preparation.



**Fig 5.1. X-Ray diffraction patter for Nano-PSi sample (no change is noticable with varying etching time).**

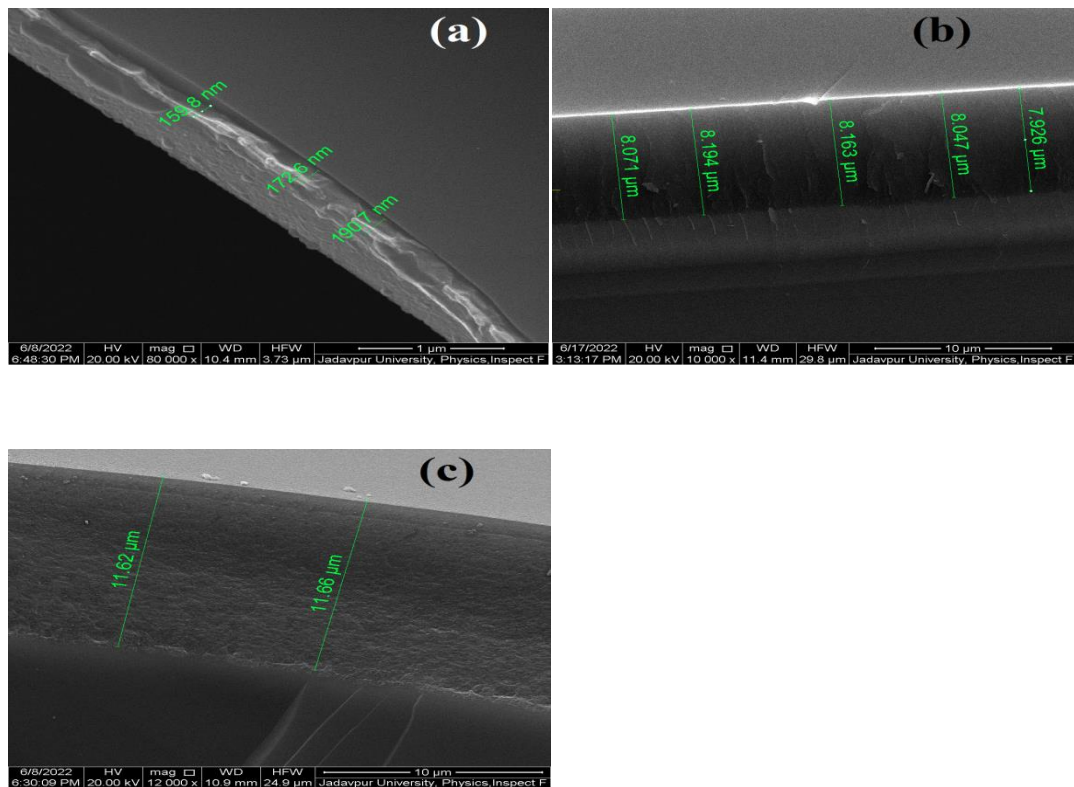


**Fig 5.2. X-Ray diffraction patter for Macro-PSi sample (no change is noticable with varying etching time).**

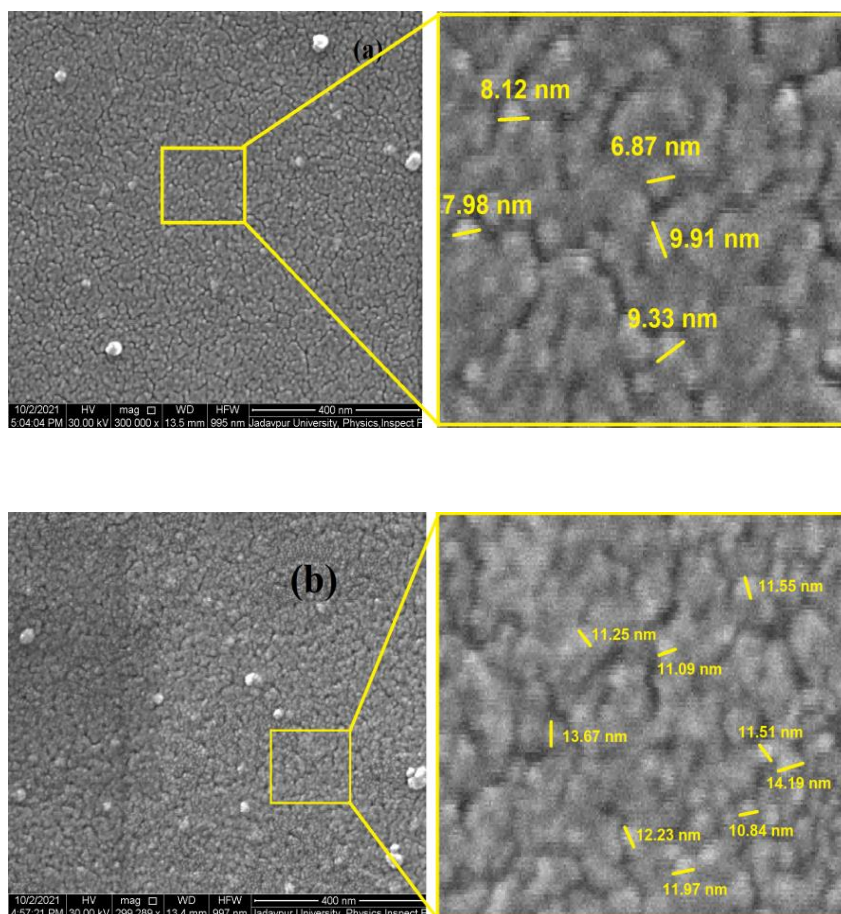
### 5.2.2 FESEM

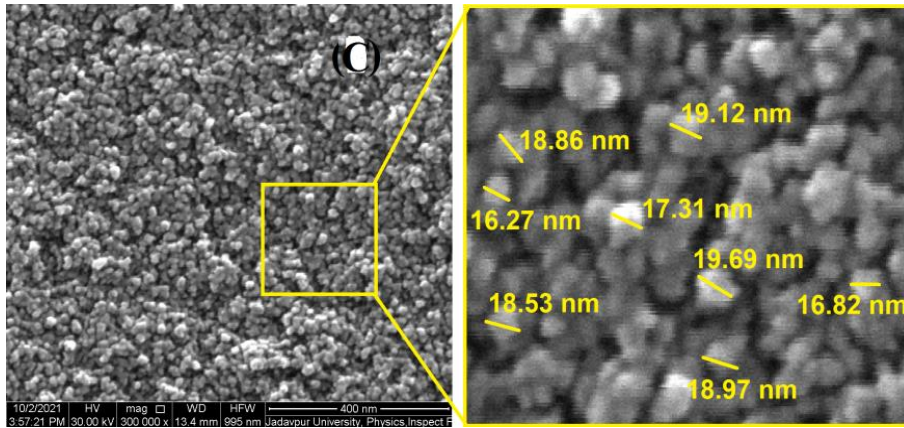
The cross-sectional FESEM images of the nano-PSi samples are shown in fig 5.3. The porous layer thickness is observed to be hugely affected by the electro-chemical etching time of preparation of the samples. The layer thickness is observed to be in 150-190nm range for PSi samples prepared under etching time of 10min in fig 5.3(a), which increases to around 8-9 $\mu$ m range on increasing etching time to 20min in fig 5.3(b). The layer thickness gets maximum for etching time of 30min in case of nano-PSi to be in the range of 11-12 $\mu$ m as depicted in fig 5.3(c)

For the top surface view of the prepared nano-PSi samples, as observed from the FESEM images in fig 5.4, “hillock-like” nano structures can be clearly seen. It is observed that the nano structure density and size both increase on increasing the etching time for nano-PSi preparation from 10min to 20min and is maximum for etching time of 30min. For nano-PSi samples prepared under etching time of 10min, the hillock like nano structure size is observed to be in the range of ~6-10nm in fig 5.4(a). When etching time of preparation of nano-PSi sample is increased to 20min the structure size is observed to have increase to ~11-14nm range in fig 5.4(b). On further increment of etching time to 30min, the structure size further increasesd to ~16-20nm range in fig 5.4(c).



**Fig 5.3. Cross-sectional FESEM image of nano-PSi with etching time (a) 10min, (b) 20min, (c) 30min.**

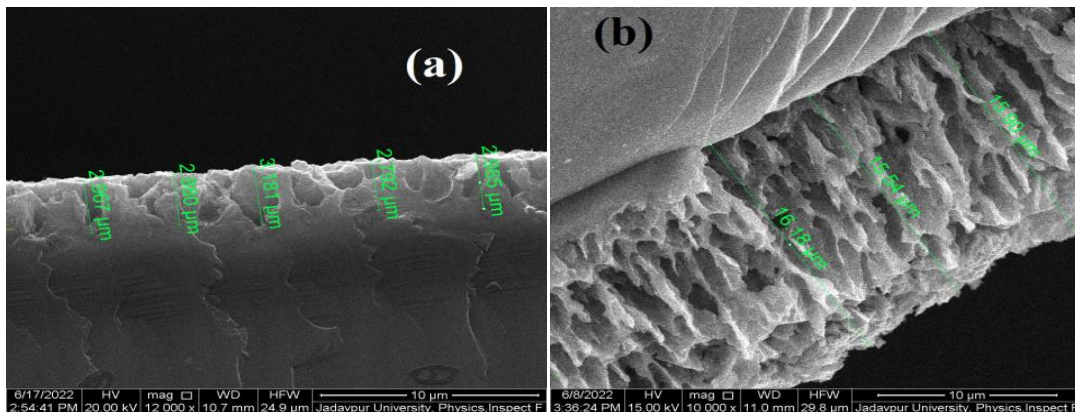




**Fig 5.4. FESEM image of nano-PSi with etching time (a) 10min, (b) 20min, (c) 30min.**

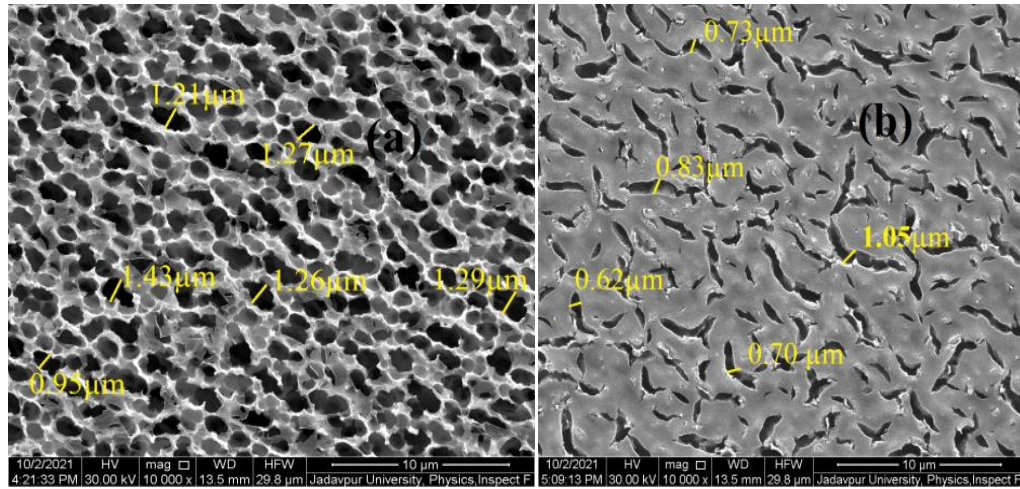
The cross-sectional FESEM image for macro-PSi samples are shown in fig 5.5. In the case of macro-PSi samples a similar observation of increasing porous layer thickness with increasing etching time is manifested. The layer thickness being in the range of 2-3 $\mu$ m for sample prepared under etching time of 10min, as in fig 5.5(a) which increases to a layer thickness of 15-16 $\mu$ m range on increasing the etching time to 30min, shown in fig 5.5(b).

In the case of macro-PSi, pore diameter is observed to have increased on increasing the etching time from 10min to 30min. For macro-PSi sample of etching time 10min the pores are visibly smaller, lesser in number and in their formative stage while the pore diameter is of range  $\sim$ 0.5-1.0 $\mu$ m as shown in fig 5.6(b). Where as well formed pores, with increased pore density are seen in macro-PSi sample with 30min etching time, the pore diameters is increased to the range of  $\sim$ 1.0-1.5 $\mu$ m as in fig 5.6(a).



**Fig 5.5. Cross-sectional FESEM image of macro-PSi of etching time (a) 10min and (b) 30min.**





**Fig 5.6. FESEM image of macro-PSi of etching time (a) 30min and (b) 10min.**

The top surface morphology for macro-PSi samples are observed to be much different from that of nano-PSi samples, as can be seen in fig 5.6. The porous structure of the macro-PSi samples is seen to be increased many-folds and much more prominent in comparison to nano-PSi, with well-formed pores and definite edges being clearly visible in the case of macro-PSi. Many-fold increase in the porous structure is evident in macro-PSi samples in comparison to nano-PSi samples, as observed from fig 5.4 and 5.6. The top surface FESEM images of both nano and macro-PSi samples show a distinct difference in porous structure distribution and density with varying etching time. The top surface view of nano-PSi samples shows distributed “hillock like” structure formation while well formed pores with distinct edges with the pores size and structure much more prominent is observed in macro-PSi samples in comparison to nano-PSi. A tabular representation of the observed difference in the FESEM images of nano and macro-PSi samples with varying etching time is depicted in table 5.2.

**TABLE 5.2: Structural Morphology of Nano and Macro-PSi with Varying Etching Time**

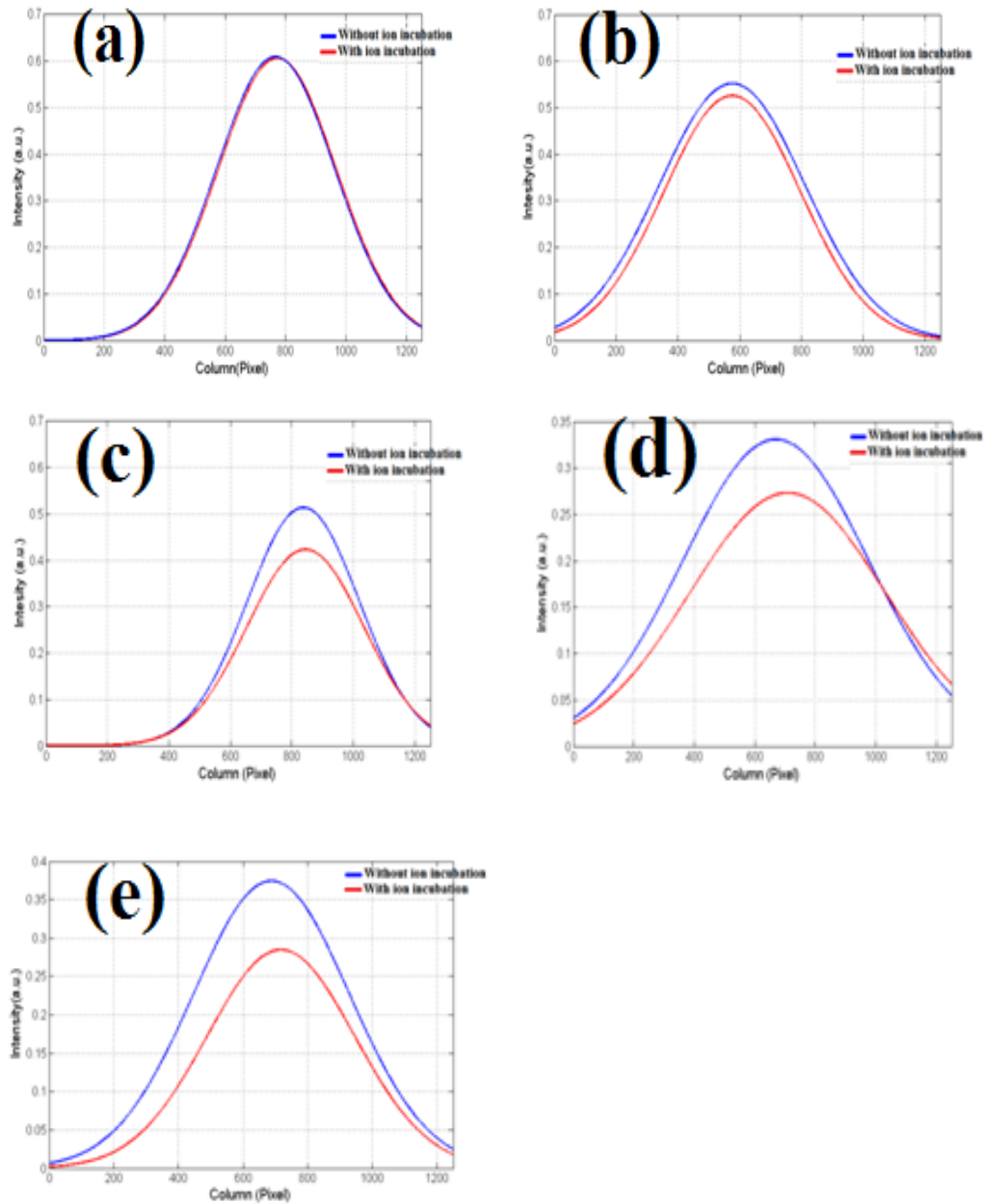
	<b>NANO-PSi</b>			<b>MACRO-PSi</b>	
<b>Etching time (min)</b>	<b>10</b>	<b>20</b>	<b>30</b>	<b>10</b>	<b>30</b>
<b>Layer Thickness</b>	150-190nm	8-9μm	11-12μm	2-3μm	15-16μm
<b>Nano-Structure size</b>	~6-10nm	~11-14nm	~16-20nm	15-16μm	~1-1.5μm

### 5.3 OPTICAL CHARACTERIZATION OF NANO AND MACRO PSi WITH CHANGING ETCHING TIME

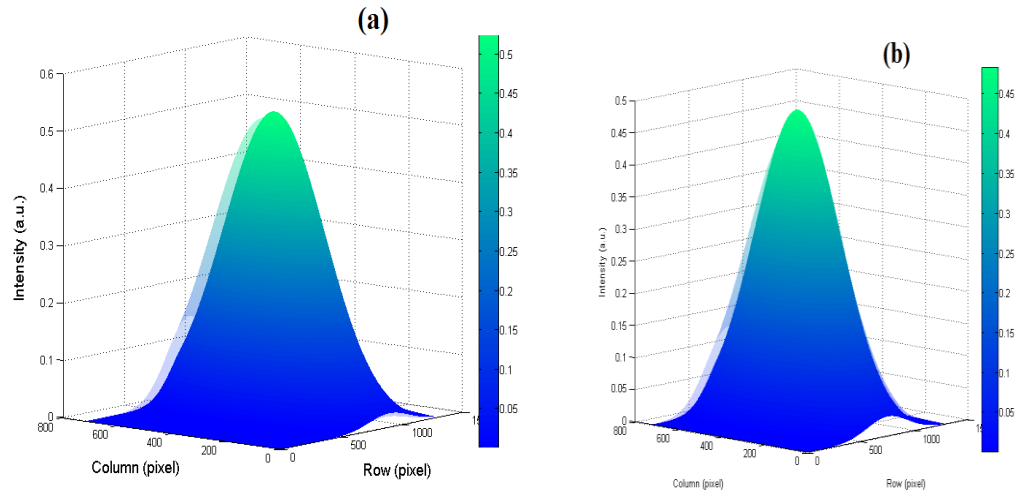
The CaM surface-functionalized nano and macro PSi- sensor surfaces, prepared under different etching time, were uniformly incubated using calcium ionic solution of biologically relevant concentration. The optical parameter analysing setup discussed in detail in the previous chapter is used for the optical data acquisition here. White light beam through the lensing arrangement is made to fall upon the sensor surface and multiple optical parameters, namely specular reflectance, scattering and absorption loss were monitored. The analysis of the reflected beam for the samples shows a significant dependence of optical response upon the etching time. On analysis of the intensity distribution matrix, fall in reflected beam intensity is observed for all the nano-PSi samples. The fall in peak intensity of the reflected beam is seen to be most prominent for nano-PSi sample of etching time 30 min, in comparison to sample prepared under 10min and 20min etching time, as shown in the 2-D Gaussian plots in fig 5.7. Though the fall in peak intensity for nano-PSi sample of etching time 20 min is more than the fall in intensity of nano-PSi sample of etching time 10min, the maximum fall in peak intensity is observed for nano-PSi prepared under 30min etching time. The fall in reflected beam peak intensity for macro-PSi samples are observed to be much more in comparison to all the nano-PSi samples. The fall in peak intensity is increased for macro-PSi samples for increasing etching time from 10min to 30min, as shown clearly in the 2-D Gaussian plots of fig 5.7.

To analyse the reflected beam scattering after calcium incubation, the 3-D Gaussian of the intensity distribution matrix is plotted for sensor surfaces prepared under varying etching time. In case of nano-PSi samples maximum scattering is observed for PSi sample prepared under etching time of 30min, as shown in fig 5.8(a). For macro-PSi samples, though the scattering is much more in comparison to nano-PSi samples, the maximum scattering is observed for macro-PSi sample prepared under 30min etching time, as clearly depicted in fig 5.8(b). The solid curve represents scattering for sensor surface without calcium incubation and the shaded one for sensor surface with calcium incubation. Thus, here too an increase in reflection beam scattering with increase in etching time is observed for both nano and macro-PSi

samples. The third optical parameter, i.e. absorption loss is obtained from the decrease in the area under the 3-D Gaussian curve. For nano-PSi samples the maximum decrease in 3-D Gaussian curve, namely the maximum absorption loss is observed for sample with etching time of 30min. similarly for macro-PSi samples the maximum absorption loss is observed for samples with etching time of 30min. Thus, in case of absorption loss the trend of increasing absorption loss with increasing etching time is maintained for both nano and macro-PSi samples.



**Fig 5.7. 2-D Gaussian plots of intensity distribution matrix for Nano-PSi with (a)10min etching time, Nano-PSi with (b)20min etching time, Nano-PSi with (c)30min etching time, Macro-PSi with (d)10min etching time and Macro-PSi with (e) 30min etching time.**



**Fig 5.8. 3-D Gaussian plots for beam scattering after calcium absorption for (a) nano-PSi of 30min etching time and (b) macro-PSi of 30min etching time.**

As discussed in the previous chapter, the quantitative optical responses of the prepared detector surfaces were obtained by the following method. The specular reflectance change ( $R_s$ ) is obtained from the drop in peak reflected beam intensity from the detector surface when incubated in calcium solution, with respect to the control. The diffused reflectance ( $R_d$ ), which is the measure of the scattering of the reflected beam from the detector surface, is calculated from the change obtained in FWHM value of the reflected beam, with and without calcium solution incubation. The decrement in the volume under the 3-D Gaussian curve of the reflected beam intensity distribution matrix, for calcium solution incubated detector surface when compared to the control, gives the data for integral reflectance ( $R_a$ ). The  $R_a$  is the measure of the effective absorption of the reflected beam by the detector surface. The mathematical expressions of the optical parameters are given as follows:

$$R_s = ((I_o - I_w) / I_o) \times 100\% \dots \dots \dots (1)$$

$I_o$  = Central peak intensity without calcium solution incubation.

$I_w$  = Central peak intensity with calcium solution incubation.

$$R_d = ((D_w - D_o) / D_o) \times 100\% \dots \dots \dots (2)$$

$D_o$  = FWHM value without calcium solution incubation.

$D_w$  = FWHM value with calcium solution incubation

.



$$R_a = ((A_o - A_w) / A_o) \times 100\% \dots \dots \dots (3)$$

$A_o$  = Volume without calcium solution incubation.

$A_w$  = Volume with calcium solution incubation.

The average optical response (R) of the detector surfaces is given by:

$$R = (R_s + R_d + R_a) / 3 \dots \dots \dots (4)$$

The tabular representation of the variation of optical parameters with varying etching time is of both nano and macro-PSi samples are shown in table 5.3.

**TABLE 5.3: Individual and Overall Change in Optical Parameter Values with Varying Etching Time for Nano and Macro-PSi detectors.**

	NANO-PSi DETECTOR			MACRO-PSi DETECTOR	
Etching time (min)	10	20	30	10	30
Peak Intensity fall ( $R_s$ ) (in %)	0.56	5.74	8.89	13.11	24.38
Scattering loss ( $R_d$ ) (in %)	0.60	2.90	7.73	19.77	21.96
Absorption loss ( $R_a$ ) (in %)	0.66	2.14	5.70	7.48	23.31
Overall Optical response (R) (in %)	0.60	3.59	7.44	13.45	23.21

## 5.4 DISCUSSION OF OPTICAL RESPONSE

It has been discussed previously that how the intensity of the reflected beam from a surface is hugely affected by parameters like specular reflectance, diffused reflectance and absorption of incident beam by the surface. As explained previously by Bruggeman [26], for a sensor having composite surface, the effects of individual reflectance of each component contributes to the effective reflectance of the composite reflecting surface.

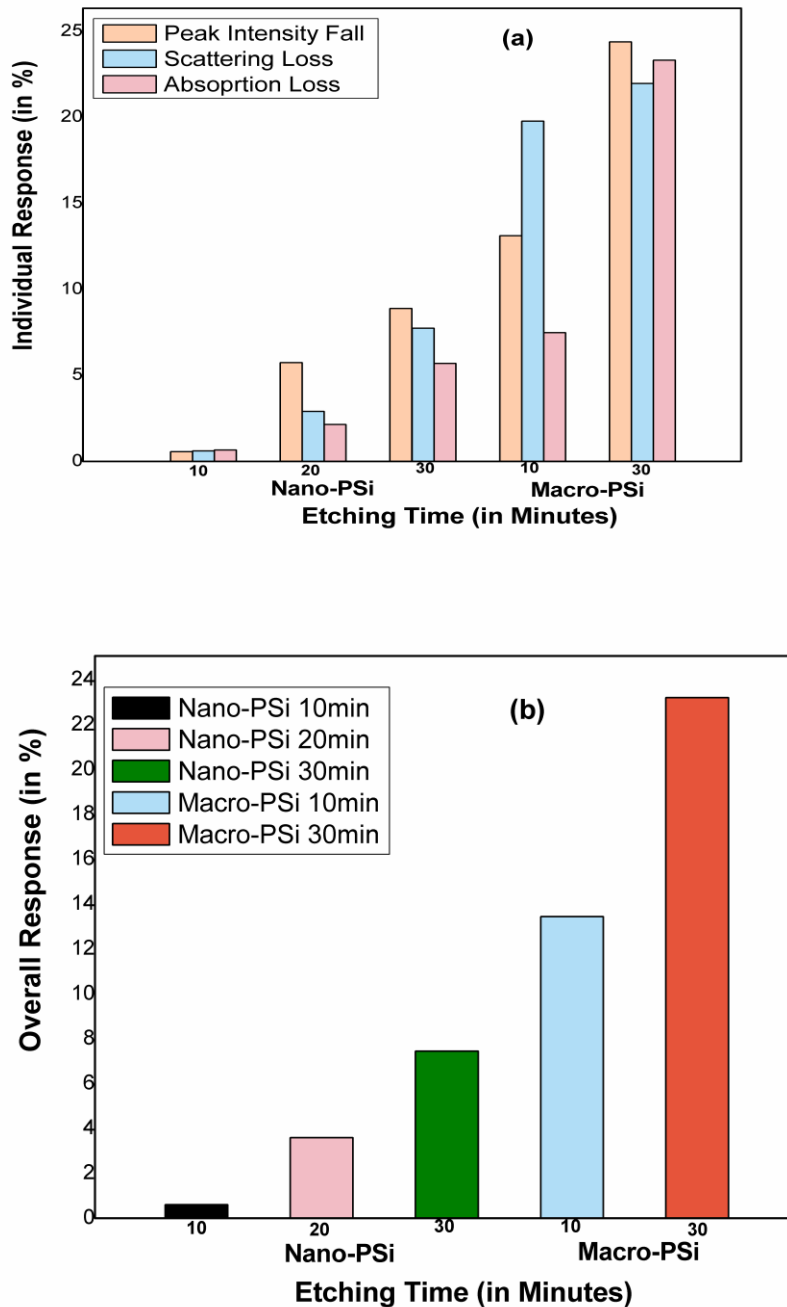
It has been established in the previous chapter that the detector surface developed here has intrinsic surface roughness owing to its porous nature. Moreover, with attachment of bio-molecules like CaM together with calcium solution incubation, its surface roughness increases as would have been the case for any molecular attachment to the porous surface [10,27]. Thus a decrease in specular reflectance is evident for the detector surface due to phenomena like shadowing and multiple reflections, common for rough reflecting surfaces [10,27,28]. This explains the fall in the peak intensity of the reflected beam value of the detector surface when solution incubated. The increase in diffused reflectance is also due to the fact that divergence and scattering of the reflected beam increases with surface roughness of the detector surface. In fact, absorption loss is also observed to increase due to the phenomenon of multiple reflections on the rough surface.

In this work, the nano-structure size, pore diameter and layer thickness, hence the surface area for absorption of P<sub>Si</sub> is observed to increase with increase in electrochemical etching time. This phenomena is consistent with previously established studies performed in this context [29,30]. Increase in porosity facilitates greater surface area for absorption and thus the optical response of the fabricated composite detecting platform should increase with increase in etching time and thus porosity. For nano-P<sub>Si</sub> samples, it is observed that the optical response of the detector surface increases with etching time. Though the optical response of the detector increases when etching time is increased, but the increase is observed to be non-linear. That is, the rate of increase of optical response is much more when etching time is increased from 20min to 30min, in comparison to the increase in optical response when the etching time is increased from 10min to 20min. The maximum optical response of the detector is observed for etching time of 30min. This phenomenon is attributed to the fact that though there is an increment in structure size and layer thickness with increasing etching time, that facilitates bio-molecule absorption to the detector surface, there is also a simultaneous, disproportionate increment in pore population in case of nano-P<sub>Si</sub> layer, with increasing etching time [6,29]. This phenomena is clearly visible in the FESEM images shown in fig 5.4 and 5.5. The images clearly show the increment in layer thickness and structure size of

nano-PSi detector surfaces with increase in etching time. This disproportionate increase in pore population causes the disproportionate increase in the response of the calcium detector with increasing etching time. Thus, increase in porosity, the hillock-like structure size together with substantial increment in porous layer thickness of the PSi layer in the detector surface must have increased the effective bio-molecule attachment capability, due to the fact the surface area of absorption increases with increasing structure size and layer thickness, for the case of nano-porous silicon. Thus it can be said that the hillock like structure size of the nano-PSi detector platform and its layer thickness increases the effective surface area for absorption and plays a predominant role for bio-molecule absorption or attachment, together with the fact that with increasing etching time the porosity and surface area of the entire nano-PSi surface increases. This increase results in the fall in specular reflectance intensity with a simultaneous increase in diffused reflectance from the detector surface which is consistent with the optical data observed.

As discussed earlier, the porous nature of macro-PSi detector platforms are much more vivid in comparison to nano-PSi, due to this many-fold increase in the porous structure, the optical response of the macro-PSi detector surface is found to be more pronounced in comparison to nano-PSi detector samples. This is due to many-fold bigger structure and pore size of macro-PSi samples that plays a determining role for molecular attachment to the porous surface of the detector. On increasing the etching time for macro-PSi samples from 10min to 30min the optical response increases owing to the phenomena of simultaneous increase in pore size, porosity and layer thickness of the PSi surface with increasing in etching time, that results in decrease in specular reflectance and a simultaneous increase in diffused reflectance as stated before. This phenomenon is consistent with the observations in the FESEM images in fig 5.5 and 5.6. Thus, the individual optical responses, namely the peak intensity fall, scattering loss and absorption loss of the detectors are found to be maximum for macro-PSi detector sample of etching time 30min. Though the response of the macro samples are higher than the nano samples owing to its manyfold increase in surface roughness, the highest optical response is recorder for nano-PSi sample prepared under 30min etching time as depicted in

fig 5.9(a). The overall optical response of the macro and nano-PSi detectors are shown in fig 5.9(b) which clearly shows the phenomena of higher optical response of the detectors fabricated with increased etching time for both nano and macrosamples.



**Fig 5.9. (a) Individual optical response of nano and macro-PSi samples of different etching time. (b) Overall average optical response of nano and macro-PSi samples of different etching time.**

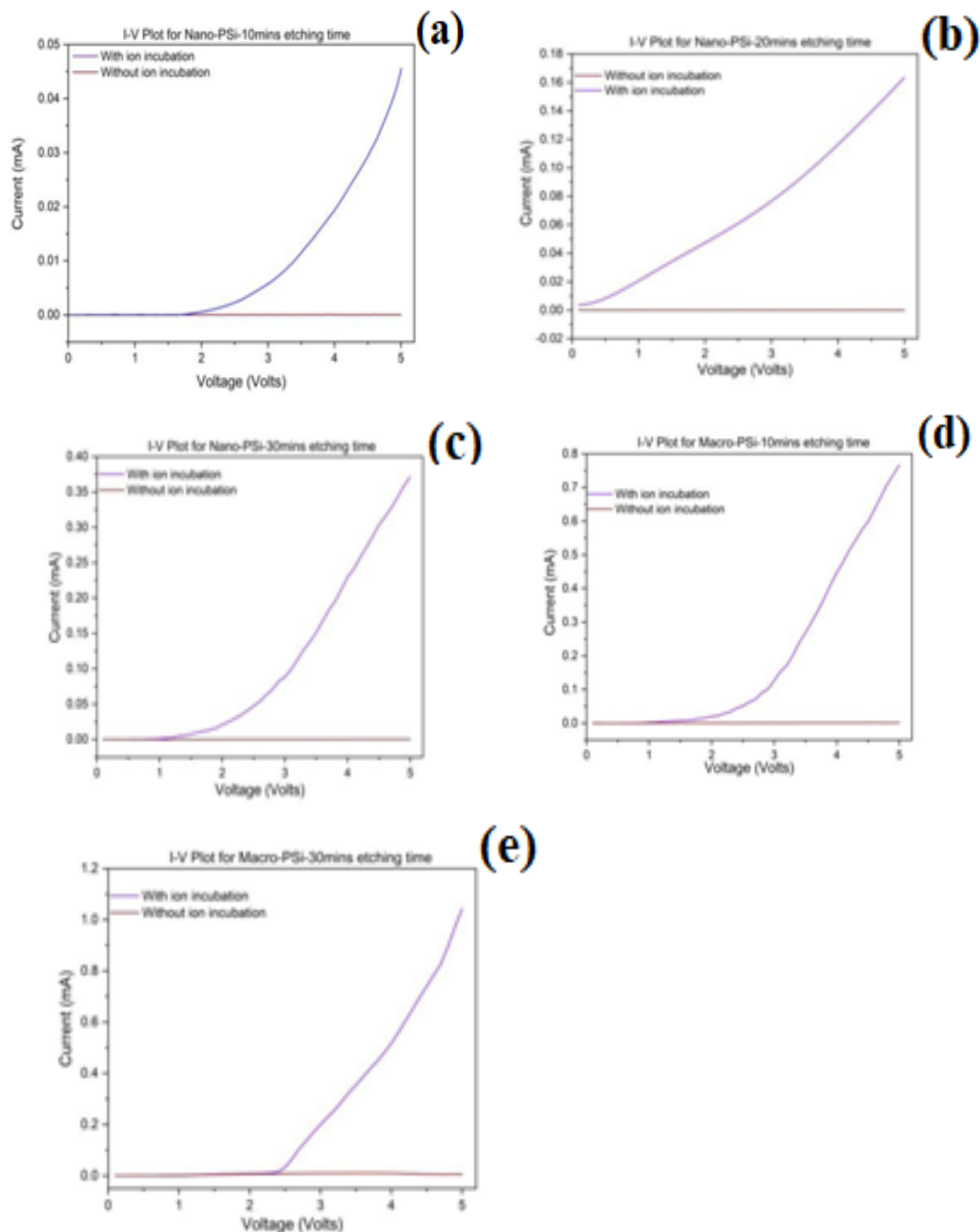
## 5.5 ELECTRICAL CHARACTERIZATION OF NANO AND MACRO-PSi WITH VARYING ETCHING TIME

The electrical conductivity of the detector surface is tested using Electrometer (Kethiley- U3606B). The electrical data were acquired for the detector surfaces through the ohmic contacts upon the detector surface and by using a data acquisition system. The response of the detectors were measured by monitoring the change in the current ( $I_w$ ) flow through the detector surface when incubated with calcium ionic solution in comparison to the current ( $I_o$ ) value of the detector surface without ionic incubation, for a steady increase in voltage ( $V$ ) across the surface. The data acquirement was performed under ambient pressure and temperature conditions.

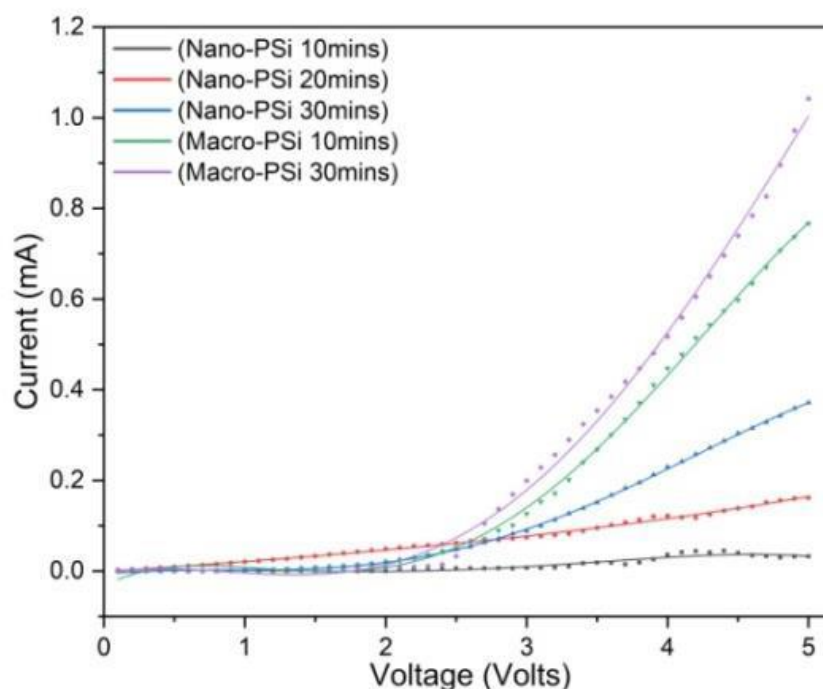
The I-V characteristics of the macro and nano-PSi detector surfaces were studied by incubating all the detector surfaces in calcium ionic solution of exactly same concentration which is in biological relevant level. The individual responses for the detectors (both nano and macro) are shown in figure 5.10 (a-e) It is observed that the rise in current value within a definite voltage range (0-5V) is almost exponential when the detector surfaces are incubated with calcium ion solution, in comparison to the current response of un-incubated detector surfaces. A drastic rise in current value is observed within a voltage range of around 2-2.5 V which continues to rise exponentially till the highest range of the applied voltage (5V).

The electrical response of the PSi based calcium detector shows high dependence upon the etching time of PSi fabrication. Though the current response of all the nano and macro-PSi detectors shows a near about exponential rise with increasing voltage (0-5V) as can be observed in fig 5.11. In case of nano-PSi detectors, the range of increase in current value is observed to have increased substantially with increasing etching time of PSi fabrication. That is, the maximum current value against the maximum voltage (5V) is observed to be relatively minimum for nano-PSi sample prepared under etching time of 10min, the maximum current value increases when etching time is increased to 20min and is maximum for nano detector sample prepared under 30min etching time as clear in fig 5.11. Though the current value of the detector surface for macro-PSi samples are much higher in comparison to nano-PSi samples, a similar trend is observed in case of macro-PSi detector samples too. That is, the trend of the increase in the current value with increasing voltage increases substantially with increase in etching time of macro-PSi

detector surface preparation. Fig 5.11 shows clearly the increase in current value for macro-PSi detector prepared under etching time of 30min is clearly much higher in comparison to detector prepared in 10min etching time.



**Fig 5.10. . I Vs V characteristics of nano and macro-PSi samples. (a) nano-PSi 10min etching time. (b) nano-PSi 20min etching time. (c) nano-PSi 30min etching time. (d) macro-PSi 10min etching time. (e) macro-PSi 30min etching time**



**Fig 5.11. Comparative I Vs V characteristics of macro and nano-PSi samples.**

## 5.6 DISCUSSION OF ELECTRICAL RESPONSE

As discussed previously that in defective solids like PSi, that bears intrinsic defective states and surface dangling bonds [30], multiple mechanism like hopping of thermally excited carriers, Poole-Frenkle (P-F) and Trap Assisted Tunnelling (TAT) attribute towards the charge transport mechanism [30]. The I-V characteristics for PSi based CaM surface-functionalized calcium detector has been discussed and established in the previous chapter.

As far as the electrical response are concerned, the response of the nano-PSi detectors developed in this work clearly shows an increment in electrical response with increasing etching time for PSi fabrication, visible in fig 5.11. This increment can be attributed to the phenomena of increase in porosity and thus the effective surface area of the nano-PSi detector surface with increase in etching time that facilitates better molecular attachment to the detector surface and hence an increase in electrical response due to the increase in defective states in the structure of the prepared sample is observed with increase in etching time of preparation of the

detector surfaces. Moreover, the increase in porous layer thickness with increasing etching time as depicted in cross-sectional FESEM images further facilitates better molecular attachment and as trap states in the structure of P<sub>Si</sub> increases with increasing porous layer thickness, that can act as hopping centers and adds to the conductivity of the P<sub>Si</sub> based detector, hence contributes to the increase in electrical response of the detectors [30].

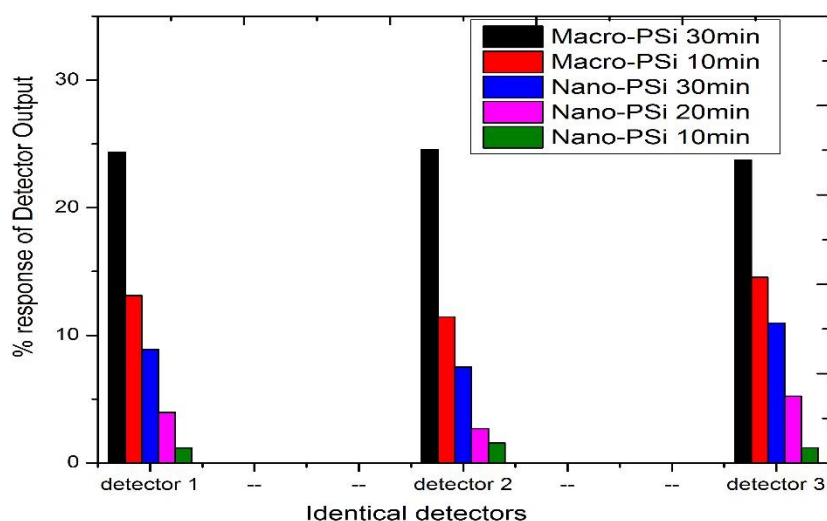
The absence of hillock like nano-structures, as in the case of nano-P<sub>Si</sub> and the presence of well-defined porous structure with hugely increased pore size with definite edges can be seen clearly in the FESEM images of macro-P<sub>Si</sub> samples. Due to this further increase in pore size and thus the effective surface area, in case of macro-P<sub>Si</sub> samples as compared to nano-P<sub>Si</sub> samples, which enables better molecular attachment to the porous surface of the detectors. Thus the effective conductivity of the macro-P<sub>Si</sub> detector surfaces increases and thus the electrical response of the macro-P<sub>Si</sub> detectors are much greater when compared to nano-P<sub>Si</sub> detector samples, evident from fig 5.11. The trend of increasing in electrical response with increasing in etching time of fabrication is very much observed in the case of macro-P<sub>Si</sub> samples too. Though the electrical response of macro-P<sub>Si</sub> detector sample prepared under etching time of 10min is higher in comparison to nano-P<sub>Si</sub> detector samples, the electrical response gets even higher when etching time of fabrication of macro-P<sub>Si</sub> sample is increased to 30min.

## **5.7 REPRODUCIBILITY STUDY OF NANO AND MACRO-P<sub>Si</sub> WITH CHANGING ETCHING TIME**

The reproducibility of all the detectors have been observed for a set of 5 detectors, two macro-P<sub>Si</sub> and three nano-P<sub>Si</sub>, each set containing three detectors each prepared under same etching time, keeping the remaining etching parameters unaltered. Thus we get three identical detectors of macro-P<sub>Si</sub> prepared with etching time of 30min, 3 identical macro-P<sub>Si</sub> detectors of 10min etching time, 3 identical nano-P<sub>Si</sub> detectors each of 30min, 20min and 10min fabrication etching time respectively. All the detectors were surface functionalized with 20 $\mu$ l of 1:1 CaM-TBS solution and incubated at 4<sup>0</sup>C for 20hours. Exactly same concentration of calcium ion solution that is, 0.01mM



calcium salt dissolved in 0.5M solvent (TBS) is prepared and 60 $\mu$ l of the same is sprayed over each detector surface.



**Fig 5.12. Reproducibility study of the developed macro and nano-PSi detectors with varying etching time.**

The decrease in specular reflected light intensity is used as the determining parameter for observing the reproducibility of the detectors under consideration. Fig 5.12 shows the response of all the macro and nano-PSi based detectors, prepared under varying etching time, towards calcium ion, observed while keeping all the fabrication and incubation parameters unaltered. The three identical macro-PSi detectors prepared with etching time of 30min shows reproducibility with a range of 0.84%. Macro-PSi detector samples of 10min etching time shows reproducibility within a range of 3.08%. For the nano-PSi samples, the 30min etching time sample's reproducibility value is within the range of 3.43%, that for sample of 20min etching time shows reproducibility in the range of 2.57% and the 10min etching time sample shows the same within 0.61% range. Thus from this study it can be said that as far as reproducibility of the response is concerned, nano-PSi based detector species, prepared under 10min etching time exhibits the best response.

## 5.8 CONCLUSION

The study described in this chapter, establishes the dependence of the optical and current response of the detector surface upon the etching time of detector

fabrication. The optical response for nano-PSi samples shows an optimum value for etching time of 30min. The optical response is observed to increase by 2.98% on increasing the etching time from 10min to 20min, there after an increase of 3.85% is observed when the etching time is further increased to 30min. for macro-PSi samples; there is a minimum increase of the optical response by 6.0%, as compared to nano-PSi samples. Though the optical response of macro-PSi samples is much higher in comparison to nano-PSi samples, a further increase in optical response of the macro-PSi detector is observed for an increasing in etching time. The optical response for macro-PSi samples is increased by 9.76%, on increasing etching time from 10min to 30min. In case of electrical response too, the response of the macro-PSi detector sample fabricated is found to be much higher in comparison to that of nano-PSi samples. A minimum increase in current value of  $\sim 0.4$  mA is observed in the current response of macro-PSi detector sample in comparison to nano-PSi ones. It is also established in this study conducted that the electrical response of the detector, like that for the optical response, for both macro and nano-PSi based detectors, increases with increase in the etching time of detector fabrication. This study provides help in the fabrication and designing of CaM surface functionalized PSi based calcium detector with increased sensitivity and response that finds use in designing of calcium and other ionic or bio-chemical sensors in further scientific studies, food and chemical industry and most importantly in medical industry for clinical diagnosis.

## Reference

1. M. Zhang, C. Abrams, L. Wang, A. Gizzi, L. He, R. Lin, Y. Chen, P. J. Loll, J. M. Pascal, J. Zhang, "Structural basis for calmodulin as a dynamic calcium sensor," *Structure*, vol. 20, no. 5, pp. 911-923, 2012.
2. D. Chin, A. R. Means, "Calmodulin: a prototypical calcium sensor," *trends in Cell Biology*, vol. 10, pp. 322-328, 2000.
3. T. W. Lin, P. J. Hsieh, C. L. Lin, Y. Y. Fang, J. X. Yang, C. C. Tsai, P. L. Chiang, C. Y. Pan, Y. T. Chen, "Label-free detection of protein-protein interactions using a calmodulin-modified nanowire transistor," *PNAS*, vol. 107, no. 3, pp. 1047-1052, 2010.
4. W. Hall, J. Modica, J. Anker, Y. Lin, M. Mrksich, R. P. V. Duyne, "Biosensing with a Calmodulin-Functionalized Plasmonic Switch," *Nano Lett.*, vol. 11, no. 3, pp. 1098-1105, 2011.
5. H. A. Hadi, T. H. Abood, A. T. Mohi, M. S. Karim, "Impact of the etching time and current density on Capacitance-Voltage characteristics of P-type of porous silicon," *World Scientific News*, vol. 67, no. 2, pp. 149-160, 2017.
6. M. J. Hussein, W. M. M. Yunus, H. M. Kamari, A. Zakaria, H. F. Oleiw, "Effect of current density and etching time on photoluminescence and energy band gap of p-type porous silicon," *optical and quantum electronics*, vol. 48, no. 194, pp. 2-8, 2016.
7. M. H. F. Suhaimi, M. Rusop, S. Abdullah, "Porosity and thickness effect of porous silicon layer on photoluminescence spectra," *International Conference on Technology, Informatics, Management, Engineering & Environment*, 2013.
8. A. Mortezaali, S. R. Sani, F. J. Jooni, "Correlation between porosity of porous silicon and optoelectronic properties," vol. 1, no. 3, pp. 293-299, 2009.
9. S. J. Kim, B. H. Jeon, K. S. Choi, N. K. Min, "Capacitive porous silicon sensors for measurement of low alcohol gas concentration at room temperature," *J Solid State Electrochem*, vol. 4, pp. 363-366, 2000.
10. D. Basu, T. Sarkar, K. Sen, S. M. Hossain, J. Das, "Multi-parametric Optical Glucose Sensor based on Surface Functionalized nano-Porous Silicon," *IEEE Sensors Journal*, vol. 18, no. 24, 2018.
11. R. C. Anderson, R. S. Muller, C. W. Tobias, "Investigations of the Electrical Properties of Porous Silicon," *J. Electrochem. Soc.*, vol. 138, no. 11, pp. 3406-3411, 1991.
12. F. A. Harraz, A. A. Ismail, M. Faisal, S. A. Al-Hajry, M. S. Al-Assiri, "Organic analytes sensitivity in meso-porous silicon electrical sensor with frontside and backside contact," *Arabian Journal of Chemistry*, DOI: <http://dx.doi.org/10.1016/j.arabjc.2017.05.015>, 2017.
13. F. A. Harraz, "Porous Silicon Chemical Sensor and Bio Sensor: A Review," *Sensors and Actuators B: Chemical*, vol. 202, pp. 897-912, 2014.
14. E. A. Kabaa, S. A. Abdulateef, N. M. Ahmed, Z. Hassan, F. A. Sabah, "A Novel Porous Silicon Multi-ions Selective Electrode Based Extended Field Effect Transistor for Sodium, Potassium, Calcium and Magnesium Sensor," *Applied Physics AMaterial Science and Processing*, vol. 125, no. 753, 2019.
15. G. N. Tovar, D. R. García, A. W. Arce, G. Palestino, S. R. Mendoza, "Mesoporous Silicon Particles Favor the Induction of Long-Lived Humoral Responses in Mice to a Peptide-Based Vaccine," *Materials*, vol. 11, no. 1083, 2018.
16. Y. M. Spivak, S. V. Mjakin, V. A. Moshnikov, M. F. Panov, A. O. Belorus, A. A. Bobkov, "Surface Functionality Features of Porous Silicon Prepared and Treated in Different Conditions," *Journal of Nanomaterials*, vol. 2016, DOI: <http://dx.doi.org/10.1155/2016/2629582>, 2016.
17. H. Saha, S. K. Dutta, S. M. Hossain, S. Chakraborty, A. Saha, "Mechanism and Control of Formation of Porous Silicon on p-Type Si," *Bull. Mater. Sci.*, vol. 21, no. 3, pp. 195-201, 1998.
18. T. Sarkar, D. Basu, N. Mukherjee, J. Das, "Comparison of Glucose Sensitivity of Nano and Macro Porous Silicon," *Materials today proceedings.*, vol. 5, no. 3, pp. 9798-9803, 2018.
19. X. Yang, F. Xi, X. Chen, S. Li, X. Wan, W. Ma, P. Dong, J. Duan, Y. Chang, "Porous Silicon Fabrication and Surface Cracking Behavior Research Based on Anodic Electrochemical Etching," *FUEL CELLS* 00, vol. 0000, no. 0, pp. 1-6, 2020.
20. H. Foell, M. Christophersen, J. Carstensen, G. Hasse, "Formation and Application of Porous Silicon," *Materials Science and Engineering R Reports*, vol. 39, no. 4, pp. 93-141, 2002.

21. P. Sarafis, E. Hourdakis, A. G. Nassiopoulou, "Dielectric Permittivity of Porous Si for Use as Substrate Material in Si-Integrated RF Devices," *IEEE transactions on electron devices*, vol. 60, no. 4, pp. 1436-1443, 2013.
22. P. Kumar, P. Huber, "Effect of Etching Parameter on Pore Size and Porosity of Electrochemically Formed Nanoporous Silicon," *Journal of Nanomaterials*, vol. 2007, DOI. 10.1155/2007/89718, 2007.
23. A. Ramizy, I. M. Ibrahim, M. A. Hammadi, "The Effect of Etching Current Density on Porous Silicon Fabricated by Electrochemical Etching Process," *International Journal of Scientific & Engineering Research*, vol. 7, no. 4, pp. 717-722, 2016.
24. M. Khardani, M. Bouaïcha, B. Bessaïs, "Bruggeman effective medium approach for modelling optical properties of porous silicon: comparison with experiment," *Physica Status Solidi C*, vol. 4, no. 6, pp. 1986-1990, 2007.
25. W. S. Yan, D. Y. Wei, S. Xu, H.P. Ahou, "Highly doped P-Type nanocrystalline silicon thin films fabricated by low-frequency inductively coupled plasma without H<sub>2</sub> dilution." *Journal of applied Ohysics*, vol. 110, np. 6, 2011.
26. K.Sen, D. Basu, S.M. Hossain, J. Das, "Calcium Selective Optical Sensor Based On Calmodulin Functionalized Porous Silicon," *Applied Physics A*, vol. 127, no. 768, 2021.
27. K. Zaki, A. Neureuther, "Scattering from a perfectly conducting surface with a sinusoidal height profile: TE polarization," *IEEE Transactions on antennas and propagation*, vol. 19, no. 2, pp. 208-214, Mar. 1971.
28. C. K. Sheng, W. M. Khairul, W. M. Zin, D. T. J. Ee, M. I. N. M. Isa, M. F. Hassan, "Etching Time Effect on Photoluminescence, Porosity, Surface Morphology and Conductivity of Porous Silicon," *Educatum Ismt*, vol. 3, no. 1, pp. 20-27, 2016.
29. D. Liu, K. Lipponen, P. Quan, X. Wan, H. Zhang, E. Makila, J. Salonen, R. Kostianen, J. Hirvonen, T. Kotiaho, H. A. Santos, "Impact of Pore Size and Surface Chemistry of Porous Silicon Particles and Structure of Phospholipids on Their Interactions," *ACS Biomaterials Science and Engineering*, vol. 4, pp. 2308-2313, 2018.
30. T. Sarkar, N. Mukherjee, J. Das, "Studies on conductivity of surface functionalized nano Porous silicon for detection of hypo and hyper glycemia", *Material Research Express*, vol. 6, 2019.





# Chapter 6: Conclusion & Future Scope

---

## 6.1 CONCLUSION

The work presented in this thesis focuses on the development of a smart diagnostic system capable of early detection of cardio-pulmonary diseases like lung cancer. Since early detection of such diseases plays a predominant role in their treatment, this work focuses on quantitative detection of these early symptoms ensuring early diagnosis and better prognosis for the patients.

One of the earliest clinical symptom of cardio-pulmonary disease like lung cancer is finger clubbing. Finger clubbing is manifested by the bulbous appearance of the fingers, namely by the disruption of certain finger parameters, namely lovi-bond angle and DPD-IPD ratio. In this work an automated, multi-parametric instrument has been developed for precise, quantitative and non-invasive diagnosis of finger clubbing that utilizes image processing and lase-photo-detector techniques for reliable diagnosis of finger clubbing. The automated instrument developed, has been used for diagnosis of finger clubbing in patients complaining of thoracic disorders and has showed reliable results.

Since diagnosis of finger clubbing does not conclusively verifies the presence of cardio-pulmonary disease in a patient, the work presented here now focuses on the development of calcium detector, capable of detecting serum calcium at biologically relevant concentrations. Since hyprecalcemia is a clinical and quiet conclusive symptom of the presence of cardio-pulmonary disorder in an individual, a detecting platform based on porous silicon (PSi) has been developed detection of calcium. Calmodulin (CaM), an enzyme common to eukaryotic cells has been surface-functionalized upon the PSi surface for selective detection of calcium detection in physiological concentration range. PSi were fabricated by electrochemical etching process, surface-functionalized by CaM and thoroughly characterized structurally. Then the performance of the calcium detector based on CaM functionalized PSi has been tested by various optical and electrical responses. Morphological and structural studies reveal effective binding of CaM to PSi surface and the detector structure fabricated was found to be highly selective towards calcium ion. When the detector

was tested with other mono-valent and di-valent cations commonly found in human blood serum, the most profound optical and electrical response of the detector was found to be for calcium ion, thus providing the high level of discrimination of the detector surface for calcium ion. Even for composite ionic mixture (containing all the ions used for testing in equal concentration), the electrical and optical response of the detector was found to be closely mimicking its response for calcium ion, which proves effective selectivity of the detector towards calcium. The response time of the detector was found to be about 54sec. The detector exhibited appreciable reproducibility, with the response of the sensor fluctuating with the limit of 0.84% for multiple times its response was tested.

Later in this work the variation of the morphological, structural, optical and electrical response of the sensor is observed with varying one of the etching parameters like etching time of PSi fabrication. Together with that the structural difference and the electrical and optical response of nano-PSi based and macro-PSi based detector are compared. It is observed that the structural morphology as well as the electrical and optical response of the detector is highly affected by etching time of fabrication. Moreover, striking morphological and structural difference, together with difference in electrical and optical response is noted on comparison of nano and macro-PSi based detector surfaces. “hillock-like” nano structure is observed on structural investigation of nano-PSi detector while well-formed porous structure is evident for macro-PSi structure. For both nano and macro samples the nano-structure size, porosity and porous layer thickness are observed to be considerably increased with increasing etching time. Though the electrical and optical response of macro-PSi based detector surface is found to be much more profound in comparison to nano-PSi based detectors, in both cases the electrical and optical response is seen to have improved on increasing the etching time of sample fabrication. As stated in this work, that the porosity and surface roughness increase with increasing etching time, the loading capacity as well as diffused reflectance increases for the detector surfaces with increasing etching time, resulting in increased optical response. Since defect states density increases with increasing etching time, an increase in electrical response is evident for the detector samples with higher etching time. Many-fold increase in surface area for absorption, defective states, and surface roughness in macro-PSi samples in comparison to nano-Psi samples results in better electrical and



optical response of the macro-PSi based detectors, though the reproducibility of nano-PSi based detectors were found to be marginally better than that for macro samples. Thus CaM surface-functionalized macro-PSi based calcium detector together with its multi-parametric approach, including electrical and optical measurement system provides ideal structures for sensitive, selective and cost-effective calcium detection at biologically relevant concentration range.

## 6.2 FUTURE SCOPE

Based on the limitations of the diagnostic system, further work can be done for improvement and further development of the system to ensure better performance.

1. The automated instrument developed in this work undertake two parameters, namely lomi-bond angle and DPD-IPD ratio for the diagnosis of finger clubbing. More parameters in form of finger clubbing markers like Crug's angle, Shine measurement of nail plate and finger temperature measurement, can be incorporated for improved sensitivity of the finger clubbing monitor.
2. The selectivity of the fabricated CaM surface-functionalized PSi based calcium detector is tested for different cations commonly found in human body. Other than calcium namely  $\text{Na}^+$ ,  $\text{K}^+$ ,  $\text{Mn}^{2+}$ ,  $\text{Mg}^{2+}$  has been used for establishing the selectivity of the detector. The detector can be put to test for more cations and anions that are commonly found in human serum as well as those not so common in human serum but are common in food processing and water management fields, to observe its performance and selectivity so that the area of application of the fabricated detector can be monitored.
3. In this work, only one etching parameter that is etching time has been varied to find the variation of structural, optical and electrical response of the detector. Other etching parameters like etching current density and electrolytic concentration that are known to affect the structural morphology of fabricated PSi can be altered and the change in electrical and optical response needs to be investigated for improving the sensitivity of the fabricated detector.

4. Further investigation is required to monitor the response of the detector with varying CaM concentration and amount with which the detector surface is functionalized.
5. Huge scope prevails for the development of calcium sensor from the fabricated detector in this work by studying the variation of the detector response with varying calcium concentration, calibration of its sensitivity and limit of Detection (LOD).
6. Finally, a portable micro-sized device can be developed from the work based on this thesis for real time blood serum calcium level monitoring. Thus, an integrated system of finger clubbing monitor and serum calcium detector can be developed for multi-parametric diagnostic approach for early detection of cardio-pulmonary disease.





# **Annexure**

---

## **Annexure I**

Matlab code for finger clubbing measurement by image processing.

## **Annexure II**

Matlab code for finger clubbing measurement by laser-photo-detector arrangement.

## **Annexure III**

Matlab code for analysis of instant snapshots for optical analysis.

## **Annexure I**

### **Matlab code for finger clubbing measurement by image processing.**

```
% reading the image in matlab
a=imread('p12.png');
i=I(890:1680,1200:2200);
imshow(i);
a1=imrotate(i,270);
% converting the image to its gray form
%%a2=rgb2gray(a1);
% setting the threshold to convert the image to its near binary form
%%b=a2(54:547,135:430);
a3=a1>130;
% converting the image to its binary form
b1=im2bw(a3);
imshow(b1);
% finding the width profile of the image length-wise
c=sum(b1==0,2);
% finding the row and column value of the one dimensional array
containing
% the width profile
[m,n]=size(c);
for i=1:(m-1)
    x=c(i)
    y=c(i+1)
    if x>(y+2);
        d=1
        break
    else
        d=0 ;
    end
end
if d==1
    disp('IPD<DPD, The finger may be clubbed')
elseif d==0
    disp('IPD>DPD the finger may not be clubbed')
end

%reading the image
I=imread('p12.jpg');
imshow(I);
i=I(912:1710,1095:2387);
imshow(i);
%converting the image to gray scale
%%i1=rgb2gray(i);
%%imshow(i1);
%setting threshold to convert the image t o binary
i2=i1>120;
imshow(i2);
B2=im2bw(i);
%converting the binary image to its complementary
BW=~B2;
imshow(BW);
%showing the size of the image
dim=size(BW)
```

```

%finding the row for the corresponding column
col1=55
row1=min(find(BW(:,col1)))
col2=75
row2=min(find(BW(:,col2)))
col3=165
row3=min(find(BW(:,col3)))
col4=175
row4=min(find(BW(:,col4)))
%drawing the line on the image
imshow(B2);
%%hold on;
%%line([col1,col2],[row1,row2]);
%%line([col3,col4],[row3,row4]);

%declaring vector and finding the angle between them
V1=[col2,row2]-[col1,row1];
V2=[col4,row4]-[col3,row3];
Angle=acos(dot(V1,V2)/norm(V1)/norm(V2));
angle1=atan(Angle);
g=rad2deg(angle1);
theta=180-g;
    %alternative method of finding angle
    %dp=dot(V1,V2);
    %length1=sqrt(sum(V1.^2));
    %length2=sqrt(sum(V2.^2));
    %angle=180-acos(dp/(length1*length2))*180/pi
%declearing equation of the two lines
syms x y
m1=(row1-row2)/(col1-col2);
equ1=((y-row2)/(x-col2))== m1;
m2=(row3-row4)/(col3-col4);
equ2=((y-row4)/(x-col4))== m2;
% solving the equation
[SolX,SolY]=solve([equ1,equ2])
refY=((row1-row4)/(col1-col4))*(SolX-col4)+row4
%choosing out of the two angle equation
if(refY==SolY)
    disp('angle is 180')
else
    if(refY>SolY)
        clubangle=theta+(2*g);
        disp(clubangle)
    else
        disp(theta)
    end
end
%showing the image with the lines
imshow(i)
hold on
line([col1,col4],[row1,row4]);
line([col1,SolX],[row1,SolY]);
line([SolX,col4],[SolY,row4]);

```

### Matlab code for finger clubbing measurement by laser-photo-detector arrangement.

```
global a dir1 stp1 dir2 stp2 val0
a=arduino('COM3');
dir1=3;
stp1=2;
dir2=5;
stp2=4;
val0=2;
a.pinMode(dir1,'output');
a.pinMode(stp1,'output');
a.pinMode(dir2,'output');
a.pinMode(stp2,'output');

% dir is assigned 1 for counterclockwise rotation of motor
%counter is initialized

%no. of steps rotated by motor
for k=1:5
    a.digitalWrite(dir,1);
    pause(0.1);
c=0;
    for j=0:500
        a.digitalWrite(stp,1);
        pause(0.0001);
        a.digitalWrite(stp,0);
        x0=a.analogRead(2)
        %y0=0
        if x0>850
            %y0=1
            %tic
            c=c+1;
        else
            continue
        end
        %if y0==1 && x0<400
            % disp('i am going mad over this
program.....')
            % t=toc
        end
    %end
    disp(c);
% v=(20.106/3200)*1000
%w=t*v
% disp(w);
% disp('data accusation complete');
disp('data accusation complete');
    w(k)=c*0.00634;
    %disp(w);
a.digitalWrite(dir,0);
pause(0.1);
    for i=0:500
        a.digitalWrite(stp,1);
        pause(0.0001);
        a.digitalWrite(stp,0);
```



```

end
disp('action complete...');
end
disp(w);
[m,n]=size(w);
for l=1:(n-1)
    x=w(l);
    y=w(l+1);
    if x>(y+2)
        d=1;
        break
    else
        d=0 ;
    end
end
if d==1
    disp('IPD<DPD, The finger may be clubbed')
elseif d==0
    disp('IPD>DPD the finger may not be clubbed')
end

```

```

global a dir1 stp1 dir2 stp2 val0
a=arduino('COM3');
dir1=3;
stp1=2;
val0=2;
dir2=5;
stp2=4;
a.pinMode(dir1,'output');
a.pinMode(stp1,'output');
a.pinMode(dir2,'output');
a.pinMode(stp2,'output');
% 1st vertical movement of motor1 to obtain x1
    a.digitalWrite(dir1,1);
    c=0;
    for j=0:150
        a.digitalWrite(stp1,1);
        pause(0.0001);
        a.digitalWrite(stp1,0);
        x0=a.analogRead(2)

        if x0<600

            c=c+1;
            else
                continue
            end

        end
    disp(c);
    x1=c*0.00634
    disp(x1);
    a.digitalWrite(dir1,0);
    pause(0.1);
    for i=0:150
        a.digitalWrite(stp1,1);
        pause(0.0001);
        a.digitalWrite(stp1,0);
    end

```

```

% horizontal short movement of motor 2
a.digitalWrite(dir2,1);
for j=0:30
    a.digitalWrite(stp2,1);
    pause(0.0001);
    a.digitalWrite(stp2,0);
end
%vertical 2nd movement of motor 1 to get x2
a.digitalWrite(dir1,1);
c=0;
for j=0:150
    a.digitalWrite(stp1,1);
    pause(0.0001);
    a.digitalWrite(stp1,0);
    x0=a.analogRead(2)

    if x0<600

c=c+1;
    else
        continue
    end

    end
disp(c);
x2=c*0.00634
disp(x2);
a.digitalWrite(dir1,0);
pause(0.1);
for i=0:150
    a.digitalWrite(stp1,1);
    pause(0.0001);
    a.digitalWrite(stp1,0);
end
% horizontal long movement of motor 2
a.digitalWrite(dir2,1);
for j=0:200
    a.digitalWrite(stp2,1);
    pause(0.0001);
    a.digitalWrite(stp2,0);
end
% vertical movement of motor1 to get x3
a.digitalWrite(dir1,1);
c=0;
for j=0:150
    a.digitalWrite(stp1,1);
    pause(0.0001);
    a.digitalWrite(stp1,0);
    x0=a.analogRead(2)

    if x0<600

c=c+1;
    else
        continue
    end

    end
disp(c);
x3=c*0.00634

```

```

disp(x3);
a.digitalWrite(dir1,0);
pause(0.1);
for i=0:150
    a.digitalWrite(stp1,1);
    pause(0.0001);
    a.digitalWrite(stp1,0);
end
% horizontal short movement of motor 2
a.digitalWrite(dir2,1);
for j=0:30
    a.digitalWrite(stp2,1);
    pause(0.0001);
    a.digitalWrite(stp2,0);
end
%vertical 2nd movement of motor 1 to get x4
a.digitalWrite(dir1,1);
c=0;
for j=0:150
    a.digitalWrite(stp1,1);
    pause(0.0001);
    a.digitalWrite(stp1,0);
    x0=a.analogRead(2)

    if x0<600

c=c+1;
else
    continue
end

end
disp(c);
x4=c*0.00634
disp(x4);
a.digitalWrite(dir1,0);
pause(0.1);
for i=0:150
    a.digitalWrite(stp1,1);
    pause(0.0001);
    a.digitalWrite(stp1,0);
end
a.digitalWrite(dir2,0);
pause(0.1);
% back movement of horizontal motor, motor2
for i=0:260

    a.digitalWrite(stp2,1);
    pause(0.0001);
    a.digitalWrite(stp2,0);
end
disp('it has come to dis');
if ((x1<x2) && (x3>x4))
    angle1= (x2-x1)/0.1268;
    angle2=atan(angle1);
    thea1=rad2deg(angle2);
    angle3= (x3-x4)/0.1268;
    angle4=atan(angle3);
    thea2=rad2deg(angle4);
    lovibond=(180-(thea1+thea2));
    disp(lovibond);

```

```

disp('it is in the first if');
end
    if ((x1>x2) && (x3<x4))
        angle1= (x1-x2)/0.1268;
        angle2=atan(angle1);
        thea1=rad2deg(angle2);
        angle3= (x4-x3)/0.1268;
        angle4=atan(angle3);
        thea2=rad2deg(angle4);
        lovibond=(180+thea1+thea2);
        disp(lovibond);
        disp('it is in the 2nd if');
    end
    if ((x1>x2) && (x3>x4))
        angle1= (x1-x2)/0.1268;
        angle2=atan(angle1);
        thea1=rad2deg(angle2);
        angle3= (x3-x4)/0.1268;
        angle4=atan(angle3);
        thea2=rad2deg(angle4);
        lovibond=(180+thea1-thea2);
        disp(lovibond);
    disp('it is in the 3rd if');
    end
    if ((x1<x2) && (x3<x4))
        angle1= (x2-x1)/0.1268;
        angle2=atan(angle1);
        thea1=rad2deg(angle2);
        angle3= (x4-x3)/0.1268;
        angle4=atan(angle3);
        thea2=rad2deg(angle4);
        lovibond=(180-thea1+thea2);
        disp(lovibond);
        disp('it is in the 4th if');
    end
    if ((x1==x2) && (x3<x4))
        angle3=(x4-x3)/0.1268;
        angle4=atan(angle3);
        thea2=rad2deg(angle4);
        lovibond=(180+thea2);
        disp(lovibond);
        disp('it is in the 5th if');
    end
    if ((x1==x2) && (x3>x4))
        angle3=(x3-x4)/0.1268;
        angle4=atan(angle3);
        thea2=rad2deg(angle4);
        lovibond=(180-thea2);
        disp(lovibond);
    disp('it is in the 6th if');
    end
    if ((x1<x2) && (x3==x4))
        angle3=(x2-x1)/0.1268;
        angle4=atan(angle3);
        thea2=rad2deg(angle4);
        lovibond=(180-thea2);
        disp(lovibond);
    disp('it is in the 7th if');
    end
    if ((x1>x2) && (x3==x4))
        angle3=(x1-x2)/0.1268;

```

```
angle4=atan(angle3);  
thea2=rad2deg(angle4);  
lovibond=(180+thea2);  
disp(lovibond);  
disp('it is in the 8th if');  
end  
  
disp(180);  
  
disp('program over');
```

### Matlab code for analysis of instant snapshots for optical analysis.

```
I=imread('Picture 1623.jpg');
%class(I)
i=rgb2gray(I);
[x,y]=size(i)
X=1:x;
Y=1:y;
Z=im2double(i);
figure; h2=surf(Y,X,Z);
set(h2,'LineStyle','none');
colorbar
colormap winter;

avarage_value=mean(mean(Z))

mx_val=max(Z(:))
c=0;
for i=1:x
    for j=1:y
        if Z(i,j)>=mx_val*0.5;
            c=c+1;
        end
    end
end

%disp(c)
%disp(Z)

a=find(Z(:)>=mx_val*(3/4));
fwhm1=size(a)
b=find(Z(:)>=mx_val*0.5);
fwhm2=size(b)

surfcint=trapz(X,trapz(Y,Z,2))
```